

Overactuated Systems Coordination

THÈSE N° 4299 (2009)

PRÉSENTÉE LE 23 JANVIER 2009

À LA FACULTE SCIENCES ET TECHNIQUES DE L'INGÉNIEUR

LABORATOIRE D'AUTOMATIQUE - COMMUN

PROGRAMME DOCTORAL EN INFORMATIQUE, COMMUNICATIONS ET INFORMATION

ÉCOLE POLYTECHNIQUE FÉDÉRALE DE LAUSANNE

POUR L'OBTENTION DU GRADE DE DOCTEUR ÈS SCIENCES

PAR

Yvan MICHELLOD

acceptée sur proposition du jury:

Prof. H. Bleuler, président du jury
Dr D. Gillet, Dr Ph. Müllhaupt, directeurs de thèse
Dr B. Kiss, rapporteur
Dr F. Pepe, rapporteur
Dr A. Terrier, rapporteur



ÉCOLE POLYTECHNIQUE
FÉDÉRALE DE LAUSANNE

Suisse
2009

A Papa

A Alexandra et Romane

Remerciements

Comme tout travail de longue haleine, celui-ci a comporté des moments d'enthousiasme débordant, comme des moments plus pénibles. J'aimerais saisir l'occasion ici de remercier toutes les personnes qui, de prêt ou de loin, m'ont apporté leur soutien.

En premier lieu, je tiens à remercier les éminences grises du laboratoire d'automatique pour m'avoir accueilli et donné la possibilité de réaliser ce travail de recherche: à savoir les professeurs Dominique Bonvin et Roland Longchamp, et surtout Denis Gillet. Merci Denis de m'avoir fait confiance en me donnant l'opportunité de travailler sur le projet prima-ddl. Merci aussi de m'avoir laissé les coudées franches pour me permettre de me développer à mon aise. La confiance que tu m'as témoignée m'honore.

Je tiens à remercier tout particulièrement Philippe Mullhaupt pour son aide précieuse, ses conseils adéquats et son éternel enthousiasme. Même lorsque les moments d'adversité avaient une forte tendance à me décourager, tu as toujours su me motiver. Ce travail, résultat de nos pérégrinations intellectuelles, n'aurait certainement pas vu le jour sans tes interventions.

Je tiens à apporter toute ma gratitude au professeur H. Bleuler ainsi qu'aux docteurs K. Balint et A. Terrier pour avoir accepté

d'évaluer ce travail en tant que rapporteurs. Leurs remarques avisées ont sans aucun doute amélioré ma compréhension du domaine.

Un tout grand merci à mes collègues de bureau actuels ou passés, Davide, Damien et Klaske qui m'ont fait l'amitié de m'encourager lors des difficultés. Nos interminables discussions font sans aucun doute partie des meilleurs moments de ce cette thèse.

J'aimerai aussi étendre ces remerciements à mes autres amis du laboratoire d'automatique, en particulier, Marc, Gorka, Mark, Basile, Sylvain, Daniel, Pierre, Sébastien, compagnons de route d'infortune, partageant d'innombrables discussions et expériences plus ou moins scientifiques. Ce sont les amis de tous les jours qui ont rendu mon cadre de travail agréable et convivial.

Un merci particulier à Christophe Saltzmann et Philippe Cuanillon qui m'ont apporté conseils et soutien technique pour la réalisation pratique du prototype de la DDL ainsi que tout au long de ces années. Merci aussi à toute l'équipe du secrétariat, Ruth, Francine, Sole, Omeira et Marie-Claire. Votre aide m'a permis de me concentrer sur l'essentiel et vos sourires ont égayé mes journées de travail. Je remercie encore tous mes collègues du laboratoire qui ont partagé un bout de chemin à mes côtés.

Un grand merci à toute l'équipe du projet PRIMA-DDL, en particulier à Francesco, pour sa confiance et son enthousiasme, à Charles et Michel, pour leurs incroyables expériences pratiques et leurs gentillesse à mon égard, à Danuta, Laurent et Thanh pour nos longues journées de test sur le prototype et nos soirées animées, à Bruno et Gilles, pour notre collaboration tout simplement, à Françoise Delplanck et Frédéric Dérie pour m'avoir donné la possibilité de participer à l'implémentation in situ (à Paranal) de notre système, à tout ceux que j'oublie de citer ici qui ont permis la réussite de notre projet.

Merci à mes compagnons de repas et d'études, amis de longue date maintenant, Grégoire W., Claude, Thomas, Grégoire Ch., Gilles et Fabien: nos discussions philosophiques sur les bienfaits de la thèse ont su maintenir ma motivation jusqu'au terme de ces recherches.

Un tout tout grand merci à vous, ma famille, pour votre soutien et votre intérêt. C'est surtout grâce à votre présence et votre amour qu'il m'a été possible de surmonter toutes les difficultés rencontrées tout au long de ce travail. Rosmarie, Thomas et Claire, Pascal et Sandrine, Régis et Odette, Eric, Laetitia, Ludivine et Coralie: merci. Je vous dédie ce travail avec plaisir. Merci à toi papa, pour tes incessants encouragements et pour m'avoir écouté lorsque je partais dans mes interminables explications souvent brumeuses. La fierté que tu avais à me voir aller jusqu'au bout de moi-même a souvent été le facteur de motivation qui me remettait en selle.

Finalement, merci à ma femme, Alexandra, et à ma fille, Romane, pour votre amour, ou simplement pour votre présence et votre patience, jours après jours. Vous m'avez donné le temps nécessaire, souvent même plus, avec compréhension, pour que je puisse me consacrer à mes travaux.

*Rien n'est meilleur,
pour sécher ses larmes que de fixer une étoile.*

Raoul Follereau

Abstract

The economic growth inherent to our nowadays society pushes the industries toward better performances. In the mechatronic context, the increasing competition results in more and more stringent specifications. Thus, the multiple objectives to track become hard to achieve without compromises. A potential interesting solution to this problematic is overactuation, in the sense that, the considered system has more actuated degrees of freedom than the minimal number required to realize a task. Indeed, overactuation enables flexible and efficient responses to a high variety of tasks. Moreover, the coordinated combination of different subsystems enables both to combine their advantages and to cancel their disadvantages.

However, the successful coordination of the supplementary degrees of freedom at our disposal, thanks to overactuation, is not trivial. As a matter of fact, the problem of unpredictable response of overactuated systems to a periodic excitation can be particularly critical. Furthermore, the flexibility brought by the overactuation is to be used efficiently in order to justify its corresponding complexity and higher costs. In this sense, the tracking of multiple simultaneous objectives are clearly enabled by the overactuation and thus constitutes a clear motivation for such a solution.

As a consequence, the constructive coordination of overactuated systems, which can be very difficult, is very important to achieve stringent objectives. This thesis aims at contributing to the improvement of the coordination of such systems. In this context, three axis of research are considered: *differential geometry*, *potential functions*

and *closed-loop control*. Each of these axis is to be taken as a separate insight on the overall coordination of overactuated systems.

On the one hand, the formalism of *differential geometry* enables a solution to the unpredictability problem raised here above. An intelligent parameterization of the solution space to a periodic task enforces the predictability of the subsystem responses. Indeed, the periodicity of the task is transferred to the latter subsystem responses, thanks to an adequate coordination scheme.

On the second hand, *potential functions* enable the coordination of multiple simultaneous objectives to track. A clear hierarchy in the tasks priority is achieved through their successive projections into reduced orthogonal subspaces. Moreover, the previously mentioned predictability problem is also re-examined in this context.

Finally, in the frame of an international project in collaboration with the European Southern Observatory (ESO), an opto-mecatronic overactuated system, called Differential Delay Line, enables the consideration of *closed-loop coordination*. The successful coordination of the subsystems of the Differential Delay Line, combining their intrinsic advantages, is the key control-element ensuring the achievement of the stringent requirements.

This thesis demonstrates that a constructive coordination of the supplementary degrees of freedom of overactuated systems enables to achieve, at least partly, the stringent requirements of nowadays mechatronics.

Keywords:

Nonlinear Control, Redundancy, Overactuation, Coordination, Trajectory Planification, Optical Delay Line.

Résumé

La croissance continue propre à notre société de consommation d'aujourd'hui amène les industries à être de plus en plus performantes pour rester compétitives. Dans le contexte de la mécatronique, cette compétitivité croissante débouche sur des spécifications de plus en plus aiguës. Les multiples objectifs à réaliser deviennent difficiles à atteindre sans compromis. Une solution potentielle à cette problématique réside dans le suractionnement, compris dans le sens où le système considéré possède plus de degrés de liberté (d'actionneurs) que cela est strictement nécessaire à la réalisation de sa tâche. Le suractionnement permet alors une réponse flexible et performante à toutes sortes de tâches. De même, la combinaison coordonnée d'actionneurs de types différents permet à la fois de cumuler leurs avantages respectifs et d'annuler leurs désavantages.

Toutefois, la problématique de la coordination des degrés de liberté supplémentaires liée au suractionnement se pose. Par exemple, le problème de l'imprévisibilité des réponses des systèmes suractionnés soumis à des tâches périodiques peut être particulièrement critique. De plus, un système avec plus d'actionneurs que strictement nécessaire se doit d'exploiter au mieux ces derniers pour justifier sa plus grande complexité et son coût supérieur. La poursuite simultanée de multiples objectifs et la flexibilité du type de réponse, amenées par le suractionnement, en sont les motivations principales.

Par conséquent, la coordination constructive des systèmes suractionnés, qui peut être particulièrement ardue, est primordiale pour atteindre les objectifs. Cette thèse vise ainsi à contribuer à l'amé-

lioration de la coordination de tels systèmes. Pour ce faire, trois axes de développement sont considérés: la *géométrie différentielle*, les *fonctions potentielles* et la *boucle fermée*. Chacun de ces domaines pris indépendamment contribue à augmenter notre connaissance globale de la coordination des systèmes suractionnés.

D'une part, le formalisme de la *géométrie différentielle* nous permet de répondre à la problématique critique de l'imprévisibilité des réponses des systèmes suractionnés soumis à une excitation périodique. En effet, la paramétrisation coordonnée de l'ensemble des réponses d'un manipulateur à une tâche périodique renforce sa prévisibilité par une répartition, elle-même périodique, de la tâche sur chacun des sous-systèmes.

D'autre part, les *fonctions potentielles* nous permettent de mettre en place un schéma de coordination flexible à objectifs multiples. Une hiérarchie claire des priorités des tâches est mise en place par leur projection dans des espaces orthogonaux restreints. La problématique de la prédictivité de la réponse du manipulateur est aussi examinée dans ce contexte.

Finalement, un projet international en collaboration avec l'observatoire européen de l'hémisphère sud (ESO) nous permet de considérer les problèmes de coordination liés à la *boucle fermée*. En effet, une ligne à retard différentiel est réalisée par un système optomécatronique suractionné. La coordination fructueuse entre les sous-systèmes de la ligne à retard différentiel combine avantageusement leurs caractéristiques intrinsèques et, de ce fait, est le garant de l'adéquation entre les performances réelles et les spécifications demandées.

Cette thèse démontre qu'une coordination constructive des degrés de liberté supplémentaires des systèmes suractionnés permet de répondre, au moins en partie, aux attentes de plus en plus pointues de la mécatronique.

Mots-clés:

Contrôle Non-linéaire, Redondance, Suractionnement, Coordination, Planification de Trajectoire, Ligne à Retard Optique.

Contents

1	Introduction	1
1.1	Motivation	1
1.2	State of the art	4
1.3	Objectives and organization of the thesis	6
2	Coordination of overactuated systems	9
2.1	Overactuation: an infinite set of solutions	9
2.2	Differentiation of the solutions	10
2.3	Constructive coordination	11
2.4	Antagonistic objectives	11
3	Preliminaries	13
3.1	Open kinematic chain	13
3.1.1	5R Robot in 3D space	15
3.1.2	3R Robot in 2D space	16
3.1.3	Example of a main-task design	17
3.2	Closed trajectories and repeatability	18
3.3	The Poincaré map	18
3.4	Direct and inverse kinematic problem	20
3.5	General inversion of the jacobian	22
3.5.1	Jacobian definition	22

3.5.2	The pseudo-inverse as a velocity backward map	22
3.6	1-forms, involutivity and integrability	23
4	Differential geometry for coordination	27
4.1	Introduction	27
4.2	Coordination through differential geometry properties	30
4.2.1	Overactuation: an infinite set of solutions	30
4.2.2	Differentiation of the solutions	31
4.2.3	Constructive coordination	32
4.2.4	Antagonistic objectives	32
4.3	Coordination to achieve periodicity	33
4.4	Conclusion	48
5	Potential functions for coordination	51
5.1	Introduction	51
5.2	Coordination through potential functions	53
5.2.1	Overactuation: an infinite set of solutions	53
5.2.2	Differentiation of the solutions	54
5.2.3	Constructive coordination	55
5.2.4	Antagonistic objectives	56
5.3	Soft extension of the jacobian	56
5.4	The Hessian as coordination solution	69
5.5	Flexibility, compliance and repeatability	73
5.6	Conclusion	77
6	Closed-loop control for coordination	79
6.1	Introduction	80
6.2	Coordination of the overactuated DDL	92
6.2.1	Overactuation: an infinite set of solutions	93
6.2.2	Differentiation of the solutions	94
6.2.3	Constructive coordination	95
6.2.4	Antagonistic objectives	100
6.3	Simultaneous coordination of 2 DDLs	101
6.4	DDL prototype performances	105
6.5	Conclusion	115

7	Conclusions and perspectives	117
A	Shoulder coordination	121
B	Blade guiding analysis	133
C	Piezoelectric hysteresis compensation	137
D	Illustrations of the Differential Delay Line	147
E	Links to illustrative movies	153
	Index	167
	Glossary	171
	Curriculum vitæ	173

Introduction

Nowadays necessity of high performances enforces the antagonism of objectives: the classical control trade-off. "Have your cake and eat it too".

1.1 Motivation

Nowadays, the society is pushing toward performances. In our daily lives, success is intimately linked to competition and therefore one should strive for best possible performances under all circumstances. In industries, increasing output productivity, reducing costs or reducing the error margin are essential in order to remain competitive on the market.

However, the desired performances are often hard to be simultaneously reached. For example, one needs to be efficient at *microscopic scale* and simultaneously, these performances are requested over a large operating area (*macroscopic scale*). Moreover, on one side, *flexibility* is enhanced as a great advantage in the sense that it allows adapting to each problem specifically, and, on the other side, the *overall* concerted action should be harmonious. The resulting opposition in objectives to reach is representative of the problem one has to solve in our every day life. There is a nice sentence expressing this: "Have your cake and eat it too". From the control engineering point of view, this antagonism corresponds to the traditional trade-off between performances (fast responses, high gains) and robustness (stability).

Solutions to overcome these limitations are twofold. First, one can improve the concerned actors capabilities. Increasing the actuator bandwidth and precision for example will push the limit further away. However, this limit will still be present and one can think that, later on, it will re-appear with the next increase in specifications. Second, combining multiple actors with different capabilities is another solution. In our common lives, team force is being widely used with more or less success. Team sports are a clear example of a trial of constructive cooperation between people to achieve common goals, which would not be possible otherwise. From an engineering point of view, *overactuation*, or redundancy, in the sense of having more actuators than the minimal number required to realize a task, is an attempt to transfer this 'team spirit' to the technical field. Therefore, overactuation is a potential solution to our high performances demand. It enables to combine together fine micro-actuators with large macro-actuators or to combine fast and strong actuators to achieve multiple objectives simultaneously. In this sense, flexibility can be achieved throughout the combination of multiple subsystems, while an intelligent control coordinating the individual subparts enables predictability and repeatability.

Coordination etymologically means harmonious functioning of parts for effective results. In this sense, the constructive coordination of the subsystems is the key element, from the control point of view, enhancing the overall performances. A well-known example of successful coordination appears in biology: the human motor coordination. This extremely complex system is incredibly well-coordinated in order to enable, on one side, gross motor skills (walking, running, jumping, ...), and on the other side fine motor skills (manipulation of small objects using small muscle movement). In particular, the fine motor skills principally concern the arms and fingers coordination. These fine motions are often using feedback information to re-fine the movement: visual contact is used to *close the loop*. Fingers are also a specially nice example of a coordinated-overactuated system. The role of the thumb (which is primordial to enable grasping for example) lies apart from the remaining of the fingers (which are in

some way redundant).

Moreover, the humans, as one of the most complex coordinated overactuated-system, are realizing multiple tasks simultaneously with different level of attention. For example, in order to carry an object (possibly a cup full of liquid) to a specified place, a human will usually use his two hands simultaneously to be more stable (overactuation). If this task request a displacement of the entire body (to be reached), this will be done while ensuring a safe posture and avoiding obstacle: this is an obvious *coordinated multi-tasking* scheme (see Figure 1.1). However, all these tasks do not have the same priority. A human

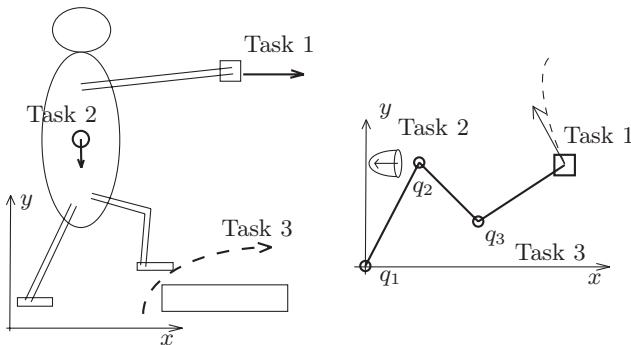


Fig. 1.1. Multiple tasks: a human-body versus an overactuated manipulator. Task 1: end-effector (hand) positioning. Task 2: posture optimization. Task 3: limits (obstacle) avoidance.

will first handle its posture in order not to fall, then concentrate on the obstacle avoidance for finally realizing its carrying task. A manipulator, which is working in a closed and safe environment, will put more emphasis on the realization of the task than on its own posture. Furthermore, these simultaneous goals are not necessarily easily decoupled: the realization of a task could prevent the successful realization of other tasks. Avoiding brusquely an obstacle in order

to remain in a safe posture could cause the carried-object to fall on the ground or to empty its load. Thus, a constructive coordination of the overall system (human body or manipulator) will consider all these objectives together with their level of priority (see Figure 1.1). With this nice example, we can feel that overactuation and coordination are intimately linked to the particular functioning of each subsystem. There is a clear classification of the individual subparts concerning their redundancy and the role they play to realize the tasks.

To sum up, in this thesis, I will focus on the constructive *coordination of overactuated systems* as a response to more and more stringent specifications and multi-tasking scheme. A particular application concerning the control of an optical Differential Delay Line, as a specific overactuated system, will also be detailed.

1.2 State of the art

Now that the substantial matter of this thesis has been introduced, the underlying problematic is highlighted through the different research axis found in the literature.

From an application point of view, redundant systems (i.e. systems having more actuated degrees of freedom than necessary for a given output task) show superior flexibility over classical systems insofar as they can accommodate not only for the main task but also for a possible secondary objective. The redundancy can be put to good effect to maximize efficiency (torque) resulting in substantial energy savings [4, 43], to optimize the time response resulting in fast responses [17, 75], to improve the accuracy of a positioning output [6, 53, 65, 69, 70, 84, 96, 105], to increase the reliability of a critical functionality [57, 99, 108] and/or to combine multiple objectives [39, 45, 54, 104].

Nevertheless, the augmented number of choices that is at the controller designer disposal makes the control design difficult so as to meet simultaneously all of these objectives. In this context, several

methods have been proposed to take advantage of these multiple possibilities. The generalized pseudo-inverse of the jacobian matrix (which corresponds to the partial differential matrix of the output with respect to the joints) first introduced by [103] to solve the redundancy, has been shown to minimize locally the kinetic energy necessary to realize the main task, while its null space is at our disposal to optimize any secondary objective [55, 56, 64]. Note that, in this thesis, the term *joint* designates an articulation of a manipulator which is actively-controlled with an actuator.

A repeatability problem was raised by [56] where several simulation experiments were run, using the Moore-Penrose pseudo-inverse control. They found that this control was not repeatable, but in some cases they observed limit cycles that did preserve repeatability. [8, 14, 42] also mentioned this repeatability problem. Since the mapping from the actuators space to the output space is a submersion (surjective map), an infinite number of different solutions exist to the coordination problem which consists in allocating the correct "amount of output" to each actuator. In particular, the differential geometry integrability condition has been shown (see [36, 37, 88, 91]) to be primordial in order to obtain repeatable solution in the joint space when realizing a periodic task at the output. In this context, [91] developed an integrability condition based on a Lie bracket test. This condition together with simple connectedness hypothesis ensures repeatable joint trajectories when tracking a closed trajectory with a redundant system. The proposed geometric reasoning, analyzes the joint space structure induced by the control strategy. Repeatability is equivalent to the existence of surfaces that are stable under the control, and for which the kinematic function is one to one. This yields the condition involving Lie brackets.

Baillieul [8, 9] tackled the inverse kinematic repeatability problem from another side. He proposed to extend the jacobian matrix in order to obtain a single possible solution to its inversion problem. This extension will impose an additional arbitrary relation between joints in order to obtain a square jacobian matrix to inverse. However,

this technique never ensures to avoid singularities in the inversion matrix problem along the trajectory path.

Gu [35,36] introduced a configuration manifold embedding model to study especially redundant robot. The ultimate objective of this model development is to explicitly show the fact that for a redundant robot, a subtask decision represented by a certain kinematic null solution is technically equivalent to the configuration manifold embedding in its dynamic modeling. In other words, once the minimum embeddable C-manifold, as the smallest dynamic model, is achieved, a one-to-one kinematic output of the redundant robot can also be determined accordingly in terms of a given main task as well as a desired subtask specification.

Topological tools have been introduced in the context of robotics in order to obtain an insight into engineering problems [15, 16, 34]. Through topology, efforts have been put on global solutions to the inverse kinematic problem.

In the context of studying the humanoid robots coordination and control, Khatib research group developed many concepts which are relevant to our research work. They developed an operational space coordination frame [51], enabling the dynamic description of all motions and tasks. Moreover, they used artificial potential functions to enable simultaneous multi-tasking (posture optimization, obstacle avoidance [50], joint limits avoidance...), enforcing prioritization of the tasks and subtasks through successive projections into task-nullspaces [52, 89, 90].

I do not have the presumption to have made a complete overview of the concerning literature, however these are some of the relevant ideas regarding the presented research.

1.3 Objectives and organization of the thesis

This thesis aims at exploring the coordination of overactuated systems. After the definition of what are the properties of an overactuated system and what is meant as coordination in Chapter 2,

Chapter 3 introduces the necessary concepts to the development of this thesis.

Afterwards, three axis of research are developed thoroughly concerning the coordination of overactuated systems, each one of them should be taken as a separate insight on the general coordination goal. First, in Chapter 4, some properties of differential geometry are demonstrated to be essential for our coordination objective. Under this scope, a constructive coordination is obtained whenever a particular involutive parameterization of the solution space ensures a periodic response of the joints to a periodic end-effector task.

Second, Chapter 5 explores the coordination of overactuated systems under the scope of potential functions and multi-tasking schemes. In this context, constructive coordination is obtained whenever multiple tasks are tracked simultaneously successfully. Moreover, a hierarchical separation of the tasks and a topological optimal solution are examined particularly.

Third, the Chapter 6 examines a particular overactuated system (the Differential Delay Line, DDL) under the scope of closed-loop coordination. In this context, constructive coordination is obtained whenever the performance-specifications are obtained and saturation of the fine stage is avoided. Furthermore, a particular overactuation scheme enforcing the coordination of multiple DDLs is also detailed. These three chapters represent respectively three different insights on the main matter of this thesis.

Finally, Chapter 7 concludes the undertaken research and highlights some future research potentialities.

As recapitulation, in this thesis, I principally aim at contributing to the optimal exploitation of the supplementary degrees of freedom of overactuated systems. This objective is realized through the three main chapters (Chapters 4, 5 and 6), where three different original insights are proposed.

Coordination of overactuated systems

Overactuation increases flexibility to the cost of a large increase in complexity. The coordination of overactuated systems includes four characteristics: infinite set of solutions, differentiation of the solutions, coordination to obtain the desired choice and antagonistic objectives.

As introduced in Chapter 1, overactuation is a solution to nowadays demand for extreme performances. Thus, in combining the respective advantages of subsystems, we tend to reach better performances. However, the appropriate combination of subsystems is not trivial and necessitates deep coordination in order to balance adequately the inherent antagonism of the objectives.

In this chapter, I introduce the four major characteristics of the overactuated-system-coordination problematic (illustrated in Figure 2.1): 1) infinite set of solutions, 2) differentiation of the solutions, 3) constructive coordination, 4) antagonistic objectives. All these concepts are re-examined specifically under the scope of each next chapter (Chapters 4, 5 and 6).

2.1 Overactuation: an infinite set of solutions

An overactuated system, as considered in this thesis, is defined such that there exists infinite different solutions to a pre-defined task. The infinite dimension of the solution set implies simultaneously the possibility to modify continuously the configuration of the system in

navigating within the set. Notice that emphasis is put on the link between the system and a predefined task. The characteristic of a system to be overactuated is only defined with respect to its task.

The existence of infinite different solutions implies a decision process realizing the appropriate choice in order to solve the overactuation problem. Having more possibilities than strictly necessary to realize a given task induces either an optimality problem, for example in term of energy, posture, or a multi-task problem. In this sense, any secondary objective can be added to the main task of the system. Flexibility is enhanced through the multiple choices at our disposal, to the cost of a higher degree of complexity. Particularly, the counterpart of flexibility consists in an indetermination problem. In the sense that for a given task, the response of a system is not always strictly identical, depending on the initial conditions.

2.2 Differentiation of the solutions

The implicit choice procedure related to the overactuation resolution necessitates a clear differentiation of the solutions. The latter have to be separated in order to enable a correct evaluation of the different possibilities. This separation process includes, first, an intrinsic characterization of the subsystems (corresponding to the particular capacities of each subsystem) and, second, a clear classification of the objectives in term of priority.

Firstly, separation includes for example bandwidth, accuracy, resolution, torque characteristics. These concepts are subsystem oriented, in the sense that they describe the intrinsic behavior of the constituting elements. Secondly, separation includes tasks and objectives orientated evaluation. In the sense that some objectives are prior to others. These concepts are eventually system oriented.

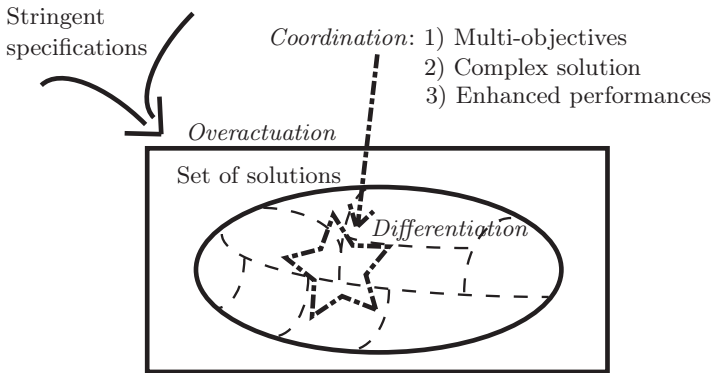


Fig. 2.1. Coordination of overactuated systems as a solution to stringent specifications and complex systems. Overactuation implies an infinite set of solutions to the same task, which have to be differentiated in order to evaluate their respective interest. Finally, a constructive coordination scheme is to be developed in order to take advantage of the flexibility at the disposal of the controller designer.

2.3 Constructive coordination

As a result of the infinity of different alternatives, a coordination strategy enhancing mutual advantages of each subsystem is to be selected. The coordination enables the constructive tracking of multiple objectives, while avoiding any type of singularities. The obtained solution should maintain the flexibility brought by overactuation while ensuring non-versatility. Notice that, in this thesis, *versatility* is understood as an unpredictable joint response, entirely dependent on the initial conditions.

2.4 Antagonistic objectives

The well-known classical control trade-off between robustness and performances find its equivalent when addressing the coordination

problem of overactuated systems. The combination of a priori antagonistic (meaning either opposed or competitive) objectives can often only be featured by overactuated systems in the sense developed in this thesis. Microscopic positioning accuracy (nm) over macroscopic area (several mm), as requested for the DDL opto-mechatronic system (see Chapter 6), is a clear example of one of these antagonisms. Some of the antagonisms which are relevant to our study are listed hereafter.

- *Flexibility*, which is often desired, is counterbalanced by *versatility*, Chapter 4.
- *Accessibility singularities* (corresponding to limitations of the workspace) are dual to the *integration singularities* (coming from the direct/inverse kinematics), Chapter 4 and 5.
- The *complexity* caused by the tracking of multiple objectives is clearly antagonistic to the *simplicity* of a single objective tracking, Chapter 5.
- *Redundancy* (overactuation) is opposed to the *unicity* of solutions for fully-actuated system, Chapters 4, 5 and 6.
- *Open-loop* coordination (handling absolute signals) and *closed-loop* coordination (handling relative error signals) are intrinsically different, Chapter 6.
- Finally, in terms of performance and specification, this antagonism is clearly visible in Chapter 6. An obvious example concerns the ratio between the requested resolution (*nanometer resolution*) and the requested working stroke (over *several millimeters*).

In Chapter 2, I introduced the major concepts linked to the problematic of overactuated system coordination. Note that each of the Sections 2.1 to 2.4 will be re-examined under the scope of Chapters 4, 5 and 6.

In the forthcoming chapter (Chapter 3), some of the mathematical tools which are needed in order to understand the future developments are reminded.

Preliminaries

Some concepts which are useful to the presentation of the following chapters are clarified hereafter.

In the forthcoming sections, some of the most important mathematical tools regarding this thesis are recalled. Almost all of them can be found in a close-form in the literature. Thus, most of my work herein concerns the re-formulation of these tools in the context of overactuated systems coordination.

Moreover, the two main examples that I use to illustrate the concepts in the following chapters (the 5R3D manipulator and the 3R2D manipulator) are introduced.

3.1 Open kinematic chain

In this section some definitions and concepts which are useful to our presentation are detailed. Moreover, (and without loss of generality), two particular manipulators are detailed: either a five rotary-serially-linked (5R) robot in 3D space, or a 3 rotary-serially-linked (3R) manipulator in a 2D plane. Additionally, an example of an output trajectory is chosen for comparison purposes.

Definition 3.1 (*Open Kinematic Chain*) *An open kinematic chain is a n -serial link manipulator arm, whose end-effector, attached to*

the last link, performs a task in \mathbb{R}^3 . The end-effector position $Y(t)$ is described with a function of the joints angle (for rotary joint) and length (for prismatic joint). Using the joint-configuration (angle and length) coordinates $(q_1, \dots, q_n) \in Q, q_i \in \mathbb{R}$, we have

$$Y = (x(q) \ y(q) \ z(q))^T \quad (3.1)$$

which for notational purposes will be written $Y = \zeta(q)$.

Notice that, in this thesis, the term *joint* designates an articulation of a manipulator which is actively-controlled with an actuator. So that the *joint configurations* correspond to a general representation of the manipulator with the individual position of each articulation as coordinates. Note also that *end-effector* designates the extremity of a manipulator, usually holding a tool (like a pincer for example), the position of which is to be controlled.

Definition 3.2 (*Working Space*) The working space $\Gamma^m \subset \mathbb{R}^m$ of a n -joints manipulator arm described by its joint configurations $Y = \zeta(q_1, \dots, q_n) \in \mathbb{R}^m, (q_1, \dots, q_n) \in Q, q_i \in \mathbb{R}$, corresponds to the end-effector bounded accessibility area in \mathbb{R}^m .

$$\Gamma^m = \left\{ Y \in \mathbb{R}^m : \exists \{q_1, \dots, q_n\} \in Q, \right. \\ \left. Y = \zeta(q_1, \dots, q_n) \right\}$$

The working space Γ^m of a manipulator denotes the ambient space in which the end-effector of a manipulator acts. The nature of the working space depends on the type of manipulator and task considered:

- \mathbb{R} : linear manipulator ($m = 1$)
- \mathbb{R}^2 : planar manipulator without orientation ($m = 2$)
- $\mathbb{R}^2 \times SO(2)$: planar manipulator with orientation ($m = 3$)
- \mathbb{R}^3 : spatial positioning manipulator ($m = 3$)
- $\mathbb{R}^3 \times SO(3)$: spatial manipulator with orientation ($m = 6$)

where m denotes the number of independent parameters necessary to specify the location of the end-effector frame in its ambient space.

Definition 3.3 (*Redundant Robot*) *A manipulator made of n joints is said to be redundant, when, for a fixed end-effector position \bar{Y} , there exist infinite different joint configurations (q_1, \dots, q_n) . Let $\bar{x}, \bar{y}, \bar{z} \in \mathbb{R}$ be a given end-effector position $\bar{Y} = (\bar{x} \ \bar{y} \ \bar{z})^T \in \mathbb{R}^3$.*

$$\Omega_q = \{(q_1, \dots, q_n) \in Q, q_i \in \mathbb{R} : \zeta(q_1, \dots, q_n) = \bar{Y}\}$$

The redundant manifold Ω is the manifold collecting the subspaces $\Omega_q \subset Q$ for all possible $\bar{Y} \in \mathbb{R}^3$.

$$\Omega = \bigcup_{\bar{Y} \in \mathbb{R}^3} \Omega_q$$

Note that the term *self-motion* is dedicated to a motion of the manipulator strictly in the redundant manifold Ω_q (i.e.: a joint motion which does not have any impact on the end-effector position).

Remark 3.1 *An obvious particularity of redundant systems is that they cannot be specified uniquely by a set of parameters that only describes the end-effector position or orientation. An independent set of end-effector configuration parameters, therefore, does not constitute a generalized coordinate frame for the whole system [51].*

3.1.1 5R Robot in 3D space

For any robot, each possible configurations of the joints defines a unique position and orientation of its end-effector. Mathematically, this characteristic is defined through a unique map ζ from the inputs, the joint coordinates $(q_i(t))$, to the output, the cartesian position and the orientation $(y(t))$ of the end-effector.

$$y(t) = \zeta(q_1(t), q_2(t), \dots, q_n(t)) \quad (3.2)$$

Thus a 5R-manipulator in 3D space corresponds to an open kinematic chain constituted of five serially linked rotary joints (5R). For

our study, this particular manipulator will realize a periodic positioning task $Y(t)$ in \mathbb{R}^3 , see Figure 3.1.

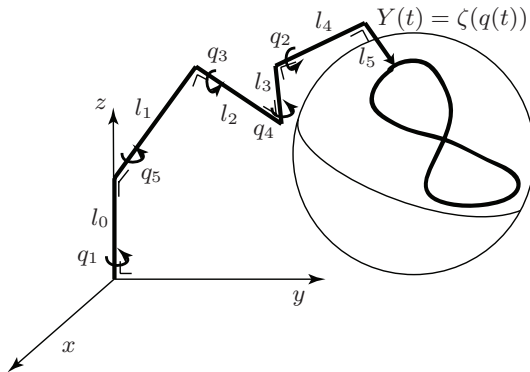


Fig. 3.1. Five rotary (5R) joints (q_1 to q_5) serially linked (l_0 to l_5) manipulator arm in \mathbb{R}^3 .

3.1.2 3R Robot in 2D space

The 3R serial manipulator in 2D space is defined with the particularity that all its three rotation axis are parallel and perpendicular to the output space \mathbb{R}^2 , see Figure 3.2. This particular manipulator thus enables a motion of its end-effector in a two-dimensional plane. As for the preceding manipulator, essentially the positioning of its end-effector (not the orientation) is considered. Considering absolute joint angles (meaning angle with respect to a fixed referential), the end-effector position (x, y) is defined as follow.

$$\begin{aligned} x &= \cos(q_1) + \cos(q_2) + \cos(q_3) \\ y &= \sin(q_1) + \sin(q_2) + \sin(q_3) \end{aligned}$$

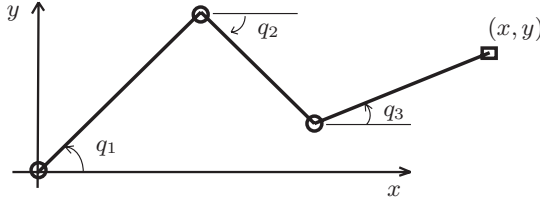


Fig. 3.2. 3R2D serial-planar manipulator with absolute angular joints q_1 , q_2 and q_3 .

3.1.3 Example of a main-task design

Only end-effector trajectories that can be embedded in a smooth manifold \mathcal{S} are considered. As the main task, the end-effector trajectory in \mathbb{R}^3 is parameterized with time. The manipulator output manifold \mathcal{S} , containing the end-effector trajectory, is selected to be a sphere. The tangent bundle ($T\mathcal{S}$) associated with the output manifold contains the velocity-vector of displacement $dY/dt = \dot{Y}(t)$.

As an example, a Lissajou curve parameterized by the following equations is selected as the main positioning task of the manipulator arm.

$$\begin{aligned} x_p(t) &= A \cos(\omega t + \varphi) \\ y_p(t) &= A \cos(2\omega t + \varphi) \end{aligned}$$

Using the rotation matrices $R_x(a)$, $R_y(b)$, $R_z(c)$ defined by [33] (pp. 146-147 and 608), the planar curve is mapped onto the output manifold (sphere) through the local diffeomorphism defined by:

$$\begin{aligned} \begin{pmatrix} x(t) \\ y(t) \\ z(t) \end{pmatrix} &= R_x(a)R_y(b)R_z(c) \begin{pmatrix} r \cos(x_p) \cos(y_p) \\ r \cos(x_p) \sin(y_p) \\ r \sin(x_p) \end{pmatrix} \\ &+ \begin{pmatrix} c_x \\ c_y \\ c_z \end{pmatrix} \end{aligned} \quad (3.3)$$

where c_x , c_y , c_z represent the sphere center coordinates and r its radius.

The velocity reference dY/dt is obtained through the time derivative of Equation 3.3.

3.2 Closed trajectories and repeatability

A closed end-effector trajectory is defined such that the end-effector follows a periodic path in the operational coordinate frame. Thus, it passes periodically through the same coordinate point.

Definition 3.4 (*closed trajectory*) *A closed trajectory $\varphi(t) \in \mathbb{R}^m$ is a periodic trajectory.*

$$\varphi(t) = \varphi(t + T) \tag{3.4}$$

where T represents its time period.

The repeatability problem introduced previously (see Section 1.2) describes the fact that, despite the tracking of a closed trajectory with the end-effector of a redundant manipulator, the joints are not necessarily following a closed path in the joints coordinate-frame. Therefore, the motion of the manipulator arm is not always predictable, which is not acceptable in most industrial environment.

3.3 The Poincaré map

The Poincaré map is defined as the intersection of an orbit in the state space of a continuous dynamical system with a certain lower dimensional subspace, called the Poincaré section, transversal to the flow of the system. The transversality of the Poincaré section basically means that orbits starting on the subspace flow through the subspace itself and not parallel to it (see Figure 3.3).

Definition 3.5 Let (\mathbb{R}, X, Φ) be a global dynamical system, with \mathbb{R} the real numbers, X the state space and Φ the evolution function (integral solution to $\dot{x} = f(x)$). Let γ be an orbit through a point p and S be a local differentiable and transversal section of Φ through p , called Poincaré section through p .

Given an open and connected neighbourhood U of p , a function

$$P : U \rightarrow S$$

is called Poincaré map for orbit γ on the Poincaré section S through point p if:

- $P(p) = p$
- $P(U)$ is a neighbourhood of p and $P : U \rightarrow P(U)$ is a diffeomorphism.

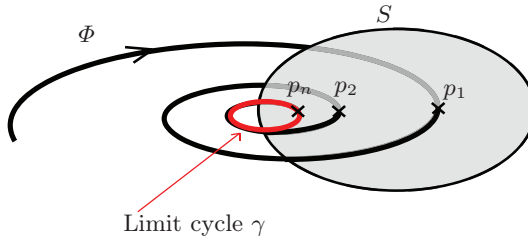


Fig. 3.3. Poincaré map: the convergence of a system ($\dot{x} = f(x)$) to a limit cycle γ happens when the discrete series $\{p_1, p_2, \dots, p_n\}$ resulting from the intersection of the evolution function Φ with the Poincaré section converges to a fixed point p_n .

A Poincaré map can be interpreted as a discrete dynamical systems with a state space that is one dimension smaller than the original continuous dynamical system. Because it preserves many properties of periodic and quasiperiodic orbits of the original system and has a lower dimensional state space it is often used for analyzing the original system.

Theorem 3.1 *Defining (Z, U, P) as the corresponding discrete dynamical system with state space U and evolution function $P : Z \times U \rightarrow U$, we have either:*

- *the periodic orbit γ of the continuous dynamical system is stable if and only if the fixed point p of the discrete dynamical system is stable, or*
- *the periodic orbit γ of the continuous dynamical system is asymptotically stable if and only if the fixed point p of the discrete dynamical system is asymptotically stable.*

The interested reader will find a proof of Theorem 3.1 in [25].

Remark 3.2 *A linear system when driven by an external periodic force will try to follow the applied force and hence oscillate with the applied frequency (after a short transient behavior). The situation is quite different for a nonlinear system. Here, depending on the strength of nonlinearity, the system shows periodic or quasi periodic or chaotic behavior. We expect that in the periodic regime the period of system should be related to the period of external force. If T is the period of external force then system period will be nT , where n is an integer. In the chaotic regime (no periodicity) n tends to infinity. Thus, the number of distinct points (over a long period of time) plotted on the Poincaré map indicates the period of the system.*

3.4 Direct and inverse kinematic problem

Definition 3.6 *(forward or direct kinematic) Consider a serial manipulator made of n independent joints $q_1, \dots, q_n \in \mathbb{R}$. The direct kinematic problem concerns the definition of the map $Y(q) = \zeta(q)$ from the joint space Q to the end-effector space $\mathcal{S} \subset \mathbb{R}^3$.*

$$\zeta : q \in Q \rightarrow \mathcal{S} \subset \mathbb{R}^3$$

$$Y(q) = \begin{pmatrix} x \\ y \\ z \end{pmatrix} = \zeta(q) \quad (3.5)$$

The map $\zeta(q)$ defines a single position/orientation of the output (end-effector position and or orientation) from the joint coordinates.

Remark 3.3 *For redundant systems, this direct map is surjective. By its surjective nature, there are many different joint configurations linked to the same end-effector position (an infinity for redundant systems).*

Remark 3.4 *There is an equivalent surjective direct map $\phi(q)$ linking the velocities of the joints \dot{q} to the motion of the end-effector \dot{Y} . This velocity map is perfectly defined by the partial differentiation of the function $\zeta(q)$.*

$$\dot{Y} = \phi(q)\dot{q} = \frac{\partial \zeta}{\partial q} \dot{q} \quad (3.6)$$

Definition 3.7 *(inverse kinematic) The inverse kinematic concerns the reverse map ζ^{-1} from the end-effector position $Y = (x, y, z)^T$ to the joint configurations (q_1, \dots, q_n) , $q_i \in \mathbb{R}$.*

$$\begin{aligned} \zeta^{-1} : \mathcal{S} \subset \mathbb{R}^3 &\rightarrow Q \\ q &= \begin{pmatrix} q_1 \\ \dots \\ q_n \end{pmatrix} = \zeta^{-1} \begin{pmatrix} x \\ y \\ z \end{pmatrix} \end{aligned} \quad (3.7)$$

Concerning redundant systems, this inverse map can only be analytically obtained for a very reduced class of manipulators [5].

Remark 3.5 *The inverse kinematic problem at velocity level for redundant manipulators, which attempts to determine the joint displacements \dot{q} needed in order to realize a predefined motion with the end-effector \dot{Y} , is very complex in the sense that an infinity of different solutions exist.*

$$\dot{q} = \phi^{-1}(\dot{Y})$$

It is therefore not possible to obtain an analytical solution to this problem, except for particular manipulators.

The mapping ζ , ζ^{-1} , ϕ and ϕ^{-1} introduced in this section are illustrated in Figure 4.1.

3.5 General inversion of the jacobian

3.5.1 Jacobian definition

Definition 3.8 (*Jacobian*) *The jacobian matrix J of an open kinematic chain is defined as the partial derivative of its end-effector cartesian position $Y = \zeta(q)$ with respect to the joints q_i .*

$$J = \nabla_q Y(q) = \frac{\partial \zeta(q)}{\partial q} \quad (3.8)$$

The jacobian matrix J defines the velocity map $\phi(q)$ (see Remark 3.4) from the joint-velocity space \dot{q} to the end-effector-velocity space \dot{Y} .

$$\dot{Y} = \phi(q)\dot{q} = J\dot{q} \quad (3.9)$$

3.5.2 The pseudo-inverse as a velocity backward map

The velocity map, see Remark 3.5 using the jacobian matrix (differential map between the tangent spaces of the operational and joint spaces), is one solution through integration to the inverse kinematic problem.

Considering the injective nature of the inverse kinematic problem defined by the reverse equation

$$\dot{q} = \left(\frac{\partial \zeta}{\partial q} \right)^{-1} \dot{Y}$$

(from Equations 3.8 and 3.9), there exists an infinity of different solutions to this problem. Among all solutions, a reasonable choice could be the local minimization of the joint velocities in order to realize the desired end-effector motion.

Theorem 3.2 *The classical Moore-Penrose pseudo-inverse of the jacobian matrix $J^+ = J^T(JJ^T)^{-1}$ is one solution to the inverse kinematic problem. Moreover, the pseudo-inverse solution tends to minimize locally the joint variations in order to realize a predefined trajectory $Y(t)$.*

Proof: Defining the cost function

$$G(\dot{q}) = \dot{q}^T W \dot{q}$$

with W , a $n \times n$ positive definite weighting matrix, we try to minimize the joint variations. Using the Lagrange multipliers method to ensure the tracking of the trajectory (the direct kinematic Equation 3.9), we obtain the following formulation.

$$G(\dot{q}, \lambda) = \dot{q}^T W \dot{q} - \lambda^T (J\dot{q} - \dot{Y}) \quad (3.10)$$

The necessary condition of optimality are two folds: first $\frac{\partial G}{\partial \dot{q}} = 0$, which induces $2W\dot{q} - J^T \lambda = 0$ or equivalently $\dot{q} = \frac{1}{2}W^{-1}J^T \lambda$ and second $\frac{\partial G}{\partial \lambda} = 0$ which corresponds to $J\dot{q} = \dot{Y}$. Eliminating the Lagrange multipliers and substituting into (3.10), we obtain finally (see [5] for details).

$$\dot{q} = W^{-1}J^T(JW^{-1}J^T)^{-1}\dot{Y} \quad (3.11)$$

Notice that, considering the jacobian matrix J to be full row-rank, $(JW^{-1}J^T)$ is a full-rank square matrix, which is thus invertible. Finally, if the weighting matrix W is taken as the identity matrix, we find that one solution, which satisfies the local necessary conditions of optimality, is the Moore-Penrose pseudo-inverse.

$$\dot{q} = J^T(JJ^T)^{-1}\dot{Y} = J^+\dot{Y} \quad (3.12)$$

■

3.6 1-forms, involutivity and integrability

Some useful concepts of differential geometry are recalled hereafter.

Definition 3.9 (*manifold*) *A manifold M^n is a topological space in \mathbb{R}^n which is locally Euclidean. In other words, it is a space where, around every point $p \in M^n$, there is a small neighborhood U that is topologically equivalent to an open unit ball in \mathbb{R}^n .*

Definition 3.10 (*homeomorphism*) A homeomorphism, also called a continuous transformation, is an equivalence relation and one-to-one correspondence between points in two geometric figures or topological spaces that is continuous in both directions. Two objects are said to be homeomorphic if they can be deformed into each other by a continuous, invertible mapping. Moreover, if this continuous mapping and its inverse are differentiable, the map is called a diffeomorphism.

Definition 3.11 (*compactness*) A topological space M is compact if every open cover of M also has a finite subcover. I.e. if U_j is an open subset of M , $U_j \subset M$, and the union of arbitrary open subsets covers M , $\cup_{j \in \Lambda} U_j = M$, then there must be a finite number of open subsets, $j_1, \dots, j_n \in \Lambda$ such that $U_{j_1}, \dots, U_{j_n} = M$.

The configuration space of a revolute-jointed manipulator is compact, since the product of compact manifolds is also compact. Figure 3.4 represents the compact configuration space of a single revolute joint. Note that, for revolute joints, a topological problem, which we will

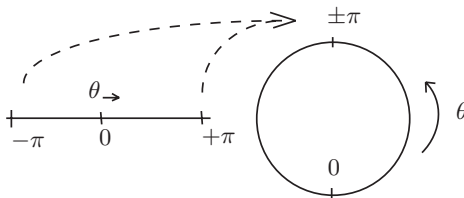


Fig. 3.4. Single revolute-joint configuration space: S^1 . Identification of $\pm\pi$.

have to take care of, results from the identification of the two distinct joint angles $\pm\pi$ in the configuration space Q (two distinct joint values have the same image in the configuration space).

The configuration space of an idealized prismatic joint q_i is not compact: the domain of its joint variable is the real line \mathbb{R} , which is

not a compact manifold. However, a prismatic joint has motion limits which limits the domain of q_i to an interval of the real line $I = [a, b]$, which is a compact manifold. Hence any serial manipulator built up from revolute and prismatic joints is consequently compact.

Definition 3.12 (*1-form*) A 1-form $\omega(q)$ is a covector field, which belongs to the dual space of the tangent bundle, T^*Q called the cotangent bundle.

$$\omega(q) = \sum_{i=1}^n c_i dq, \quad c_i \in \mathbb{R}, \quad q \in Q$$

An exact 1-form is directly obtained by the derivation of a function $h(q)$ so that $\omega = dh$. Thus, the exact 1-form of a function corresponds to the gradient of the same function. An integrable 1-form becomes exact after multiplication with an arbitrary function.

A 1-form can also be seen as an application ψ mapping any vector fields $f \subset \mathbb{R}^n$ to \mathbb{R} .

$$\psi : f \subset \mathbb{R}^n \rightarrow \mathbb{R}$$

The notation $\langle \cdot, \cdot \rangle$ can be used to feature the application ψ such that: $\langle \psi, f \rangle = r \in \mathbb{R}$. Moreover, if the vector field f belongs to the tangent bundle of an integral manifold $M^n \subset \mathbb{R}^n$, the application ψ maps the vector field f to 0.

Definition 3.13 (*involutivity*) A distribution of vector fields $\{f_1, f_2, \dots, f_n\}$ is said to be involutive when:

$$\begin{aligned} \forall f_i, f_j, i, j = 1, \dots, n \\ [f_i, f_j] \in \text{span}\{f_1, f_2, \dots, f_n\} \end{aligned}$$

where $[f_i, f_j]$ corresponds to the Lie bracket operator.

Definition 3.14 (*integrability*) A distribution of n vector fields $\{f_1, f_2, \dots, f_n\}$ is integrable, if this distribution defines the tangent space of an unique hyper-surface of dimension n . Equivalently, a system of integrable 1-forms ω_i exists and represents the normals to the hyper-surface.

Theorem 3.3 *A collection of n vector fields $\{f_1, f_2, \dots, f_n\}$ defines an integrable distribution, if and only if the distribution is involutive.*

The interested reader will find a proof of Theorem 3.3 in [73].

Remark 3.6 *The jacobian matrix (see Definition 3.8) of a n -link open kinematic chain manipulator can be expressed using the three exact 1-forms $\omega_x(q) = dx$, $\omega_y(q) = dy$ and $\omega_z(q) = dz$.*

$$J = \nabla_q Y(q) = \begin{pmatrix} \omega_x \\ \omega_y \\ \omega_z \end{pmatrix} \quad (3.13)$$

Theorem 3.4 Bendixon-Poincaré

If a state trajectory remains in a closed simply-connected set of a two dimensional submanifold Σ , then one of the three following propositions is true:

- *The trajectory converges to an equilibrium.*
- *The trajectory converges asymptotically to a limit cycle.*
- *The trajectory is itself a limit cycle.*

For a proof of Theorem 3.4, the interested reader can refer to [25] or [38].

In Chapter 3, some of the mathematical tools which are used in the following chapters are recalled. In particular, the *Bendixon-Poincaré theorem* (Theorem 3.4), the meaning of a *1-form* (see Definition 3.12) and the concepts of *involutivity* and *integrability* (Definitions 3.13 and 3.14) are very useful for the next chapter.

In the forthcoming chapter (Chapter 4), in the context of solving the inverse kinematic problem (see Definition 3.7) for a serial manipulator, a constructive open-loop coordination scheme is developed. The pre-cited differential geometry properties are used in order to derive a condition ensuring repeatable joint responses to a periodic excitation.

Differential geometry for coordination

In this chapter, the coordination of an overactuated serial manipulator is understood as an appropriate repartition of the end-effector position-reference through all joints (open-loop control) under the scope of differential geometry. A constructive coordination is obtained whenever repeatable (meaning periodic) joint responses are obtained to periodic excitation of the end-effector, while keeping the initial flexibility brought by overactuation.

Overactuation, as defined in this thesis, implies the existence of supplementary degrees of freedom with respect to the main task to be realized. These supplementary degrees of freedom increase the flexibility of the system's response. In this context, the repeatability of the joint responses to a periodic excitation becomes uncertain when solving the inverse kinematic problem (see Definition 3.7). This chapter attempts to develop some differential-geometry properties in order to overcome this predictability issue.

4.1 Introduction

The present chapter considers as an output task the positioning of the end-effector of an overactuated serial manipulator (constituted of n serially-connected rotary joints) so as to track a closed orbit on a working surface in the three dimensional space (3D). Only the position is considered, the orientation is left unspecified.

In the sequel, a set of vector fields (defining velocities in the joints configuration manifold) is shown to play a key role when using the pseudo-inverse of the jacobian of the forward kinematics in achieving a periodic movement of all joints while realizing the periodic output task. Using the pseudo-inverse of the jacobian of the forward kinematics is not new. [103] suggested first the use of the pseudo-inverse of the jacobian to solve the redundancy, he also first stated the link between the redundancy property and the output task. [64] extended the pseudo-inverse approach to include self-motions using the null space of the jacobian matrix. Recently, [76] focuses on a recursive algorithm to obtain the inverse kinematic of redundant manipulators for which the joint motions are shown (experimentally) to become periodic after convergence.

[36, 37, 88, 91] developed an integrability condition based on a Lie bracket test which has been shown to be primordial in order to obtain repeatable solution in the joint space when realizing a periodic task at the output. This condition together with simple connectedness hypothesis ensures repeatable joint trajectories when tracking a closed trajectory. However, this reasoning is not constructive. It is more an analytical tool in order to inspect whether or not the vector fields used to parametrize the displacement are involutive (see Theorem 3.3 to recall the link between involutivity and integrability). The way these vector fields are obtained is still unspecified and remain mainly a trial and error process.

As the main contribution in this chapter, a constructive coordination strategy is developed based on differential geometry properties (the proposed method constructs the involutive basis introduced here above). The latter coordination scheme ensures a periodic (repeatable) response of the joints while keeping the initial flexibility brought by the overactuation.

4.1.1 Overactuation VS redundancy

Importance is put on the difference between redundancy and overactuation through the notion of an output manifold. Definitions 4.1,

and 4.2 are new and specific to the work undertaken. They are especially useful for the results derived in Sections 4.3.2 to 4.3.4.

Definition 4.1 (*Output Manifold*) *The smooth manifold \mathcal{S} containing the end-effector trajectories $Y(t)$, is called the output manifold.*

The overactuation property of a manipulator is intimately linked to the end-effector task. This observation motivates the following extension of the redundancy definition, so as to include the output manifold.

Definition 4.2 (*Overactuation*) *A redundant manipulator is said to be overactuated, when its number of internal degrees of freedom $(q_1, \dots, q_n) \in Q, q_i \in \mathbb{R}, i = 1, \dots, 5$, is larger than its end-effector motion capabilities $(x, y, z)^T \subset \mathbb{R}^3$, on a predefined output manifold \mathcal{S} .*

$$\forall Y(t) \in \mathcal{S} \subset \Gamma^3, \exists \text{ at least } q(t) \text{ and } \bar{q}(t), q(t) \neq \bar{q}(t) : \\ Y(t) = \zeta(q(t)) = \zeta(\bar{q}(t))$$

Whenever the robot is redundant, the jacobian matrix J that realizes the map ϕ between the tangent spaces has not full-column rank and therefore can not be exactly inverted. For every trajectory of the end-effector in the working space of the redundant robot, there exists an infinite number of corresponding joint motions. Figure 4.1 illustrates the main symbols and terminology. The output manifold is called \mathcal{S} and embedded in \mathbb{R}^3 . At a given point of \mathcal{S} , the tangent space is labelled $T_s\mathcal{S}$. Here s is a point of \mathcal{S} . The corresponding point in \mathbb{R}^3 is also labelled s and corresponds to $(x, y, z)^T$. The context should clarify which of the two is considered. The configuration manifold is noted Q with the tangent space at the configuration q written T_qQ . $\zeta(\cdot)$ is a submersion for which ϕ is the corresponding surjective map from the tangent space T_qQ to the tangent space $T_{\zeta(q)}\mathcal{S}$, where $\zeta(q) = s$. $T\mathcal{S}$ and TQ are the respective tangent bundles.

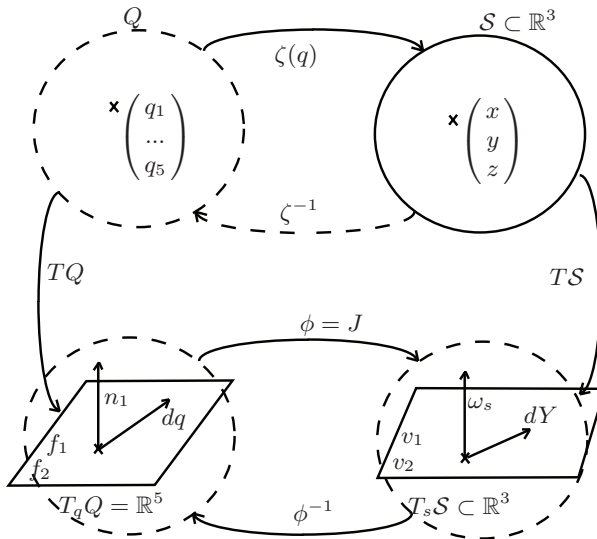


Fig. 4.1. Direct (inverse) kinematic map ζ , (ζ^{-1}) between end-effector position and its corresponding joints configuration. Identically, direct (inverse) kinematic map ϕ , (ϕ^{-1}) between end-effector velocity and its corresponding joints motion.

4.2 Coordination through differential geometry properties

The 3D positioning of a 5R serial-manipulator end-effector is considered (see Section 3.1.1). Achieving a constructive coordination of the constitutive joints in order to fulfill the positioning task is the aim of this chapter.

4.2.1 Overactuation: an infinite set of solutions

The considered manipulator has 5 internal degrees of freedom, since it has 5 independent rotary joints. As we consider the positioning

of the end-effector in the 3D space (orientation is left unspecified), the manipulator is clearly overactuated ($5 - 3 = 2$ degrees of redundancy).

$$\text{Dim}(\Omega) = 2$$

where Ω is the redundant manifold as introduced in Definition 3.3. The configuration manifold Q

$$S^1 \times S^1 \times S^1 \times S^1 \times S^1 = Q$$

where S^1 corresponds to the manifold of a single rotary joint and, thus, Q is compact by definition.

The working manifold, defined by the space in which the end-effector is moving, corresponds to $\mathbb{R} \times \mathbb{R} \times \mathbb{R} = \mathbb{R}^3$. Moreover, the output manifold \mathcal{S} , as introduced in Definition 4.1, is included in the working manifold.

$$\mathcal{S} \subset \mathbb{R}^3$$

Therefore, there exists an infinite number of different configurations corresponding to the same position and/or trajectory in the output manifold.

4.2.2 Differentiation of the solutions

Navigating within the set of acceptable solutions to a fixed end-effector position (or predefined trajectory) within the redundant manifold Ω enables to modify freely the configuration of the manipulator. Thus, flexibility is enhanced by the infinite number of different configurations at our disposal.

However, with the flexibility, *versatility* (see Section 2.3) of the obtained responses to an identical excitation is also enforced. From the infinite different choices at our disposal, the difficulty of determining efficiently the adequate configuration increases a lot. Within all solutions, there is a particular parameterization (2 involutive vector fields, see Definition 3.13) which forces some kind of foliation of the solution space. This foliation is directly linked to the involutivity of

our parameterization and induces repetitive (meaning identical) responses of the joints to a periodic excitation of the end-effector. A repeatable (periodic) motion of the robot in its coordinate frame is highly desirable, while realizing the main task, since the repeatability induces also predictability, [37, 76, 91]. Repeatability means here the possibility of realizing a periodic motion of *all* joints (closed trajectories) while not “blocking” specific joints.

4.2.3 Constructive coordination

The first coordination task means adequate repartition of the displacement through all joints in order to realize a specified trajectory with the end-effector. In other words, see Figure 4.1, the submersion map ϕ^{-1} from the tangent space TS of the output manifold S to the tangent space TQ of the configuration manifold Q is to be defined correctly in order to fulfill the positioning task of the end-effector $Y(t)$.

The second coordination task is defined such that a periodic excitation of the end-effector induces closed joint trajectories. Focus is put on realizing a periodic movement of the end-effector in the output manifold S while trying as best as possible to also achieve periodic movements of all joints in Q .

To meet both objectives, without losing the redundant property (i.e. keeping $n > 3$), is not a trivial matter and need good coordination throughout all joints.

4.2.4 Antagonistic objectives

The incredible flexibility brought by the overactuation of the manipulator (∞ different configurations corresponding to same end-effector output) has a clear counterpart in versatility of joint responses. This versatility means mainly unpredictability of the joint configurations, which is not acceptable for most of the applications.

The latter consideration enforces our design in pushing toward constructive coordination so as to obtain closed joint trajectories for periodic end-effector tasks.

4.3 Coordination to achieve periodicity

In this section, we are concerned with the constructive coordination of a 5R serial manipulator $(q_1, \dots, q_5) \in Q$ such that a periodic positioning end-effector task $Y(t) \in \mathbb{R}^3$ is realized, while periodic joint trajectories are enforced.

4.3.1 Direct Jacobian Inversion

The pseudo-inverse of the jacobian (see Section 3.5.2) of the forward kinematics (see Definition 3.6) $J^+ = (JJ^T)^{-1}J^T$ can be used to express one choice of joints velocity dq associated with a given velocity of the end-effector dY/dt (see Figure 4.2). Recall from Section 3.1.3, that the desired end-effector velocity $\dot{Y} = dY/dt$ is obtained from the time derivative of Equation 3.3.

$$dq/dt = J^+ dY/dt \quad (4.1)$$

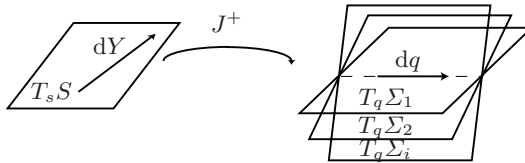


Fig. 4.2. The inverse map based on J^+ selects locally *one* of the existing tangent planes $T_q \Sigma_i$.

Example 4.1 *As an example of this map based on the pseudo-inverse of the jacobian, the results of integrating Equation (4.1) for the 5R3D serial manipulator (introduced in Section 3.1.1) are shown in Figure 4.3. The following parameter were used:*

- *Joints initial conditions:* $q_1(0) = 0.298$, $q_2(0) = 0.165$, $q_3(0) = 0.260$, $q_4(0) = 1.24$, $q_5(0) = 4.37$;
- *Output manifold, sphere:* $R = 1.5$, $c_x = 0$, $c_y = -0.5$, $c_z = 0.2$;
- *Manipulator arms length:* $l_0 = l_1 = l_2 = l_3 = l_4 = 1$, $l_5 = 0.5$;
- *Task parameters:* $\omega = 0.4$, $A = 0.6$, $\phi = \frac{\pi}{2}$, $a = \frac{\pi}{4}$, $b = \frac{\pi}{4}$, $c = 0$.

Realizing the submersion (map from $T_s\mathcal{S}$ to $T_q\Sigma$) with the pseudo-inverse of the jacobian matrix J^+ as proposed herein presents one clear advantage (see Section 3.5.2): the local norm of the joint velocities ($\|\dot{q}_1, \dot{q}_2, \dots, \dot{q}_n\|$) is minimized in order to realize the desired displacement of the end-effector $\dot{Y}(t)$ (see Theorem 3.2).

Even though the robot performs perfectly the first coordination task (see Figure 4.3(a)), the displacement along the Lissajou curve induces a completely chaotic and unpredictable motion in the joint space (see Figure 4.3(b)).

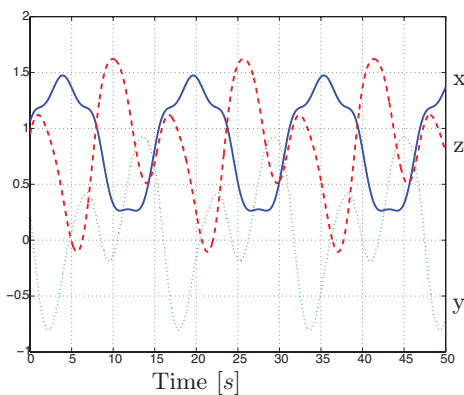
The choice of joints velocity is fortunately not unique for a prescribed motion of the end effector (thanks to redundancy). The next section explores another possibility which takes advantage of the distinction between overactuation and redundancy (that is, by explicitly using the defining equations of the output manifold).

4.3.2 Improving the Periodicity

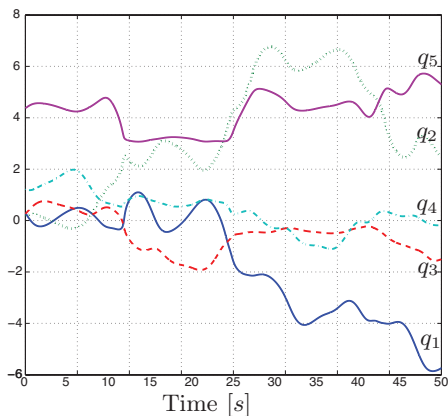
In order to improve the periodicity of joint movements, I propose to use the structure of the output manifold (see Definition 4.1) for constructing the displacement vector dY/dt .

Consider the exact 1-form ω_1 (see Definition 3.12) associated with the spherical output manifold \mathcal{S} through the gradient of its equation $h(x, y, z) = (x - c_x)^2 + (y - c_y)^2 + (z - c_z)^2 - R^2$, that is

$$\begin{aligned}\omega_1 &= dh \\ &= 2(x - c_x)dx + 2(y - c_y)dy + 2(z - c_z)dz.\end{aligned}$$



(a) Output evolution through time: the periodic Lissajou is perfectly realized.



(b) Joints evolution through time.

Fig. 4.3. Direct pseudo-inversion of the velocity vector leads to an erratic unpredictable behavior of the joints, even if the Lissajou periodic task is perfectly realized (reference and real positions are perfectly superimposed).

Proposition 4.1 *Except for the points on the equatorial line $(y - c_y)^2 + (z - c_z)^2 = R^2$ and $x = c_x$, the vector fields*

$$v_1 = \begin{pmatrix} -(z - c_z) \\ 0 \\ (x - c_x) \end{pmatrix}, \quad v_2 = \begin{pmatrix} -(y - c_y) \\ (x - c_x) \\ 0 \end{pmatrix}$$

(i) span a two dimensional subspace and (ii) are involutive. Therefore except on this line, they locally define an integrable distribution.

Proof: The only way for $v_1(s)$ and $v_2(s)$ (with $s = (x \ y \ z)^T$) not to span a two dimensional subspace is that $x = c_x$. Using the defining equation for \mathcal{S} gives $(y - c_y)^2 + (z - c_z)^2 = R^2$ which gives an equatorial line. By construction $\langle \omega_1; v_1 \rangle = 0$ and $\langle \omega_1; v_2 \rangle = 0$ (see Definition 3.12). Because $d\omega_1 = 0$ by exactness, Formula (1.25) of [77] yields

$$\begin{aligned} 0 &= \langle d\omega_1; v_1, v_2 \rangle \\ &= v_2 \langle \omega_1; v_1 \rangle - v_1 \langle \omega_1; v_2 \rangle - \langle \omega_1; [v_1, v_2] \rangle \\ &= - \langle \omega_1; [v_1, v_2] \rangle . \end{aligned}$$

so that the bracket $[v_1, v_2]$, being annihilated by the same 1-form ω_1 as for v_1 and v_2 , belongs to the span of v_1 and v_2 , which means that v_1 and v_2 are involutive vector fields whose distribution is locally integrable. ■

Remark 4.1 *The Euler characteristic of \mathcal{S} is an obstruction in finding global expressions for v_1 and v_2 (see [27]). The best one can obtain are smooth vector fields that only vanish at a single point (instead of the whole equatorial line).*

As long as the above singular points can be avoided, which is the case for the chosen output task, the end-effector motion dY/dt , defined by the time derivative of equation (3.3), is then expressed in this involutive basis using the two scalars α and β .

$$\frac{dY}{dt} = \alpha v_1 + \beta v_2 \quad (4.2)$$

Finally, the joint motions are obtained through the local inverse map from $T_s\mathcal{S}$ to $T_q\mathcal{Q}$ based on the pseudo-inverse of the jacobian matrix J^+ (Figure 4.1). With $f_1 = J^+v_1$ and $f_2 = J^+v_2$ the joints velocity becomes

$$\frac{dq}{dt} = \alpha f_1 + \beta f_2 \quad (4.3)$$

Example 4.2 *A simulation, using Equations 4.2 and 4.3 with the 5R3D serial manipulator realizing a Lissajou curve on the sphere \mathcal{S} is undertaken (see Figure 4.4). The same simulation parameters as those introduced in Example 4.1 are used.*

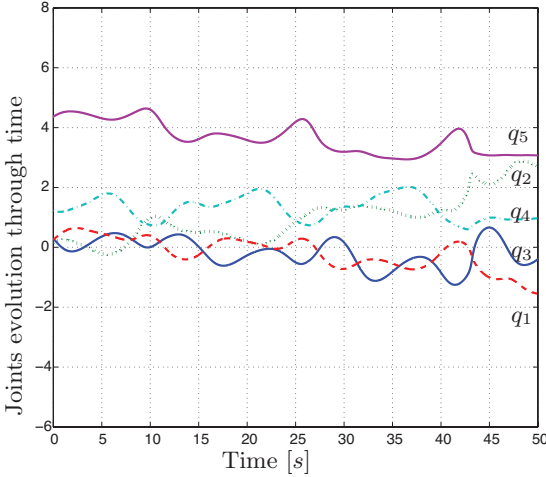


Fig. 4.4. An involutive basis of the output manifold helps in reducing the unpredictable behavior. (Since the Lissajou task is perfectly realized, as in Figure 4.3(a), it is not shown again here.)

The displayed trajectories still fail to be periodic. The results are nevertheless better than those obtained using the first method, since the resulting trajectories are closer to periodicity than with the direct Jacobian inversion of the tangent vector of the Lissajou curve (that is, introducing an involutive basis of the tangent bundle TS helps in reducing the erratic and unpredictable characteristics of the motion in the joint space).

However, since exact joints periodicity is not achieved yet, the next section aims at developing a sufficient condition ensuring its full realization.

4.3.3 A Sufficient Condition for Joints Periodicity

In the proof of the following theorem, the Poincaré-Bendixon theorem (see Theorem 3.4) is used to derive a sufficient condition for periodicity.

Theorem 4.1 *Let f_1 and f_2 be two involutive vector fields such that $f_1(q)$ and $f_2(q)$ belong to T_qQ for all q . Moreover, assume that for all q , $v_1 = J(q)f_1(q)$ and $v_2 = J(q)f_2(q)$ are independent vectors in $T_{\zeta(q)}S$. Now, if the following two conditions hold, namely:*

- *The integral manifold of f_1 and f_2 is simply connected and compact.*
- *The end-effector movement $Y(t)$ is periodic.*

then the joints motion obtained after decomposing (4.2) and integrating (4.3) is also periodic or converges to a limit cycle.

Proof: Because by hypothesis (f_1 and f_2 are involutive), the integral manifold of f_1 and f_2 exists. Therefore, $q(t)$ is confined to a 2-dimensional submanifold of Q . Because this submanifold is also assumed to be simply connected, the hypotheses of Poincaré-Bendixon theorem (Theorem 3.4) are satisfied. The result then follows after noticing that, by hypothesis (the end-effector trajectory is periodic and f_1 and f_2 are in correspondence with v_1 and v_2), convergence

to an equilibrium point is excluded. Moreover, divergence of $q(t)$ to infinity as $t \rightarrow \infty$ is prohibited since the manifold is assumed to be compact (i.e. closed and bounded). ■

In Section 4.3.2, although the basis of the tangent bundle TS is ensured by involutive vector fields v_1 and v_2 , the vector fields f_1 and f_2 could very well not be involutive. It is known that, whenever $z = \phi(x)$ is a diffeomorphism, then the bracket commutes with the push forward:

$$\left[\frac{\partial \phi}{\partial x} v_1 \circ \phi^{-1}(z), \frac{\partial \phi}{\partial x} v_2 \circ \phi^{-1}(z) \right] = \frac{\partial \phi}{\partial x} [v_1, v_2] \circ \phi^{-1}(z)$$

However, when ϕ is a submersion, as it is the case here (the jacobian is a surjective map; it has a non trivial kernel), then the Lie-bracket does not necessarily commute with the pseudo-inverse.

Lemma 4.1 *Whenever ϕ is a submersion, then $\phi^+[v_1, v_2]$ is not necessarily equal to $[\phi^+v_1, \phi^+v_2]$.*

Proof: If both expressions in the lemma were equal then the involutivity of v_1 and v_2 would imply the one of ϕ^+v_1 and ϕ^+v_2 (by linearity of the pseudo-inverse). However, this is not necessarily the case as the following example testifies. Consider the submersion $\phi : q \rightarrow x$ from \mathbb{R}^3 to \mathbb{R}^2 defined by $x_1 = q_1$ and $x_2 = q_2 + q_1q_3$. Let $v_1 = (1 \ 0)^T$ and $v_2 = (0 \ 1)^T$ define two trivially involutive vector fields. Now, $f_1 = \phi^+v_1 = (1 + q_3^2 \ q_3 \ q_1q_3)^T$ and $f_2 = \phi^+v_2 = (q_3(2 + q_1^2 + q_3^2) \ 1 + q_1^2 + q_3^2 \ q_1(1 + q_1^2 + q_3^2))^T$ are not involutive since

$$\det[f_1, f_2, [f_1, f_2]] = -(1 + q_1^2)^2 \neq 0.$$

■

The Example 4.3 illustrates the loss of involutivity through the pseudo-inverse of the jacobian map (see Lemma 4.1) with a planar 3R2D manipulator.

Example 4.3 Consider the 3R serial-planar manipulator defined in Figure 4.5 with equally-lengthed arms ($l = 1$). The output end-effector position is considered.

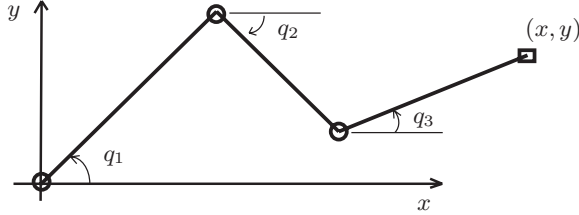


Fig. 4.5. 3R serial-planar manipulator with absolute angular joints q_1 , q_2 and q_3 .

$$x = \cos(q_1) + \cos(q_2) + \cos(q_3) \quad (4.4)$$

$$y = \sin(q_1) + \sin(q_2) + \sin(q_3) \quad (4.5)$$

The associated jacobian matrix is obtained through partial differentiation of the equations 4.4 and 4.5.

$$J = \begin{pmatrix} -\sin(q_1) & -\sin(q_2) & -\sin(q_3) \\ \cos(q_1) & \cos(q_2) & \cos(q_3) \end{pmatrix}$$

Consider the two trivially-involutive vector fields $v_1 = (1, 0)^T$ and $v_2 = (0, 1)^T$, spanning the entire plane (x, y) . Their image $f_1 = J^+v_1$ and $f_2 = J^+v_2$ through the pseudo-inverse of the jacobian $J^+ = J^T(JJ^T)^{-1}$ map does not form an involutive basis of the configuration space, (the determinant of the matrix $\{f_1, f_2, [f_1 f_2]\}$ is not null).

$$f_1 = \begin{pmatrix} 2 \sin(q_1) + \sin(q_1 - 2q_2) + \sin(q_1 - 2q_3) \\ -\sin(2q_1 - q_2) + 2 \sin(q_2) + \sin(q_2 - 2q_3) \\ \sin(2q_1 - q_3) + \sin(2q_2 - q_3) - 2 \sin(q_3) \end{pmatrix} \cdot 1/\alpha \quad (4.6)$$

$$f_2 = \begin{pmatrix} -2 \cos(q_1) + \cos(q_1 - 2q_2) + \cos(q_1 - 2q_3) \\ \cos(2q_1 - q_2) - 2 \cos(q_2) + \cos(q_2 - 2q_3) \\ \cos(2q_1 - q_3) + \cos(2q_2 - q_3) - 2 \cos(q_3) \end{pmatrix} \cdot 1/\alpha \quad (4.7)$$

$$\alpha = (-3 + \cos(2q_1 - 2q_2) + \cos(2q_1 - 2q_3) + \cos(2q_2 - 2q_3)) \\ \text{Det} \{f_1, f_2, [f_1 \ f_2]\} \neq 0 \quad (4.8)$$

Because the trajectories displayed in Figure 4.4 are not periodic in the joint space q , the vector fields f_1 and f_2 are either: (i) not involutive or (ii) involutive and the underlying submanifold Σ is not simply connected (Theorem 4.1) or (iii) involutive and the underlying submanifold Σ is not compact (Theorem 4.1) or (iv) the convergence of the joint trajectories to their periodicities is not completed yet, in the sense that the integration time considered is too short.

Notice that this is not a numerical inaccuracy in computing the pseudo-inverse as one might initially suspect, but it is an inherent limitation of pulling back the involutive vector fields v_1 and v_2 along a submersion.

Now, based on the sufficient condition I developed in Theorem 4.1, an involutive basis of the tangent bundle TQ for the 5R3D manipulator is built in the next section. The aim is to finally enforce periodic joint responses whenever the excitation (end-effector positioning task to be realized) is periodic.

4.3.4 Involutive basis of the 5D tangent bundle TQ

Because a submersion has a kernel, there exist many different f_1 and f_2 that map to a basis of \mathcal{S} in the working space, most of which are not involutive. By preventing the usage of certain directions of the kernel while constructing f_1 and f_2 , involutivity is guaranteed. The following theorem constructs first f_1 and f_2 in this way, before computing v_1 and v_2 .

Theorem 4.2

1. Define $\omega_x = dx$, $\omega_y = dy$, $\omega_z = dz$ where x , y , z are the end-effector positions.
2. Let ω_4 and ω_5 be complementary integrable 1-forms in the sense that ω_x , ω_y , ω_z , ω_4 , and ω_5 span the cotangent bundle T^*Q .
3. Define f_1 , f_2 as the dual vector fields to the three 1-forms ω_1 , ω_4 , and ω_5 , that is,

$$\begin{pmatrix} \omega_1 \\ \omega_4 \\ \omega_5 \end{pmatrix} (f_1 \ f_2) = 0,$$

where ω_1 is the 1-form associated with the output manifold \mathcal{S} .

Under these assumptions, f_1 and f_2 are involutive and $v_1 = \frac{\partial \zeta}{\partial q} f_1 \circ \zeta^{-1}(x)$ and $v_2 = \frac{\partial \zeta}{\partial q} f_2 \circ \zeta^{-1}(x)$ constitute a basis for TS .

Proof: First notice that ω_1 , ω_4 , and ω_5 are always independent since ω_1 is a linear combination of ω_x , ω_y , and ω_z , which are, in turn, independent from ω_4 and ω_5 (by construction). This means that f_1 and f_2 are well defined (no rank loss in the defining 1-forms). Involutivity follows by construction since ω_1 is exact and ω_4 and ω_5 are integrable. The only subtle point is that v_1 and v_2 do never cancel and span TS . On this purpose, notice that f_1 and f_2 cannot be mapped to a zero vector through $\frac{\partial \zeta}{\partial q}$, for if this was the case (say $\zeta \phi q f_1 = 0$), then this would mean that

$$\begin{pmatrix} \omega_x \\ \omega_y \\ \omega_z \end{pmatrix} f_1 = 0.$$

Noticing that $\omega_4 f_1 = 0$ and $\omega_5 f_1 = 0$ as well, together with the fact that ω_x , ω_y , ω_z , ω_4 , and ω_5 are independent would lead to $f_1 = 0$, which is a contradiction. ■

Remark 4.2 *Finding the two integrable complementary 1-forms ω_4 and ω_5 can either be done by inspection or in a more systematic way using Cartan's equivalence method (see [77]) which generalizes the canonical form of Darboux to more than a single 1-form. This gives all possible choices of ω_4 and ω_5 . This step does not require the knowledge of the output manifold \mathcal{S} , but depends only on the type of redundant robot used through the specific Lie group structure of the robot.*

Lemma 4.2 *The induced hyper-surface Σ can be modified through the redundant basis $R_i \in T\Omega \subset \mathbb{R}^n$ to keep the flexibility of the redundant manipulator.*

Proof: To prove this, it is sufficient to demonstrate that all non-null redundant vector fields $R \in T\Omega$ do not belong to $T\Sigma$. By this way, R forces the manipulator to quit the present hyper-surface Σ , relaxing the complementary constraints. Without loss of generality, we will restrict the proof to the case with $n = 5$ joints.

$$R \in T\Omega^5 : \begin{pmatrix} \omega_x \\ \omega_y \\ \omega_z \end{pmatrix} \cdot R = 0 \quad (4.9)$$

$$R \in T\Sigma^5 : \begin{pmatrix} \omega_1 \\ \omega_4 \\ \omega_5 \end{pmatrix} \cdot R = 0 \quad (4.10)$$

Since $\omega_x, \omega_y, \omega_z, \omega_4, \omega_5$ are independent by construction and ω_1 is a linear combination of the three first 1-forms, the only possible vector in \mathbb{R}^5 satisfying the two equations (4.9 and 4.10) (representing six constraints) simultaneously is $R = 0$. ■

With Lemma 4.2, the manipulator has been shown not to be constrained in a unique periodic solution. Through the redundant basis R_i , the latter solution can be modified freely, ensuring the initial flexibility of the manipulator.

The following example applies Theorem 4.2 to the 5R3D manipulator in order to enforce a periodic joints response.

Example 4.4 Consider the 5R serial-link manipulator and a spheric output manifold \mathcal{S} , 2 arbitrary additional (complementary) 1-forms ω_4 and ω_5 are added to the initial 1-form ω_1 representing the sphere \mathcal{S} .

$$\begin{aligned} h &: (x(q) - c_x)^2 + (y(q) - c_y)^2 + (z(q) - c_z)^2 = R^2 \\ \omega_1 &= \nabla_q h \\ \omega_4 &= [1 \ 0 \ 0 \ 0 \ 1] \\ \omega_5 &= [0 \ 1 \ 0 \ 1 \ 0] \end{aligned}$$

Based on these 1-forms, Theorem 4.2 gives the 5-dimensional involutive basis $\{f_1, f_2\}$ of the tangent bundle $T\Sigma^n$. Using the direct map ϕ based on the well-defined jacobian J , the local image of the hyper-surface $T\Sigma = \text{span}\{f_1, f_2\} \subset \mathbb{R}^n$ into \mathbb{R}^3 is built, see Figure 4.1.

$$v_1 = Jf_1 \quad v_2 = Jf_2$$

The joint trajectories of the 5R serial manipulator realizing a Lissajou curve on the sphere \mathcal{S} , using the same simulation parameters as in Example 4.1, are illustrated in Figure 4.6.

The constant complementary 1-forms ω_4 and ω_5 , introduced via Theorem 4.2, limit the possible configurations of the manipulator. They define a foliation of the hyper-surface Σ , on which the system remains, ensuring a periodic joints response.

This last example illustrates that the integration, using a combination of 1-forms, enforces involutivity: the robot joint motions are completely predictable (periodic) and remain in a reduced hyper-plane (foliation) of the configuration space. The manipulator joint configurations are constrained and periodic, while realizing perfectly the Lissajou main task. See Appendix E for a link to an illustrative movie.

Constructive coordination of the joints is achieved so as to fulfill both objectives defined in Section 4.2.3. The periodic task of the end-effector is perfectly realized while closed joint trajectories are enforced.

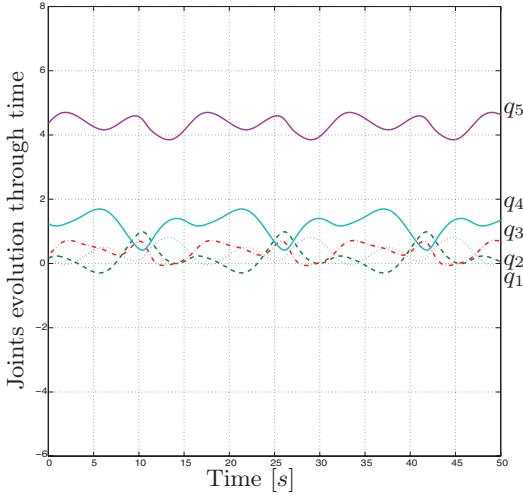


Fig. 4.6. Periodic motion of the joints. The vector fields f_1 and f_2 are involutive. (Since the Lissajou task is perfectly realized, as in Figure 4.3(a), it is not shown again here.)

Future research should address the particular construction of this simply connected integral manifold for redundant robots, and especially the choice of ω_4 and ω_5 so as to guarantee both simple connectedness (using for instance de Rham cohomology (see [27])) and compactity (using Riemannian geometry) of the integral manifold of f_1 and f_2 . In this context, an interesting research-guess could use Lie Groups and Lie Algebra as in [72, 87].

Remark 4.3 *A particular constructive method to obtain the complementary 1-form for a 3R2D serial manipulator, enforcing compliance and flexibility, is detailed in Section 5.5.*

In this section, I developed a particular parameterization of the solution space through the use of an involutive basis of vector fields (see Theorem 4.2). This basis, built from the constructive combina-

tion of 1-forms, ensures a periodic response of the joints (see Figure 4.6) to a periodic positioning task: constructive coordination (see Section 4.2.3) is achieved.

4.3.5 Convergence to a limit cycle

Remark 4.4 *Long-term integration of the pseudo-inverse pulled-up velocity (as proposed in Section 4.3.1, Equation 4.1), over several periods of the end-effector task, tend to be periodic (for the 5R3D manipulator), see Figure 4.7. But the obtained joints period is a high multiple of the task period and thus is not reducing the unpredictability of the manipulator.*

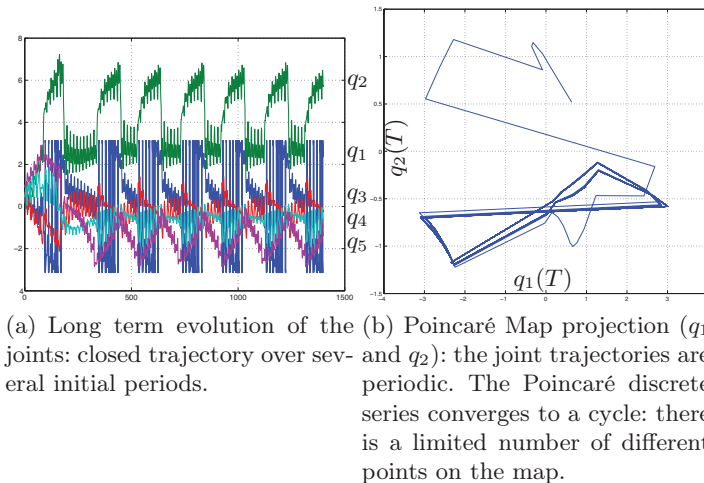


Fig. 4.7. A long term integration, over several period of the main task, shows that the joints trajectory is finally closed but over a very high multiple of the initial period. This kind of periodicity is certainly not increasing the predictability of the manipulator.

Remark 4.4 tends to illustrate the complexity of the underlying problematic. On one hand, in order to ensure the periodicity of the joints, we enforced some kind of foliation of the solution-space (integral manifold Σ) using the involutivity property of our vector fields parameterization (see Section 4.3.4). This foliation (which is clearly a limitation of the whole solution space) was demonstrated to be closely related to the joints periodicity (see Theorem 4.1). Moreover the obtained periodicity is directly of the same order than the end-effector task.

On the second hand, the pseudo-inverse of the jacobian, which does not ensure the existence of any integral manifold, tends also to a periodic solution for some tasks and manipulators, even if this periodicity is several order of magnitude larger than the end-effector excitation (see Figure 4.7).

Conjecture 4.1 *When considering the pseudo-inverse pulled-up velocity $dq = J^+dY$, together with a manipulator made of serially-connected rotary joints, the dimension of the redundant manifold $\delta = \text{Dim}(\Omega)$ (i.e. the number of supplementary actuators with respect to a given task) is closely linked to the convergence to a limit cycle of the joints for a closed-trajectory of the end-effector.*

- *If δ is larger than 2: the joints trajectory is neither periodic, nor converges to a limit cycle.*
- *If $\delta = 1$ or 2 : the joints trajectory converges to a periodic limit cycle (faster for $\delta = 1$).*
- *If $\delta = 0$: the system is not redundant and thus a single (eventually periodic) solution exists.*

Some elements of proof are pointed out hereafter. In some way, the redundant manifold Ω (which contains all possible self-motions of the manipulator generated by the realization of the main periodic task) is linked to the task. At every point of the end-effector task, a manifold Ω_q exists and represents all possible configuration which are accessible from the given output position (see Definition 3.3). The degree of redundancy δ defines the dimension of this local (linked to

a fixed end-effector position) manifold Ω_q as well as the dimension of Ω , the redundancy manifold corresponding to the collection of all local manifolds Ω_q .

If the dimension δ is null, the system is fully-actuated and the joint responses are directly periodic. If $\delta = 1$, the redundant manifold is homomorphic to a closed-interval of the real line or to a circle: $I \subset \mathbb{R}^1$ or S^1 . And if $\delta = 2$, the redundant manifold is homomorphic to a limited plane, a sphere or a torus: $I^2 \subset \mathbb{R}^2$ or S^2 . Thus, because the redundancy manifold Ω is compact over the full periodic task, any induced self-motion (by the realization of the main task) is enclosed in it. Moreover, if Ω is simply connected, all hypothesis of Bendixon-Poincaré Theorem (3.4) are satisfied, ensuring a convergence either to an equilibrium point, or to a limit cycle (compactness excludes divergences) of any induced self-motion. If $\delta > 2$, any induced self-motion is living in an, at least, 3D space: no convergence is guaranteed.

If the induced self-motion of the manipulator (caused by the execution of the main periodic task) is converging to a fixed-point on Ω , the overall joints motion converges to a periodic cycle.

If the induced self-motion of the manipulator is converging to a limit cycle on Ω , it is reasonable to think that its period is a multiple of the end-effector period. If this hypothesis is true, the overall joints motion converges also to a periodic cycle.

Remark 4.5 *The simply-connected hypothesis of the underlying integral manifold is only specified in order to exclude the trajectories with irrational period-ratio (see Figure 4.8). As long as this singular case is not appearing, this hypothesis can be relaxed.*

4.4 Conclusion

The following original contributions have been detailed in this chapter. First, the definition of the output manifold enabled the extension of the pure redundancy concept to overactuation (Definitions

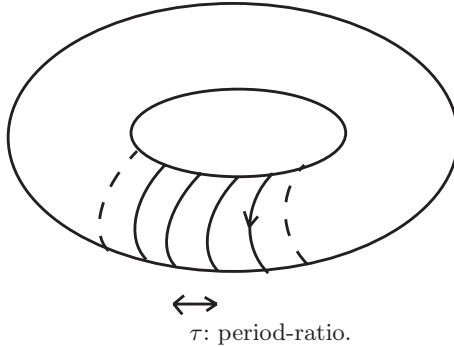


Fig. 4.8. Self-motion trajectory on the redundant manifold Ω . τ represent the period-ratio on this manifold homeomorphic to a torus ($S^1 \times S^1$).

4.1 and 4.2). Second, constructive coordination through differential geometry properties using the 1-form formalism enabled adequate repartition of the joint trajectories in order to obtain a repeatable response to a periodic excitation. In particular, a sufficient condition for joints periodicity has been established (Theorem 4.1) and a clear method, using the 1-form formalism, ensured the involutivity of the vector fields parameterization of the solution space (Theorem 4.2). The proposed constructive coordination, which enforced a foliation of the configuration space, ensured repeatable joint responses (see Figure 4.6 of Example 4.4).

In the forthcoming chapter (Chapter 5), the stringent mathematical constraint (through the complementary 1-forms) ensuring a rigorously periodic response of the joints is partly released. Still in the scope of solving the inverse kinematic problem (see Definition 3.7) as for Chapter 4, a smoother method using the gradient of potential functions is proposed. I will demonstrate that the latter method enforces a convergence of the joints trajectory to a limit cycle instead of being immediately periodic. Moreover, the coordination-scheme based on potential functions will enable the flexible tracking of multiple objectives.

Potential functions for coordination

In this chapter, coordination of an overactuated manipulator is understood as an appropriate repartition of the end-effector position reference through all joints (open-loop control). Constructive coordination is obtained whenever hierarchized multi-tasking is achieved. Furthermore, repeatability issues (as defined in the preceding chapter) are examined under this scope. Finally, a particular solution using the Hessian matrix of the main task is examined.

Overactuation implies the existence of supplementary degrees of freedom with respect to the main task to be realized. These supplementary degrees of freedom give some free room either for an optimization of the task, or directly for multi-tasking, when solving the inverse kinematic problem (see Definition 3.7). The flexibility brought by the overactuation is to be used efficiently in order to justify its corresponding complexity and higher costs. In this sense, the tracking of multiple simultaneous objectives are clearly enabled by the overactuation. One solution to the coordination of this multi-tasking scheme is obtained through the use of potential functions.

5.1 Introduction

Recall the example of the human-body multi-tasking scheme illustrated in Figure 1.1. One of the solution to enable coupled multi-tasking is the use of potential functions in order to dispatch the

different goals over different potential functions (see [51, 52, 89, 90]). Each objective is linked to a potential function with its global maximum (or minimum) at the place where the task is to be achieved. The task achievement becomes thus equivalent to a dynamic extrema research.

As presented in the preceding chapter, repeatability, meaning closed-trajectories of the joints for periodic tasks, is always desirable in the sense that predictability is an advantage. The latter is examined under the scope of potential functions and multi-tasking. However, the predictability objective should not prevent the flexibility brought by overactuation.

In this chapter, the application of potential functions to the multi-tasking scheme of overactuated manipulator is considered. Some considerations about closed-joint-trajectory responses to a periodic excitation and hierarchical secondary objectives are made. Moreover, a particular solution to the inverse kinematic problem using the Hessian matrix of the task is examined.

When not specified differently, we will consider a planar (2D) 3R manipulator (with equally length arms $l_1 = l_2 = l_3 = 1$), similar to the one depicted in Figure 3.2, tracking a circular trajectory $h(q(t))$ with its end-effector.

$$h(q) = (y_1(q) - c_1)^2 + (y_2(q) - c_2)^2 - R^2 \quad (5.1)$$

This manipulator will be labelled *3R2D manipulator* in order to emphasize its structure made of three rotary joints and to emphasize its two-dimensional working space.

5.1.1 Task manifold

The concept of *task manifold* is introduced hereafter in order to differentiate it from the output manifold defined in the preceding chapter (Definition 4.1).

Definition 5.1 (*Task manifold*) Consider a manipulator configuration manifold Q together with its coordinate frame q_1, \dots, q_n (the manipulator joint angles). The submanifold $\mathcal{Y} \subset Q$ which contains the

predefined positioning task $h(q)$ (Equation 5.1) and all self-motion paths (Definition 3.3) of the manipulator is called task manifold.

Remark 5.1 *The task manifold \mathcal{Y} contains the collection of all fibers $\mathfrak{S}_k(q)$ of the redundant space Ω associated to the main task trajectory $h(q)$ (see Equation 5.1).*

The task manifold \mathcal{Y} describes all possible responses of a manipulator to a periodic task $h(q)$. As long as the joint trajectories belong to this manifold, the manipulator is always compatible with its main positioning task: either the motion of its end-effector is along the reference trajectory or it is fixed and the elbow moves in the redundant space.

An example of a task manifold \mathcal{Y} for a 3R2D manipulator realizing a circular task h (Equation 5.1) is illustrated in Figure 5.1.

5.2 Coordination through potential functions

5.2.1 Overactuation: an infinite set of solutions

The 3R compact configuration manifold \mathcal{Y} (task manifold) corresponding to the realization of a circle on a 2D plane is homeomorphic (see Definition 3.10) to the torus $S^1 \times S^1$ (see Figure 5.1). The shape of the torus and the existence or not of the hole depends on the task h (Equation 5.1) to be realized. For example, the positioning of the task c_x and c_y is one of the elements influencing the shape of the manifold. Roughly speaking, the fact that two different configurations can be joined by two different self-motions through rotations of the elbow (not straightly) suggests the existence of a hole in the task manifold.

The task manifold \mathcal{Y} considered is compact and continuous by construction. Its continuity implies the existence of an infinite set of different solutions corresponding to the same end-effector position. In Figure 5.1, all trajectories in blue correspond to self-motions of

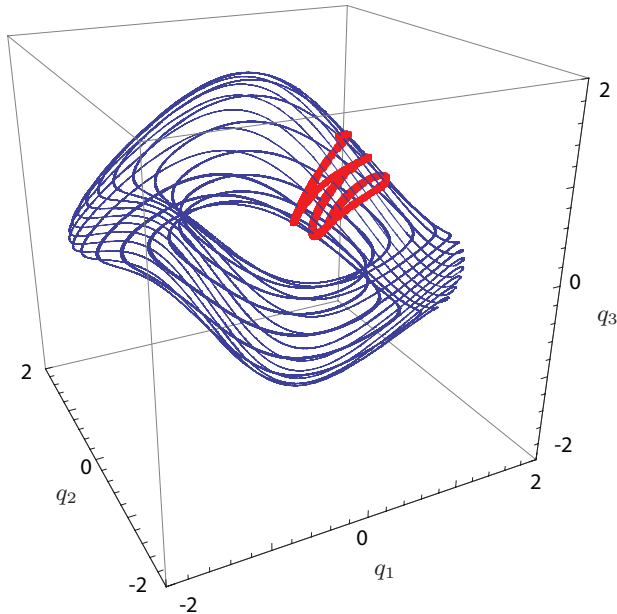


Fig. 5.1. Task manifold \mathcal{T} of the 3R2D manipulator tracking a circle as main task: a torus $S^1 \times S^1$ (task manifold). In blue, the purely redundant self-motions and, in red, one choice of realization of the task through the pseudo-inverse of the jacobian (two and a half period of it).

the manipulator and thus, correspond to the same end-effector position. This illustrates clearly the infinite dimension of the solution space.

5.2.2 Differentiation of the solutions

Navigating within the redundant manifold of the manipulator enables to modify freely its configuration. The flexibility brought by the overactuation enables the tracking of multiple objectives as long

as the secondary objectives do not interact with the main task. Thus, the tracking of a second objective (or several) in the redundant manifold, simultaneously to the realization of the primary task enable multiple task realization. Moreover, the enforcement of a prioritized hierarchy of all tasks establishes a clear differentiation between the solutions through the level of priority linked to each task.

Furthermore, within all potential solution to a periodic positioning task of the end-effector, repeatable joint motions are highly desirable in the sense that it enforces the predictability of the manipulator.

Finally, the set of solutions of the manipulator to a predefined task (task manifold), represented in Figure 5.1 for a particular choice of parameters, through its asymmetric shape, does illustrate clearly the inequivalences between the potential solutions. As an example, the closed-trajectory realizing the main task successfully along the shortest joint path is interesting. With respect to Figure 5.1, the shortest closed-transversal-trajectory (in red) to the torus would correspond to this choice.

5.2.3 Constructive coordination

Constructive coordination in this context means successful realization of the different tasks and convergence to a limit cycle of the joints trajectory for repeatability. The main task corresponds to the periodic positioning of the end-effector. The secondary tasks are defined as gradient of potential functions projected onto the tangent of the manipulator redundant-manifold. A prioritized hierarchy of the task and subtasks is to be established in order to enforce their decoupling.

Predictability of the joint motions is obtained through periodic joint trajectories whenever the end-effector task is closed. Constraints on the potential function scheme in order to ensure the convergence of the joints trajectory to a predictable limit-cycle will be stated.

Finally, a constructive solution minimizing the joint displacements along the whole task could be particularly interesting. This solution

corresponds to the shortest closed integral-curve on the task manifold realizing the positioning task.

5.2.4 Antagonistic objectives

The first clear antagonism concerns the multiple-task scheme which clearly differ from a unique task realization. Moreover, antagonism between the simultaneous objectives is obvious in the sense that they are tracked at the same time. Finally, algorithmic singularities (induced by the particular algorithmic solution to the inverse kinematic problem) and manipulator-configuration singularities (accessibility limitations or rank loss in the jacobian matrix) are antagonist (meaning different) because, even if they both induce the trajectory planning algorithm to fail, they have different causes.

The solution to the inverse kinematic problem I propose in the next section (Section 5.3.3) overcomes the algorithmic singularities.

5.3 Soft extension of the jacobian

In the aim of coordinating multiple-tasks together through the use of potential functions, the null-space of the jacobian matrix (see Definition 3.8) plays a key role. In this sense, rigid (Section 5.3.2) and soft extension of the jacobian (Section 5.3.3) are introduced hereafter.

5.3.1 Null space of the jacobian

The null space N of a matrix J (which is row deficient) is defined as the set of all vectors \dot{x} that are orthogonal to the matrix.

$$\begin{aligned} J\dot{x} &= 0 \\ NN^T\dot{x} &= (I - J^+J)\dot{x} \end{aligned} \tag{5.2}$$

where $J^+ = J^T(JJ^T)^{-1}$ is the pseudo-inverse of the matrix and $(I - J^+J)$ the projection-operator of the vector \dot{x} into the null space of J .

When considering a manipulator with jacobian J together with its main positioning task \dot{x} , the null space of the jacobian $N = \{\dot{x} | J\dot{x} = 0\}$ represents the orthogonal space to the tangent of the manipulator workspace. Therefore a state's change along one of the null space's directions has no influence on the end-effector position. In other words, we do influence the robot configuration (the elbows are moving), but the end-effector position is fixed.

Any displacement exclusively along the null space of the jacobian is thus a *self-motion*, as defined in Definition 3.3 and has no impact on the main task (end-effector positioning). Considering Figure 5.1, displacement along the null space directions corresponds to the blue trajectories, while the realization of the circular positioning task is along its perpendicular direction (red).

Therefore, as introduced by [67], one general solution to the inverse kinematic problem for redundant manipulators can be described by

$$\dot{q} = J^+\dot{x} + (I - J^+J)\phi \quad (5.3)$$

where \dot{x} is the velocity reference corresponding to the positioning task, ϕ is an arbitrary secondary differential relation projected into the null space of the jacobian.

5.3.2 Rigid extension of jacobian

Considering the inverse kinematic problem and the repeatability problem already raised in the preceding chapter, Bailleul [8, 9] proposed to extend the jacobian matrix J in order to build a full row-rank matrix, which is thus invertible by construction (see Definition 5.2). The extended jacobian thus includes secondary differential relations G which are satisfied by the manipulator, simultaneously to the real positioning task.

Definition 5.2 (*Rigid extended jacobian*) Originally introduced by [8, 9]. Consider the jacobian $J(q)$ of an overactuated manipulator, which is not full row-rank. The extended jacobian is a construction made from the initial jacobian to which we append one or more additional differential relations $G(q)$, independent of the rows of $J(q)$.

$$J_{ext}(q) = \begin{bmatrix} J(q) \\ G(q) \end{bmatrix} \quad (5.4)$$

The extended jacobian $J_{ext}(q)$ is thus full rank by construction and its inverse does exist and is unique. This solution will be labelled extended jacobian in this thesis. It fixes rigidly and a priori the extension of the jacobian.

Through the extended jacobian method, as long as the row-independence between G and J is maintained over the entire trajectory, the inverse kinematic problem is entirely defined and has a unique solution corresponding to J_{ext}^{-1} .

$$dq = J_{ext}^{-1} \begin{bmatrix} dx \\ 0 \end{bmatrix}$$

Since the inverse solution is unique, the response to a closed-trajectory excitation (the end-effector realizes a periodic task) is also periodic with the same period than the task. This solution enhances predictability through a unique solution to the inverse kinematic problem.

The rigid extension imposes an arbitrary relation $G(q)$ between joints in order to obtain a square jacobian matrix to inverse. However, it is not explained how to guarantee the row-independence of $G(q)$ with respect to $J(q)$ over the full trajectory path in the joint space. Along this path, the differential relation $G(q)$ could become linearly dependent to the initial jacobian $J(q)$ and thus the inversion of the matrix J_{ext}^{-1} would not exist anymore (algorithmic singularity). The obtention of G is more like a trial and error process along a realization of the task. If one period is fully accomplished without algorithmic singularities, then the solution is validated.

Finally, this solution fixes a priori completely the manipulator responses to any excitation: no free space is let to flexibility. A fixed, unique solution and configuration corresponds to the initial excitation (see [8, 9, 68]).

5.3.3 Soft extension of the jacobian

In order to release the rigidity of the extended jacobian solution introduced in Section 5.3.2 and retain the initial flexibility of overactuated manipulator, a softly augmented jacobian based on the general solution formulation (see Equation 5.3) introduced by [67, 103], is proposed. This softly-augmented jacobian should avoid algorithmic singularities. The repeatability of the system response is still desired.

Definition 5.3 (*Softly-augmented jacobian*) Originally introduced by [67, 103]. The solution to the inverse kinematic problem based on the direct pseudo-inverse of the desired motion J^+dx combined with the gradient of positive definite potential functions g projected into the null space of the jacobian N is called softly-augmented jacobian solution.

$$dq = J^+dx + NN^T [-\nabla_q g]^T g.$$

The proposed softly-augmented jacobian method uses gradients of potential functions as additional differential relations Φ (see Equation 5.3), in order to define completely the map between the end-effector desired displacement and the joint trajectories.

$$\Phi = [-\nabla_q g]^T g$$

This softly-augmented map is more flexible than the rigid-extension solution in the sense that the obtained-solution can converge to a limit cycle, while the previous rigid extension of the jacobian is entirely fixed by its initial conditions and the additional differential relation G . The convergence rate and trajectory depends on the initial conditions.

Through the use of a pseudo-inverse map (not a full matrix inversion) for the main task (J^+dx) combined with projected-gradient

onto the null space of the jacobian ($NN^T [-\nabla_q g]^T$) for the secondary tasks, the algorithmic singularities (coming from the matrix-inversion singularities along the path) do not exist. Furthermore, if the used potential-functions correspond to secondary tasks, this scheme enables multiple tasks to be tracked simultaneously. However, the tracking of the secondary objectives is made in a soft manner regarding the main task. The main task is exactly realized through the pseudo-inverse map, and the secondary tasks are tracked softly in the sense that the manipulator tends towards their realization, without any guarantee of success. In particular, the successful realization of the secondary tasks is highly dependent on the main task and on the dimension of the redundant space. The larger the redundant space is, the more chances the manipulator fulfill its secondary tasks.

The use of potential functions, even if it does not ensure the success of the secondary tasks, has been widely used in the literature in order to complete the differential map between end-effector and joints (see [50, 52, 68, 89, 90] for examples). However, their relations to predictive response is not well-established and will be further developed hereafter.

Convergence to a fixed point for a fixed end-effector position

This section tends to examine the self-motion of the manipulator on its own, when driven by potential functions. Without loss of generality, the 3R2D manipulator is considered.

Proposition 5.1 *Consider the 3R2D manipulator (with the joints q_1 , q_2 and q_3 defining the absolute angles) together with a fixed end-effector position. The self-motion induced by the inverse kinematic based on the softly-augmented jacobian (as defined in Definition 5.3) with a convex potential function $g(q) > 0 \quad \forall q$ (with a global minimum) converges to a fixed point.*

Proof: The end-effector fixed position implies $dx = 0$ which in turns means that (see Definition 5.3)

$$dq = NN^T [-\nabla_q g]^T g \quad (5.5)$$

where N designs the null space of the jacobian matrix J of the manipulator. The $[3 \times 3]$ matrix NN^T is positive definite by definition and of rank 1 (the rank corresponds to the dimension of the redundant manifold). Consider the semi-definite positive Lyapunov candidate function $V = g > 0$. We have:

$$\dot{V} = \frac{\partial V}{\partial q} dq = \nabla_q g \begin{bmatrix} dq_1 \\ dq_2 \\ dq_3 \end{bmatrix} \quad (5.6)$$

Combining Equations 5.5 and 5.6, we obtain:

$$\dot{V} = -[\nabla_q g] NN^T [\nabla_q g]^T g \quad (5.7)$$

Calling P the scalar product between the gradient of the potential-function $[\nabla_q g]$ and the null space N , we obtain finally:

$$P = [\nabla_q g] N \quad (5.8)$$

$$\dot{V} = -PP^T g \leq 0 \quad (5.9)$$

At this stage, two possibilities can happen: either the scalar product P is null or not.

If $P = 0$, this means that, at this particular point q , no existing self-motion of the manipulator can influence further the potential function g . Moreover, from Equations 5.5, 5.8 and 5.9, we have $\dot{V} = dq = 0$. Thus, the manipulator stabilizes itself at this fixed point.

If $P \neq 0$, we have $\dot{V} < 0$. Thus, the Lyapunov function V establishes clearly that the self-motion induced by the initial state converges toward an equilibrium point whenever the end-effector is fixed. ■

Proposition 5.1 establishes that the manipulator, when not disturbed by the end-effector main task, converges toward an equilibrium point. This equilibrium corresponds either to the minimum of the potential function g (if accessible in the redundant space) which

realizes completely the secondary task or, to its closest projection (best approximation) onto the redundant space of the manipulator.

Finally, considering again the main positioning task, the limit cycle (obtained after convergence, see Figure 5.2) and its corresponding self-motion in the redundant manifold can be interpreted as two moving attractive points for the manipulator. The first attractive point in the working space drives the motion of the end-effector toward the reference trajectory ($J^+ dx$) and the second attractive point in the redundant space ($NN^T [-\nabla_q g]^T g$) drives the self-motion toward the secondary objectives.

Convergence to a limit cycle: predictable response

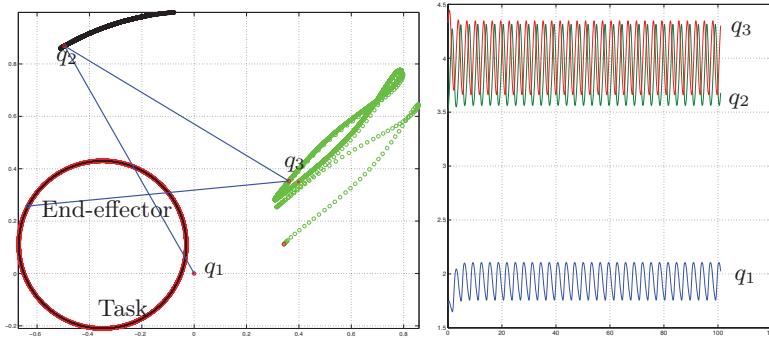
In this section, it is demonstrated that through the soft-extended jacobian coordination scheme (see Definition 5.3), under particular conditions on the potential functions, the joint responses of the 3R2D manipulator converge toward a limit cycle. Notice that, once the limit cycle is obtained (after convergence), any initial conditions that matches exactly a point on the cycle, will keep the manipulator on the same trajectory. Thus, the obtention of the corresponding cycle is interesting to our purpose of predictability.

Also the following theorem is demonstrated for a particular potential function g and a particular task h , the result can be easily generalized.

Theorem 5.1 *Consider the 3R2D manipulator together with its periodic circular task $\mathcal{S} = h = (y_1 - c_1)^2 + (y_2 - c_2)^2 - R^2$. Consider also, without loss of generality, that the desired end-effector velocity $dx \in TS$ is constant such that the period of the task T is constant. The inverse-kinematic solution based on the softly-augmented jacobian (see Definition 5.3)*

$$dq = J^+ dx - (NN^T) [-\nabla_q g]^T g$$

with the quadratic potential function $g = \alpha(q_1 - \pi/2)^2$, $\alpha \in \mathbb{R}^+$, converges to a limit cycle of same period T .



(a) Convergence to a closed-trajectory; (b) Joint convergences toward (red) main task; (black) trajectory of periodic responses. first elbow; (green) periodic trajectory of second elbow.

Fig. 5.2. 3R manipulator convergence to a limit cycle through the use of a secondary potential function: predictability is obtained.

Proof: The task manifold \mathcal{Y} corresponding to this particular 3R2D manipulator and task is homeomorphic to a torus (see Figure 5.3 for a schematic view of it). Notice that this manifold is compact by definition.

The inverse-kinematic solution based on the softly-augmented jacobian can be divided into two parts: the first part realizing the main task through the pseudo-inverse map $J^+ dx$ and the second part tracking a secondary objective defined as the gradient of a potential function g projected into the redundant space $-(NN^T)[\nabla_q g]^T g$.

The norm of the pseudo-inverse map ($J^+ dx$), as long as singular points (loss of rank in the jacobian J) are avoided, is limited by the reference-trajectory realized with the end-effector of the manipulator and thus is bounded.

$$\|J^+ dx\| \leq \|J^+\| \|dx\| \leq \lambda, \lambda \in \mathbb{R}^+ \quad (5.10)$$

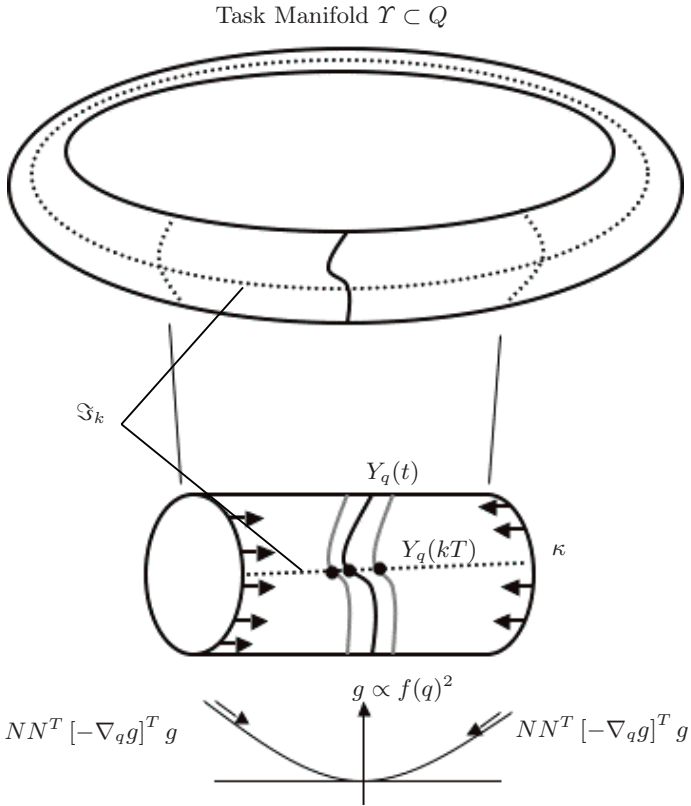


Fig. 5.3. Subpart of the task manifold $\kappa \subset \mathcal{T}$ (cylinder) of the 3R2D manipulator tracking a circle h as main task on which the joints trajectory $Y_q(t)$ is constrained by the potential function g . The realization of the periodic task ensures that the joints trajectory crosses periodically (every T periods) the same redundancy fiber \mathfrak{S}_k .

Consider the Lyapunov candidate function $V = g(q) \geq 0$, we have:

$$\begin{aligned}
\dot{V} &= \frac{\partial V}{\partial q} dq \\
&= [\nabla_q g] \left(J^+ dx - (N N^T) [\nabla_q g]^T g \right) \\
&= [\nabla_q g] J^+ dx - [\nabla_q g] N N^T [\nabla_q g]^T g. \tag{5.11}
\end{aligned}$$

In order to obtain $\dot{V} < 0$ at the border of the submanifold κ (corresponding to the 2D cylinder represented in Figure 5.3)), which enforces the cylinder (κ) to be an invariant set, consider together Equations 5.10 and 5.11. The following condition can be formulated.

$$\begin{aligned}
0 &< \| [\nabla_q g] \| \| J^+ dx \| \leq \| [\nabla_q g] \| \| N N^T \| \| [\nabla_q g]^T g \| \\
\iff \| J^+ dx \| &\leq \lambda \leq \| N \|^2 \| [\nabla_q g] \| g \\
\iff \frac{\lambda}{\| N \|^2} &\leq g \| \nabla_q g \| \tag{5.12}
\end{aligned}$$

Equation 5.12 imposes conditions on the choice of the potential function. For our particular choice $g = \alpha(q_1 - \pi/2)^2$, the latter can be reformulated:

$$\begin{aligned}
\frac{\lambda}{\| N \|^2} &\leq 2\alpha^2 |q_1 - \pi/2|^3 \\
\iff -q_1 + \frac{\pi}{2} &\leq \sqrt[3]{\frac{\lambda}{2\alpha^2 \| N \|^2}} \leq q_1 - \frac{\pi}{2} \tag{5.13}
\end{aligned}$$

These conditions define the bounds of the invariant set κ . This means that every joint trajectories passing at some point in the submanifold κ will never leave it. As a consequence, the maximal drift along the redundancy-fiber \mathfrak{S}_k , in the submanifold κ , caused by the pseudo-inverse map (see Remark 5.2) is always compensated by the gradient of the potential function g (see Figure 5.3). Thus, the joints trajectory is constrained on a 2D compact surface.

Since the cylinder κ has been shown to be an invariant set, the realization of the periodic task h of period T ensures that the joints trajectory $Y_q(t)$ crosses periodically (every T periods) the same redundancy fiber \mathfrak{S}_k (see Remark 5.1 and Figure 5.3)

$$\kappa \cap \mathfrak{S}_k = \mathfrak{S}.$$

Therefore, let q_k designate the point $Y_q(t_0 + kT) \cap \mathfrak{S}$ corresponding to the intersection of the joints trajectory with the redundancy fiber in κ . The periodic task yields a sequence of points q_k that can be mapped on the closed interval $[0, 1]$. Moreover, the q_k sequence is ordered: either

$$q_{k_1} \geq q_{k_2} \geq \dots \geq q_{k_i} \dots$$

or

$$q_{k_1} \leq q_{k_2} \leq \dots \leq q_{k_i} \dots$$

Indeed, if this is not the case, this would mean that the joints trajectory $Y_q(t)$ would self intersect in κ , which is not possible.

The ordered sequence of intersection points q_k in the invariant set κ can either converge to a fixed value $\bar{q} \in [0, 1]$ or be such that $q_{k_i} = q_{k_{i+1}} = \bar{q}, \forall i > 0$. In the first case, the joints trajectory $Y_q(t)$ converge to a T -periodic trajectory. In the second case, the joints trajectory is directly T -periodic. ■

Remark 5.2 *Taken on its own (without additional potential function), the pseudo-inverse map (see Section 4.3.1) will introduce drift along the redundancy axis (consequence of its local properties) preventing the joints trajectory to be periodic of period T .*

Remark 5.3 *The potential function acts as a spring pulling the joints trajectory toward the center of the invariant set. The parameter α of the particular potential function g modulates the strength of this virtual spring and also enables to modify the size of the invariant set κ .*

5.3.4 Extension to 5R-3D manipulators

Consider the 5R serial manipulator defined in Section 3.1.1, realizing the periodic Lissajou positioning task on a spherical output manifold. The latter method, adding secondary potential function in the null

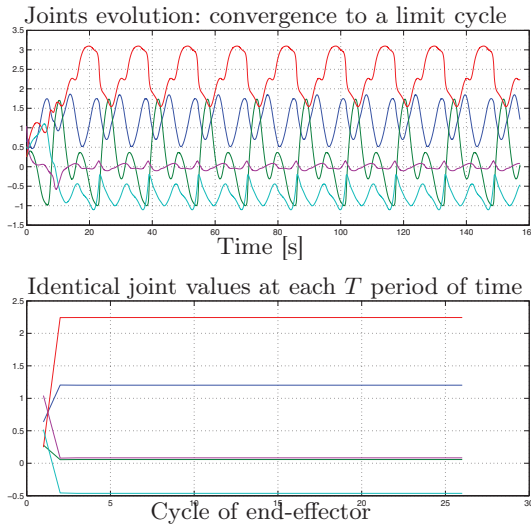


Fig. 5.4. Extension of the potential approach to a 5R3D manipulator. Convergence to a limit cycle is obtained through the use of 2 secondary potential functions.

space of the jacobian, enforces periodicity of the joints (see Figure 5.4).

Conjecture 5.1 *Theorem 5.1 is valid for any redundant serially-linked manipulator, also in the 3D space, as long as enough additional potential functions are added to compensate for the dimension of the redundancy manifold.*

5.3.5 Hierarchical adjunction of potential functions

As introduced previously, some kind of hierarchy in the objectives is desirable in the sense that tasks priority define the relation between them. This hierarchy is introduced through successive projections of

the gradients (defining the secondary tasks) into reduced null spaces [50, 52, 68, 89, 90].

Definition 5.4 (*prioritized tasks and reduced null spaces*) Originally introduced by [89]. Hierarchy in the different tasks Γ_i to be realized by a manipulator is obtained through prioritized projection onto reduced null spaces N_i . The reduced null spaces are defined with respect to the preceding tasks in the hierarchy

$$N_i = N_1 \cdot N_2 \cdot N_3 \cdot \dots N_{i-1}.$$

Thus, the reduced null space of a task is defined as the space of motion with no impact on any of the higher priority tasks.

The prioritized combination of the tasks is obtained through:

$$\Gamma = \Gamma_1 + N_1^T (\Gamma_2 + N_2^T (\Gamma_3 + N_3^T (\dots)))$$

where Γ corresponds to the combined overall task.

The usage of reduced null spaces reduces the redundant space with each new task and enforces the decoupling of the low-level task with respect to higher priority tasks.

For example, to prevent the manipulator from violating a constraint, the latter is expressed as a high-priority subtask. Any other task is then tracked in the null space of the previous constraint.

Considering together Definition 5.3 and 5.4, a prioritized softly-augmented multi-tasking scheme is defined such as:

$$dq = J^+ dx + N_1 N_1^T [-\nabla_q g_1]^T g_1 + N_2 N_2^T [-\nabla_q g_2]^T g_2 + \dots$$

The latter scheme not only enforces the decoupling between the tasks in introducing a clear hierarchy between them (1. End-effector motion (dx) 2. g_1 3. g_2 ...), but also avoids any algorithmic singularities such as the one potentially-obtained with the rigid extension of the jacobian (see Section 5.3.2).

5.4 The Hessian as coordination solution

The particular closed-solution minimizing the joint displacements along the full task is another desirable solution. The latter corresponds to the shortest closed integral-curve on the task manifold realizing the positioning task, see Figure 5.1 and 5.5.

Thus, the combination of several objectives is considered: the minimization of the joint displacements while still realizing successfully the main positioning task h together with a closed-response to a periodic excitation.

The following paragraphs describe an algorithm solving locally the inverse-kinematic problem toward the objectives described above. Indeed, the algorithm uses local information about the task acceleration to tend toward the shortest joints trajectory realizing the main positioning task (see Remark 5.4).

Recall that, in our 3R2D serial-manipulator context, we consider a circular positioning task

$$h = (y_1 - c_1)^2 + (y_2 - c_2)^2 - R^2 \quad (5.14)$$

with its corresponding 1-form $\omega_h = \nabla_q(h) = \left[\frac{\partial h}{\partial q_1} \dots \frac{\partial h}{\partial q_n} \right]$. Since, by definition of the 1-form, ω_h is orthogonal to the considered positioning-task h in the 2D working manifold, any displacement in the latter manifold, orthogonal to ω_h is along the reference trajectory. In order to consider the manipulators task entire output space, we construct the following set of vector field $\kappa \in T\mathcal{T}$:

$$\omega_h \cdot \kappa = 0 \quad (5.15)$$

which, by construction, spans all motion along the reference trajectory. The κ integral manifold corresponds to the Torus $S^1 \times S^1$ represented in Figure 5.5. This topological representation of the manipulator task manifold is now to be used in order to achieve our multiple objectives.

The end-effector acceleration corresponding to the task h , represented in the configuration space Q , is defined as the Hessian-matrix

(second derivative) of the task with respect to the joints.

$$H = \nabla_q(\nabla_q(h)) \quad (5.16)$$

H is a symmetric $n \times n$ dimension matrix where n is the number of joints. Notice that the diagonal elements of H correspond to the second derivative of the task with respect to each joint $\frac{\partial^2 h}{\partial q^2}$.

An eigenvector decomposition $\Delta[\cdot]$ of the projection of the Hessian matrix on the κ integral manifold is considered.

$$V = \Delta [\kappa^T \cdot H \cdot \kappa]$$

From this decomposition $V = [V_1 \ V_2 \dots V_i]$, only the eigenvector corresponding to the maximal eigenvalue (absolute value), is considered. This corresponds to the local maximal-curvature direction on the task manifold. Note that the dimension of the latter decomposition V is defined by the number of joints n and the dimension of the task in the working space d :

$$i = n - d.$$

In the context of the 3R2D manipulator ($n = 3$ and $d = 1$), the obtained 2D-vector corresponds to the direction of the local maximal curvature of the task manifold realizing the task h . In other term, following at each instant this direction tends to ensure that the obtained-integral path will be the shortest to realize the task (as long as the task manifold is smooth and simple, see Remark 5.4).

Expressing back the latter identified vector in the full configuration space (joint space) $f_1 = \kappa \cdot V_1$, the optimal direction (maximal curvature of the manifold) from the Hessian of the task is obtained. The correct scaling of the vector f_1 in order to realize the task correctly with respect to the reference v_{ref} (also in time) is obtained through the direct kinematic of the manipulator.

$$\begin{aligned} v_1 &= J \cdot f_1 \\ v_{ref} &= dx = \alpha v_1 \end{aligned} \quad (5.17)$$

Finally, the manipulator joint motions are obtained through the map of Equation 5.18.

$$dq = \alpha f_1 \quad (5.18)$$

The results from this procedure are illustrated in Figure 5.5 and 5.6.

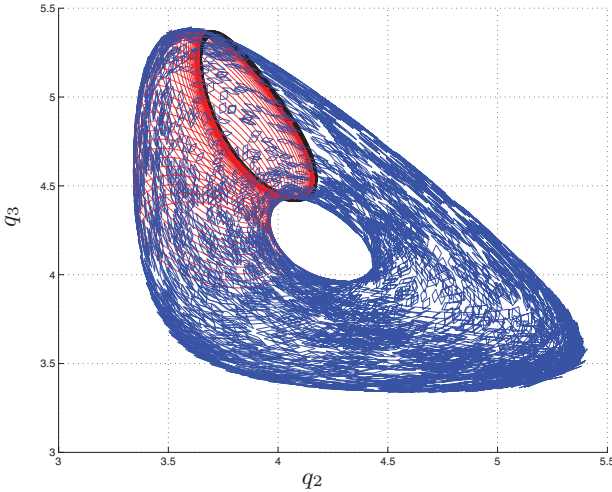


Fig. 5.5. Projection on the q_2 , q_3 plane of the task manifold \mathcal{T} of the 3R manipulator tracking a circle as main task (blue). Convergence (red) to the Hessian best solution (black) to realize the task.

Two very interesting considerations are to be underlined considering the latter method:

- The system tends locally toward the hessian-optimal solution (red path in Figure 5.5): topological optimal repartition of joint displacements.

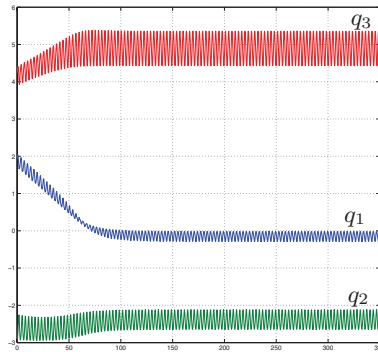


Fig. 5.6. Convergence of the joints trajectory to the Hessian local best solution.

- The joints trajectory converges to a limit cycle and remains on it (black path in Figure 5.5): periodic response to a periodic excitation.

Notice finally that this method mathematically excludes algorithmic singularities. In fact, an alignment of the vector f_1 with a purely redundant direction (algorithmic singularity) is not possible by construction. Indeed, the proposed-algorithm tracks locally (along the entire integral-path on the task manifold) the most sensitive direction of the acceleration with respect to the joints (through the maximal singular value). This ensures that if a non-redundant direction exists, which by definition is always the case on the task manifold (manipulator-singularities are excluded), the most reactive direction with respect to the task is tracked.

Remark 5.4 *The smoothness of the task manifold is necessary for this algorithm to converge to the hessian optimal solution, since it tracks **locally** the highest curvature of it. If the manifold has a complex shape with a spring-like maximal curvature all around it, the algorithm could remain indefinitely therein and never converge to*

the shortest path.

Hopefully, the shape of the task manifold is usually smooth, at least for simple end-effector trajectories.

5.5 Flexibility, compliance and repeatability

A parameterization of the complementary 1-form ω_c (introduced in Section 4.3.4) ensuring compliance and flexibility of the 3R2D manipulator, while keeping the predictability of its joints response, is proposed hereafter (see Figure 5.7 and 5.8).

Consider the task manifold \mathcal{T} (see Definition 5.1) associated to $h(q) = (y_1(q) - c_1)^2 + (y_2(q) - c_2)^2 - R^2$ its positioning task equation. Recall that this task manifold is homeomorphic to a torus, see Section 5.2.1. Define the following items (illustrated in Figure 5.7):

- \mathfrak{S}_m the redundancy fiber corresponding to the initial conditions of the manipulator q_o and $T\mathfrak{S}_m$ its associated tangent bundle,
- C as the center of the smallest ball in $Q \subset \mathbb{R}^3$ containing the entire redundancy fiber \mathfrak{S}_m ,
- the exact 1-form $\omega_h = \nabla_q h$ corresponding to the gradient of the positioning task,
- $Y_q(t)$ the joints trajectory on the task-manifold \mathcal{T} realizing the main positioning task h ,
- $\bar{q} = Y_q(t) \cap \mathfrak{S}_m$ as the intersection of the joints trajectory with the redundancy fiber \mathfrak{S}_m (all these variables are illustrated in Figure 5.7).

Choose any vector $v \neq 0$, such that $v \in T_{\bar{q}}\mathfrak{S}_m$, where $T_{\bar{q}}\mathfrak{S}_m$ corresponds to the subspace of tangent vectors to the fiber \mathfrak{S}_m at the point \bar{q} .

Now, let us choose the complementary 1-form ω_c with constant coefficients, i.e.:

$$\omega_c = \sum_{i=1}^3 c_i dq_i, \quad c_i \in \mathbb{R} \quad (5.19)$$

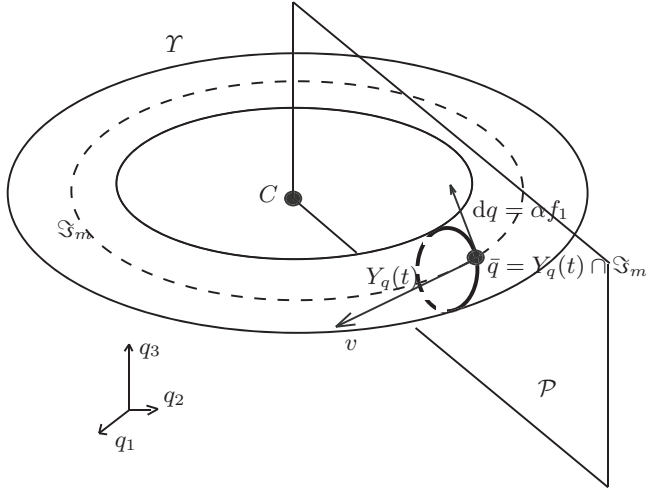


Fig. 5.7. Parameterization of the complementary 1-form ω_c through the center of the torus C and the intersection \bar{q} of the joints trajectory $Y_q(t)$ with the master redundancy fiber \mathfrak{S}_m .

such that $\begin{pmatrix} c_1 \\ c_2 \\ c_3 \end{pmatrix} = v \in T_{\bar{q}}\mathfrak{S}_m$. Because the coefficients are constant, ω_c is integrable and its integral manifold is the plane \mathcal{P} . The plane \mathcal{P} containing the center of the redundancy fiber C is necessarily intersecting the task manifold \mathcal{Y} . The latter intersection between \mathcal{P} and \mathcal{Y} defines a set of points in the joint-coordinate space Q which realizes the main positioning task.

$$\mathcal{P} \cap \mathcal{Y} = \{Y_q(t), t \in \mathbb{R}^+\} \quad (5.20)$$

Let us consider now, that $\{Y_q(t), t \in \mathbb{R}^+\}$ is a manifold, which will be \mathcal{Y} . Extending Theorem 4.2 to our 3R2D manipulator, we can now define the vector field f_1 dual to ω_c and ω_h ,

$$\begin{pmatrix} \omega_h \\ \omega_c \end{pmatrix} \cdot f_1 = 0 \quad (5.21)$$

such that $\text{span}\{f_1\} = T\mathcal{Y}$. Defining the weighting α , such that :

$$\begin{aligned} \dot{Y}(t) &= J \frac{dq}{dt} \\ &= \alpha J f_1 \end{aligned} \quad (5.22)$$

the desired velocity of the end-effector is obtained.

Figure 5.9 illustrates the perfectly-periodic joint responses corresponding to the realization of the task h over several periods T .

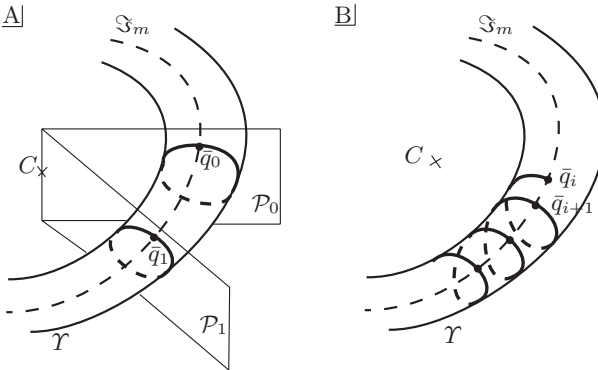


Fig. 5.8. A) The compliance of the manipulator is obtained through the free choice of the intersection point \bar{q} on the redundancy fiber \mathcal{S}_m . A different, but still periodic, response is obtained for each choice of \bar{q} . B) Illustration of a characteristic non-periodic response of the joints: the joints trajectory is drifting along \mathcal{Y} and is not closed on itself.

Indeed, the f_1 parameterization of the solution to the inverse kinematic problem for the 3R2D manipulator ensures repeatability of the

joint responses (see Figure 5.8 and 5.9). By construction, the joints trajectory is constrained in the manifold $\mathcal{Y} = \mathcal{P} \cap \mathcal{Y}$, whose dimension is one. This ensures a closed-trajectory. Furthermore, flexibility and arm-compliance of the manipulator is obtained through the flexible obtention of $\omega_c(\bar{q})$, (see Figure 5.8). Indeed, any motion along the

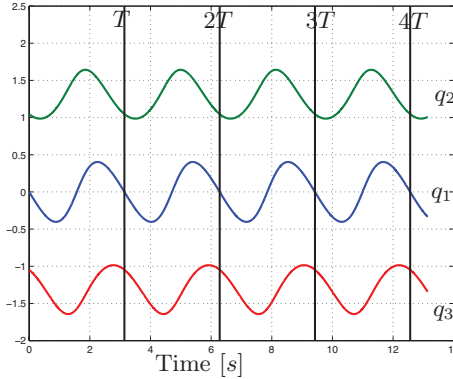


Fig. 5.9. Perfectly-periodic joint responses to the circular positioning-task h of period T . For this simulation, the following parameters were used: $l_1 = l_2 = l_3 = 1$, $c_x = 1.5$, $c_y = 0$, $R = 0.5$, $q_1(t = 0) = 0$, $q_2(t = 0) = \pi/3, q_3(t = 0) = -\pi/3$, $T = \pi$.

redundancy fiber is compliant with respect to the main task, since it has no impact with it. Thus, the intersection point $\bar{q} = Y_q(t) \cap \mathfrak{S}_m$ can be modified freely. A different limit cycle corresponds to each intersection point.

5.6 Conclusion

5.6.1 Link to the preceding chapter

The present chapter, using gradient of potential functions to enforce the coordination of the multi-tasking scheme can be, in some way, interpreted as a relaxation of the stringent condition of exact-periodicity introduced in Chapter 4. Indeed, through the potential functions coordination scheme, the joints response is not directly constrained on an arbitrary planar parameterization of the solution (through the complementary 1-forms) as for the preceding chapter. But it slowly converges to a local parameterization (not necessarily planar) inducing the desired predictable limit-cycle.

5.6.2 Contributions

The following four original contributions have been detailed in this chapter. First, the task-manifold concept has been introduced to describe all solutions to a predefined task, including the self-motion of the manipulator (Definition 5.1 and Figure 5.1). Second, in Section 5.3.3, the potential functions together with the soft-extension of the jacobian as defined in this thesis have been demonstrated to enable a constructive coordination for the main positioning-task and for multi-tasking. It has been demonstrated that toward the use of potential functions, the 3R2D manipulator joints trajectory converge to a limit cycle for a periodic excitation (Proposition 5.1 and Theorem 5.1). Third, an interesting solution (minimal joints closed-path solution) was tracked through the task Hessian-matrix eigenvector-decomposition (Section 5.4). And fourth, based on the task-manifold, a flexible, compliant and predictable parameterization of the solution space for the 3R2D manipulator was finally developed (Section 5.5).

Closed-loop control for coordination

In this chapter, a dedicated controller including a closed-loop coordinator for a dual-stage optomechatronic system is detailed. The successful coordination of the dual-stage is the key element enabling the desired performances. Moreover, a higher level of coordination implying simultaneously 2 DDLs is introduced in order to enhance further the performances.

The third axis of research on coordination, detailed in this chapter, handles the closed-loop control-scheme of a particular overactuated application. The entire argumentation concerning *the closed-loop coordination* leans on the PRIMA-DDL project. Contrarily to the two preceding chapters, where the discussed theoretical elements were illustrated through simulations, this chapter builds the coordination concepts in the project context.

Another major difference with the preceding chapters consists of the *closed-loop* control scheme (only open-loop schemes were previously considered). Instead of working with absolute signals as for the open-loop schemes, the entire coordination is based on relative signals, corresponding to tracking errors.

6.1 Introduction

6.1.1 Project context

The Very Large Telescope (VLT) is an European Southern Observatory (ESO) operated observatory on Cerro Paranal in Chile. It consists of four 8m-telescopes, the Unit Telescopes (UTs), and an optical interferometer, the VLTI. The VLTI allows to combine the four UTs and four movable 1.8m-telescopes, the Auxiliary Telescopes (ATs) [32].

Astrometry measures the angular position of stars. The precision of this basic method depends on the aperture size. In optical interferometry the angular resolution is increased by combining the light from multiple telescopes. Herein, the resolution parameter equivalent to the aperture size is the maximum distance between the combined telescopes, the baseline. When two light beams coming from the same source are being picked up at two different positions on earth, they follow different path lengths. The combination of the received light beams interfere. When they arrive in phase they superimpose and produce bright fringes (white-light-fringes), and when they arrive out of phase they cancel each other out. The main aim of optical interferometry is to find the white-light-fringes of the observed object. They provide information about the distance, the angular size and the angular separation of the observed objects. According to the difference in the baseline, the rotation of the earth and atmospheric disturbance the beams' paths are not of equal length. This difference in length has to be altered in order to produce the required interference pattern. Therefore, the optical path difference (OPD) between the two beams of light can be varied by internal delay lines to produce these fringes [74].

Figure 6.1 shows the light beams originating from the same source, travel through the focus of the telescopes, pass the delay lines and their final combination in the interferometry lab in order to produce interferometry fringes [32].

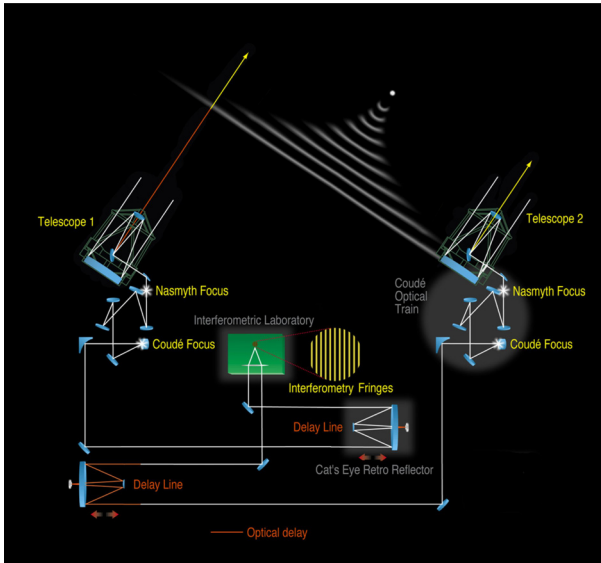


Fig. 6.1. The optical layout of the VLTI with two telescopes. Notice that the 4 DDLs are not represented and will be placed on each of the optical beam before they interfere (*Figure source: ESO [32]*).

The VLTI contains many different subsystems, a short overview of these systems is given in [32]. The Phase-Referenced Imaging and Micro-arcsecond Astrometric facility (PRIMA) expands the VLTI by the possibility to observe two stars simultaneously, a so called dual feed capability. This enhancement allows to observe fainter objects and achieve higher resolutions on the other VLTI instruments. Furthermore PRIMA's key objective is to expand the search for extra-solar planets and their birth environment. In addition to that, the high precision astrometry will increase the reach of the VLTI [22].

The principle of phase referenced imaging and micro-arcsecond astrometry with an interferometer is shown in Figure 6.2. A bright

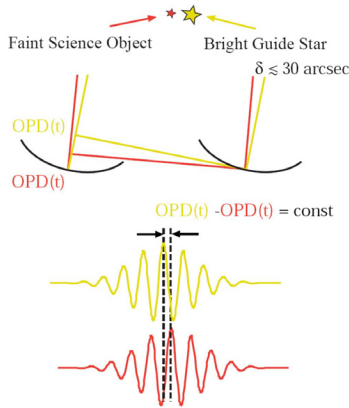


Fig. 6.2. Basic scheme of PRIMA (*Figure source: ESO [32]*).

star and a reference object are observed simultaneously in one telescope. One star is focused and therefore the fringe motion is to be the motion of the other object. The differential delay between these two beams of light has to be equalized to observe the fringe motion. This variation of the differential length of the two paths is simultaneous to the compensation of the OPD described before. As the angle between the two stars in one telescope is smaller than the angle between the two objects in different telescopes, the atmospheric disturbance has less impact on the wave front of the light and therefore a higher precision is achievable. For best performance the internal delay, the length of the baseline vector and the measurement of the fringe phase have to be known very precisely (nanometer accuracy $\approx 1/100$ radian accuracy) and the light paths throughout the system should be closely matched [60].

PRIMA requires four subsystems to commit its tasks: star separators, DDLs, two fringe sensors/trackers and a high accuracy metrology. This chapter provides a control algorithm for the DDLs, so only the DDL is briefly explained in the following paragraph. The other

systems are well described in [21]. The star separator splits the light beams of one telescope in the beam of the faint science object and the bright guide stars beam. These beams are fed through the large VLTi delay lines. Simultaneously to the main delay lines canceling the OPD, the DDL's task is to alter the path length between the two beams to cancel out the differential delay. A total differential optical path difference of up to 70 mm has to be compensated by the DDL within a 5 nm tracking accuracy. PRIMA could be operated without the DDLs - then the delay would have to be compensated by the VLTi delay lines - but a much lesser resolution would be achieved as the bandwidth of the delay lines is a lot smaller than the bandwidth of the DDL and the positioning in the delay line not as accurate [22]. A further objective of the DDL is the atmospheric disturbance compensation. Usually the atmospheric disturbances have a frequency content of up to 300 Hz. Using the DDL's high-bandwidth will improve the performance of the VLTi instruments in compensating for these perturbations.

6.1.2 ESO-Specifications

The atmospheric disturbance to be compensated can be well described by a Kolmogorov signal. The Kolmogorov signal describes the perturbation of the wave front arriving at the telescope in terms of a stochastic model. This signal has a frequency content of up to 250Hz , wherein small amplitudes ($|x| < 1\mu\text{m}$) come along with high frequencies ($f > 50\text{Hz}$) and large amplitudes with low frequencies. The residual tracking error is to be under 70nm root mean squared (RMS). Further the system is operated under vacuum. Therefore the power dissipation of the DDL is required to stay under 5W . In addition, according to the observation duration over a whole night, the system is in need of a full stroke of 70mm [70].

6.1.3 Proposed mechatronic solution

In order to achieve this high accuracy (nanometer) a system separating the requirements of a coarse stroke and high nanometer accuracy was proposed (see [85, 95]). A piezoelectric stack actuator (S-325 from PI) provides the nm-accuracy at a short stroke with a high bandwidth. And a coarse actuator (NEMA 23 from Ultramotion) provides the large stroke at a low bandwidth. So a combination of the actuators joins the advantages of each actuator and eliminates their disadvantages. Altering the length of the OPD, in terms of large μm -scale- and very accurate nm-scale strokes, yields, that both actuators have to act on the same output, the length of the light path. This light beam is reflected through the optics into a cat's eye which reflects the light further on its path. Changing the light beams length, by moving the cat's eye or altering the path difference in the cat's eye, varies the OPD. The coarse actuator, a permanent-magnet (PM) stepper motor, moves, over a leadscrew, a blade-guiding structure (a double parallelogram flexure with notch hinges, [82]) on which the cat's eye is mounted (see Appendix B). The mirror in the center of the cat's eye is attached to the top of a tripod piezoelectric and is able to be positioned at nanometer scale.

Figure 6.3 shows the simplified structure of the DDL. The light beam enters the cat's eye on the top left, is reflected in the cat's eye, passes the mirror mounted on top of the piezoelectric and leaves the cat's eye on the bottom beam. One can easily see that changing the expansion of the fine stage or moving the whole blade-guiding-system by the action of the coarse stage alters the light beams path length.

6.1.4 DISO Dual-Stage state of the art

The dual-stage concept as found in the DDL has been applied in the control of Hard-disk drives (HDD). The disk drive read/write head is positioned over a track within μm accuracy. The two stages are the arm, onto which the head is mounted and which is driven by a voice-coil motor for the coarse movement, and a microactuator

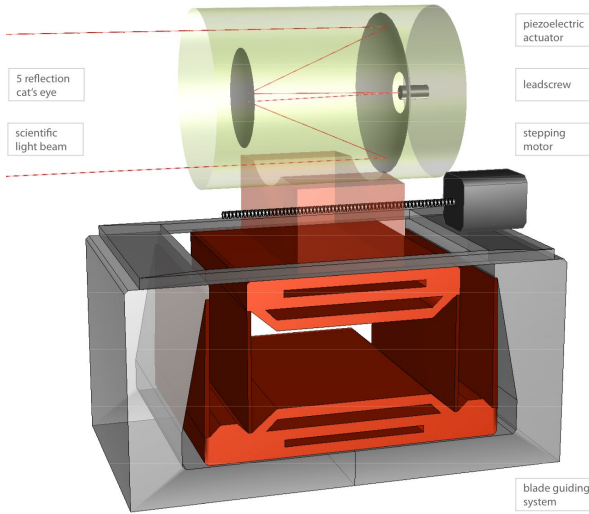


Fig. 6.3. Schematic representation of the DDL including the double parallelogram flexure with notch hinges (see Appendix B).

that is used to precisely position the head over the reference track. According to the increasing growth of the HDD market in the end of the 1990s and the rising accuracy requirements of data density many approaches have been taken to control this special DISO structure. These approaches include SISO- and MIMO - control structures. A very important point is the distribution of the tracking signal on the two stages. [3]

The SISO control approaches either regard the dual stage system as a sequence of SISO systems and design a controller by frequency shaping techniques, or decouple the two stages and regard them as two independent systems [3]. Modern multivariable con-

trol approaches have also been applied in order to increase stability margins, gain robustness towards parameter variations, enhance the tracking performance and raise the systems bandwidth. Most optimal control approaches are based on μ -synthesis and H_∞ -control which include uncertainties on modeling, and lead to increased track follow, very fast track seek and improved settling performance [63]. Further, the LQG controller was applied to the dual-stage design. Because of missing robustness guarantee and stability margins, Loop Transfer Recovery (LTR) was used, as it can be found in [44] and [101]. The desired frequency characteristics of the tracking performance is formulated according to the target feedback loop and is achieved by choosing the process noise and measurement noise covariance matrices of the Kalman filter. The LTR procedure recovers this design at the output of the plant by designing a linear quadratic regulator. The big advantage of this method is the avoidance of trial-and-error pole placement procedures [101]. The disadvantage of the optimal controllers are two folds: first the high order of the obtained controllers makes it difficult to implement in practice [3], [63]; second they present a very high sensitivity to model and identification errors.

Notice that, in HDD application the coarse stage actuator is the main tracking actuator. Therefore the voice-coil actuator usually tracks the reference while the microactuator is tracking an estimate of the relative position error between coarse and fine stage, e.g. [62], [98].

When multivariable state feedback controllers are applied a term is needed to split the one dimensional reference signal between the two stages. In [98] a command matrix is proposed to split the signal. Further, when the plant is regarded as a multivariable plant, rather than two single stages, output feedback is applied. Basically, two possibilities of feeding the tracking signal to the loop have been applied. The most common approach is to subtract the feedback signal from the tracking signal and feed the resulting state error to the controller. Another possibility is to feedforward the reference to the controller's voltage output in terms of a feedforward gain. [63] states that the feedforward term on the voltage output of the piezoelectric actuator

increases the error tracking performance with respect to satisfactory time and frequency responses.

6.1.5 DDL control problem

The small mass ratio that exists between the fine and the coarse stage highlights the uncoupled nature of the DDL system (see Section 6.1.3). Furthermore, a bandwidth decoupling also exists between the stages. The stacked piezoelectric device can indeed react much faster than the PM stepper motor. Moreover, the stochastic reference signal to be tracked by the DDL follows a Kolmogorov distribution (see Section 6.1.2). It varies slowly over large amplitudes and rapidly over small amplitudes. This structural information is perfectly in line with the bandwidth specifications of the actuators. A dedicated closed-loop coordinator is designed (see Section 6.2) to handle the interactions in-between the stages of the DDL, see Figure 6.4.

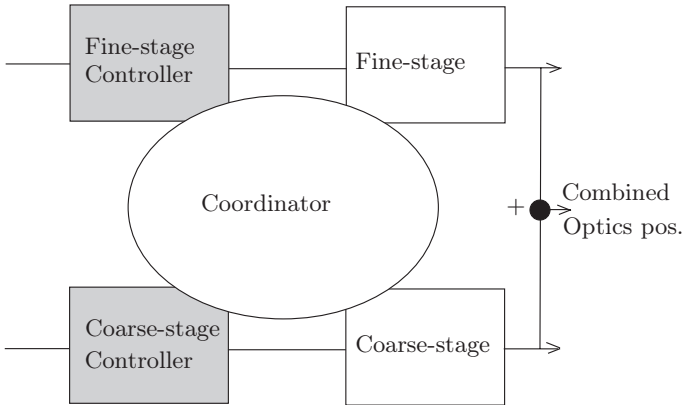


Fig. 6.4. DDL coordination problem.

In the next subsections (sections 6.1.6 and 6.1.7), the two individual controllers of the constitutive stages of the DDL (for the piezoelectric stack actuator and for the permanent magnet stepper motor) are detailed.

6.1.6 The piezoelectric as a fast and precise actuator

Nanometer positioning systems are generally using piezoelectric actuators as they are friction-free and present fast responses. In this context, the main concerns regarding piezoelectric-stack-actuators control are their well-known hysteresis and resonant frequencies which deteriorates their precision in positioning. Feed-forward model inversion [19, 23, 24, 31, 102], closed-loop high gains [47, 70, 83] and robust control [46] are the main control solutions to these two problems. Another major concern using the piezoelectric-stack actuators, is their short stroke. The usage of some kind of flexure lever to enlarge the output stroke [47, 107], or the combination of the piezoelectric actuators with other macro-actuator [7, 66, 70, 96] are some of the solutions which can be found in the literature.

Stack piezoelectric controller

According to the hardware solution (from a control design point of view), the coarse stage deviation acts as a disturbance (see Figure 6.10) on the fine stage loop. Unfortunately, the latter deviation is due to a stochastic reference signal that is a priori unknown. Nevertheless, it is possible to reject the mean value reference position of the PM stepper motor, as long as a convenient model of the disturbance is included in the fine stage controller (due to the internal model principle [26]). A simple model of this perturbation is an integrator which adjusts itself according to the low-frequency content of the stochastic signal. Thus, the controller has to include an integral term. As the piezoelectric device is used far below its resonant mode, there are no particular difficulties to control it with a classical Proportional Integral (PI) controller (see Figure 6.6).

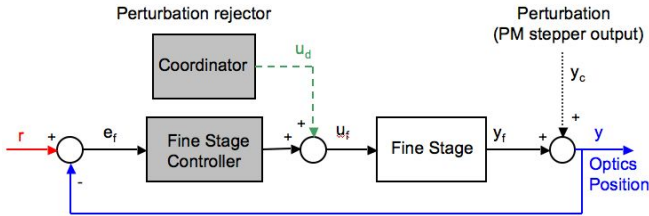


Fig. 6.5. Fine stage control structure.

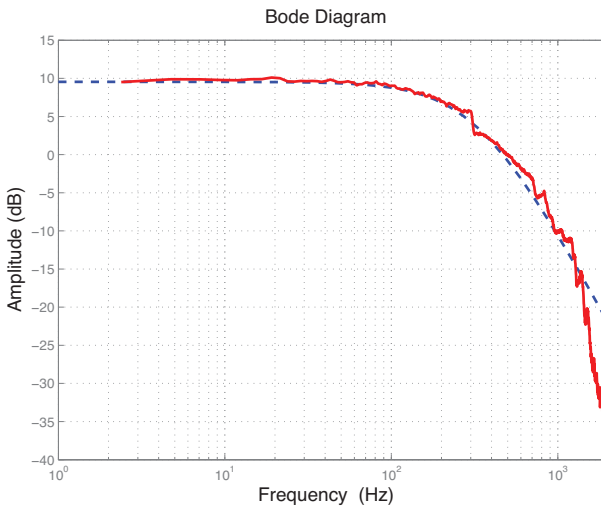


Fig. 6.6. Identified model of the piezoelectric stack actuator S-325 device (solid line), with its second-order approximation (dashed line). The estimated bandwidth is approximately 300 Hz and the static gain is approximately 3 (corresponding to a 10 V input to 30 μm output scaling).

Furthermore, in the context of nano-positioning, the hysteresis of stack piezoelectric actuators remains a major limitation to their precision. Such a degradation of the performance cannot be tolerated in

applications such as atomic-force microscopes [61], or high-accuracy optical systems [70].

The hysteresis of the piezoelectric device is partly rejected through the integral term of the controller. Since, an external metrology measures the real optical-path length, the hysteresis of the stacked piezoelectric device is seen through the feedback as a perturbation and is rejected by the integrator of the controller. Another option is to add a model-based feed-forward prediction of the hysteresis in parallel to the control scheme. In this context, different methods have been proposed to model the hysteresis appearing in piezoelectric actuators, but the most popular one remains the classical Preisach model. However, the basic method is not really suitable for a real-time compensation of a stochastic signal as it is required for the above setup in Chile. In addition, in the case of the atmospheric disturbances, no information is given at the beginning of the compensation about the future piezo expansion. Since very few studies have investigated such a problem [94], a method in order to invert the classical Preisach model has been developed (some details are discussed in Appendix C). The obtained pre-compensator can be added in parallel to the closed-loop scheme.

6.1.7 The permanent magnet stepper motor as coarse actuator enabling the complete stroke

Classical control approaches for PM stepper motors use the Park transformation to modify the considered referential [2, 11, 12, 18, 109]. H_∞ control with a simplified model [18], state feedback linearization [11, 12], or passivity and flatness-based controllers [92] are the main modern control methodologies used.

PM stepper controller

The proposed control law for the PM stepper motor is based on a direct sine/cosine control of the stator generated magnetic field (see

[70,96] for a detailed description of this approach). Indeed, the system is intrinsically stable for small angle (between the magnetic field generated at the stator and the rotor) and low frequency excitations. Under these conditions, if the load is neglected, the rotor always aligns itself with the magnetic field generated by the stator [49]. Thus, as long as the excitation is restricted to small angles with low frequency content, a simple integral controller summing continuously the position error automatically drives the PM stepper motor to the correct position.

Consequently, the following controller is proposed:

$$\begin{aligned}
 i_a(k) &= I_{peak} \sin(\alpha(k)) \\
 i_b(k) &= I_{peak} \cos(\alpha(k)) \\
 e_c(k) &= r_c(k) - \hat{y}_c(k) \\
 e_i(k) &= e_i(k-1) + K_i(h/T_i)e_c(k) \\
 &\quad \text{if}(e_i(k) > \text{Max}) \implies e_i(k) = \text{Max} \\
 &\quad \text{if}(e_i(k) < \text{Min}) \implies e_i(k) = \text{Min} \\
 \alpha(k) &= \alpha(k-1) + e_i(k)
 \end{aligned} \tag{6.1}$$

where α is the controlled phase of the stator magnetic field; h the sampling period; I_{peak} is the peak current applied to the coils of the motor; Max and Min are the rate-limits of the PM stepper; e_c is the coarse stage tracking error, i.e. the difference between the estimated position of the PM stepper motor \hat{y}_c and the low-pass filtered reference r_c of the DDL fed to the coarse stage.

The feedback information for this closed-loop scheme is provided through the coordinator, which estimates the coarse stage position (\hat{y}_c) based on the fine stage model (see subsection 6.2.3). A slow time constant T_i is chosen for the controller to avoid exciting the approximatively identified resonant mode ω (see Figure 6.7) and for ensuring a sufficient bandwidth difference between the stages.

This simple slow integral controller also has the advantage of being very robust to load variations, such as the ones caused by the double-parallelogram flexure with notch hinges (see Appendix B).

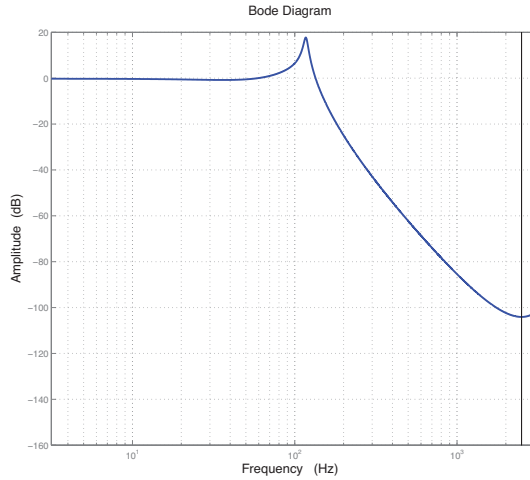


Fig. 6.7. Identified harmonic transfer function of the permanent magnet PM stepper motor coupled to the flexures. The electromechanical resonant mode can be clearly identified at 120 Hz.

So as to avoid any de-synchronization between the rotor and the generated magnetic field, on which the rotor tends to align, the variation of the controlled angle α is limited (see Equation 6.1). This limitation ensures that the acceleration is not above the physical limitations of the PM stepper motor coupled to the flexure. Moreover, this limitation ensures also the restriction of the excitation to small angles, for which the model and the controller are valid.

6.2 Coordination of the overactuated DDL

The successful constructive-coordination of the constituting stages of the DDL is the key element enabling the desired performances. Taken

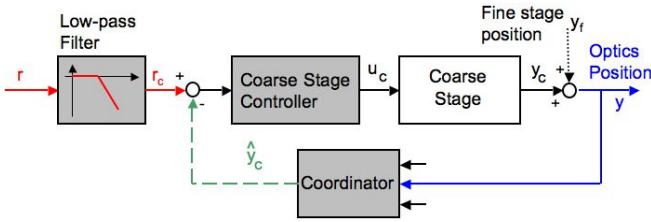


Fig. 6.8. Coarse stage control structure.

apart from the other, neither stage is able to fulfill the stringent requirements on its own. Overactuation and closed-loop coordination, as proposed in this thesis, are the only solutions to fully reach the objectives.

6.2.1 Overactuation: an infinite set of solutions

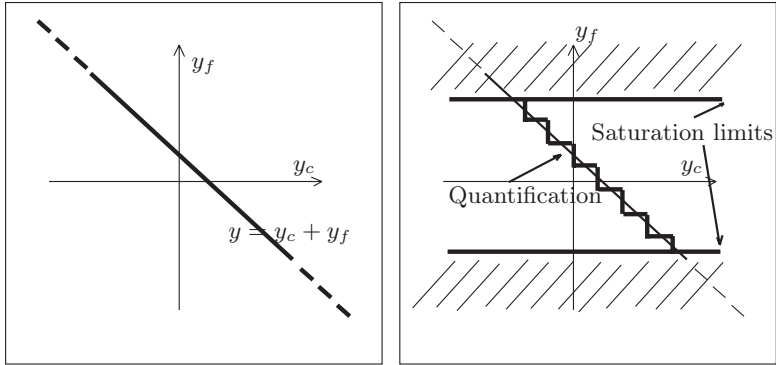
Not considering the limitation of each actuator, a single positioning task is performed by two fully independent actuators which thus provide two degrees of freedom.

The main output task y (dynamic control of the differential optical path length realized through the physical positioning of a reflective mirror) features a single translation axis realized either by the fine stage y_f or by the coarse stage y_c . The presence of these two stages acting similarly (at least theoretically) on the single output enables an infinity of different possible configurations corresponding to the same output position.

$$y_r = y_c + y_f \quad (6.2)$$

This extra degree of freedom is thus enabling an infinity of different choices: any combination of y_c and y_f satisfying the constraint (6.2) is a solution to the positioning problem (see Figure 6.9(a)).

The configuration manifold of a 2 dof overactuated manipulator, combining prismatic joints, corresponds to the 2D plane generated by $\mathbb{R} \times \mathbb{R}$.



(a) Infinity of different configurations y_c and y_f satisfying the output constraint y . (b) Restriction of the existing solutions by the actuators characteristics (saturation limits and quantification).

Fig. 6.9. Overactuated DDL: intrinsic characterization of the solutions. *Quantification* as stated herein features the less accurate coarse stage, acting at a macroscopic level.

6.2.2 Differentiation of the solutions

Of course, the two stages are not identical and we do combine them in order to take advantage of their own characteristics. In this context, some solutions are not even feasible regarding the intrinsic characteristics of each stage.

On the one hand, bandwidth, accuracy, repeatability, dry friction or saturation limits are intrinsic characteristics of the stages that distort the considered space of configuration.

Concerning the DDL, the saturation limits of the fine stage are very restrictive: the limited stroke is cutting down the complete configuration space to a short band along the y_c axis (see Figure 6.9(b)). These strong stroke-limitations of the fine stage justify directly its coordination with a coarse stage in order to enlarge the DDL working-space.

Moreover, the less-accurate (because of dry friction) and slower (lower bandwidth) coarse-stage of the DDL is not sufficient to ensure the desired performances and thus, necessitates its combination with a second actuator.

On the second hand, some solutions to Equation (6.2) are preferable than others. Considering the DDL in particular, two objectives can be underlined (a multi-tasking scheme as introduced in Section 5.2). Of course, the main task (goal 1) remains the realization of the positioning of the output y (as in Sections 4.2.3 and 5.2.3). However, in the complete configuration space satisfying the position constraint (position reference), a subpart of the existing solutions is preferable. The more distant the fine stage (with a very limited stroke) is from its saturation limits, the better it is (goal 2).

This second objective can be easily justified by the fact that the only actuator enabling the bandwidth and the accuracy which are required is the fine one. Thus, if it reaches one of its stroke limitations, it loses locally its ability to move toward this direction, resulting in not realizing fully the first objective.

To sum up: two simultaneous objectives are tracked. Firstly, the best-positioning possible of the DDL regarding its reference is to be achieved. This objective is mainly realized by the fine stage (the coarse stage being only used to enlarge the working space). Secondly, the distance to fine-stage saturation-limits is to be maximized. This second objectives is optimal when the fine stage remains in the center of its own working space (the coarse stage realizing the tracking).

6.2.3 Constructive coordination

The constructive coordination of both stages of the DDL in order to track the objectives successfully is the key control element. As detailed in the preceding section, among the infinity of different solutions, some are preferable regarding the objectives to be tracked and the intrinsic characteristics of the subsystems. The closed-loop coordination-scheme detailed hereafter enforces their successful tracking.

Global coordination scheme

The proposed parallel control structure with two SISO control loops (see Figure 6.10) enforces both the mass and the bandwidth decoupling of the DDL (see Section 6.1.5). The coarse stage handles the large amplitude component of the reference signal in the low frequencies, while the fine stage handles the small amplitude over the full bandwidth. The fine-stage loop (which is the main stage of the DDL, providing accuracy and bandwidth) is intentionally closed on the combined contributions of both stages, in order to ensure an efficient tracking of the optics position. Neither a model nor an observer is placed in the loop (see Figure 6.10) for avoiding any model-mismatch error. Moreover, to efficiently orchestrate the relative and absolute displacements of the two stages, the control structure integrates a dedicated coordinator.

The main advantage of this structure is that the stages can be considered independently for designing the controller, which makes it more intuitive by far. This is not the case when a multivariable design approach [41, 44, 62, 81] or a traditional PQ one [69, 80, 86] is considered. In the latter, an abstract representation of the dual-stage system is constructed.

Traditionally in dual-stage systems and especially in hard disc drives (HDD), the fine stage is only added to the coarse one for reducing the high-frequency tracking error. Thus, the main actuator is the coarse one and is essential to the functioning of the HDD [53, 58, 78, 79]. The bandwidth is usually decoupled through high-pass filtering at the fine stage level, letting the coarse stage handle the remainder of the excitation. However, in the context of the DDL, the system is not operable uniquely with the coarse stage, since the nanometer accuracy and the bandwidth, which are needed for astrometry purposes, are exclusively provided by the fine stage. The fine stage cannot deal exclusively with the high frequency content, since it provides the accuracy and rejects the coarse stage deviation (which is by design low-frequency). Hence, it is proposed rather to enforce the bandwidth difference using a low-pass filter at the coarse stage level. The fine

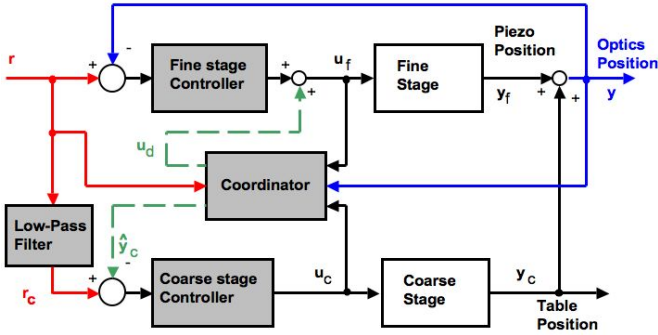


Fig. 6.10. Control structure with r , r_c , u_f , u_d , u_c , y_f , y_c , \hat{y}_c and y corresponding to reference signal, filtered reference signal, fine stage input voltage (stacked piezoelectric device), feed-forward fine stage input, coarse stage control signal (PM stepper motor), fine stage position, coarse stage position, estimated coarse stage position and optics output position, respectively. The global control structure illustrated here groups a low-pass filter, the fine stage controller, the coarse stage controller, and the stages' coordinator.

stage covers the full bandwidth, including the low-frequency part, in order to ensure an accurate tracking of the reference and also an efficient rejection of the coarse stage deviation. Here, the fine stage can be considered as the main stage.

The successful coordination of this dual-stage opto-mechatronic system necessitates three tasks: the repartition of the different information signals (feedback and reference) to the 2 subsystems, the adaptation of these signals to our purpose (filtering) and, finally, the enforcement of the cooperation between stages (pre-compensation) and between DDLs. These tasks are detailed in the following paragraphs.

Repertition of signals between stages

The reference signal (current desired-position to be) which is provided to the DDL system has to be divided into the subsystems (see Figure 6.10). This repertition need to ensure not only the tracking of the desired position (main objective) but also the secondary objective, which is the fine-stage distance to stroke-limitations maximization.

One particularity of the coordinator of the DDL is its closed-loop structure. In fact, closing the loop improves the accuracy of the tracking in providing additional informations to the system through the coordinator. The feedback information (position read by the sensor), together with the reference signal need to be adapted and distributed to the two stages. The feedback information is divided into two parts. One part, which is fed back to the fine stage, corresponds to the DDL combined output position. This crucial information is not modified by any model neither any filter in order to avoid any model mismatch. The second part is transformed to estimate the coarse stage position. This adaptation is realized with a filter representing a model of the coarse stage position, see [70] for more details.

Filtering of the coarse-stage reference

The reference signal fed to the coarse stage is modified in order to enforce the bandwidth separation between the stages (see Figure 6.10). The coarse-stage reference r_c (which is fed to the coarse-stage controller) is filtered with a third order Butterworth low-pass filter at 10 Hz, so as to keep only the low-frequency content while avoiding any excitation of high frequency resonant modes (see Figure 6.8).

This frequency separation is useful to decrease the perturbation by the coarse-stage motion on the combined output. Any motion realized by the coarse stage is seen as a perturbation by the DDL. Thus, enforcing a low frequency behavior (meaning slow) of the latter will help the compensation of its motion by the fine stage.

Pre-compensation of coarse stage motion

Taking into account, as explained here above, that any motion of the coarse stage is seen as a perturbation on the complete system position, a feed-forward prediction of the coarse stage movement will help compensating it. Hence, accuracy of the overall DDL is improved through a pre-compensation of the coarse stage movement (see Figure 6.10). Since the feedback information enforce the tracking accuracy of both stages (direct feedback for the fine stage and coordinator-adapted feedback for the coarse stage), meaning that their real positions are close to what is desired, the compensation is realized directly from the filtered reference of the coarse stage. This signal is transformed into fine-stage voltage (simple second order model) and fed directly to its input.

Enhancing advantages of each subsystem

Now that the global coordination strategy has been detailed, a particular problem, *the dual-stage destructive interference* that may occur between the stages (the two stages fighting against each other up to canceling their respective contribution) is studied. This is a major concern in HDD literature [53,69,80,86]. See Figure 6.11 for a graphical illustration of what is destructive interference. This interference is not intrinsically a problem for the accuracy of the DDL, since the overall position is directly controlled. However, uncontrolled opposite displacements of the stages could inject undesired vibrations and resonances into the system (see the specifications detailed in Section 6.1.2).

The classical PQ method (for Hard Disk Drives dual stages) mainly deals with this destructive interference between the two stages: the controller is designed in order to avoid the conditions causing these interferences (a phase difference of 180° between the two stages and, simultaneously, two identical static gains, see [63,80,86]). However, in our case, this potential problem is intrinsically dealt with the bandwidth difference imposed on our two stage system by design.

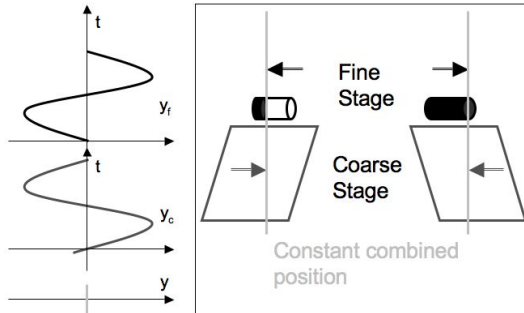


Fig. 6.11. Illustration of a dual-stage destructive interference. The two stages are moving in opposite directions, thus having no effect on the output. The two destructive-interference conditions (π phase difference between the two stages and identical gain) are met.

Through the low-pass filtered reference fed to the stepper (see Figure 6.8) and through the low-bandwidth of the stepper controller itself, a large bandwidth difference is imposed between the two stages (at least a factor ten). Therefore, since the piezoelectric device is at least ten times faster than the stepper motor and its controller, its dynamics are too fast by far to generate any uncontrolled oscillation between the two stages. The two destructive-interference conditions are never met, since the piezoelectric device, through its large bandwidth, still has a static gain of one when the coarse stage reaches its 180° phase with a static gain far less than one. Thus, the phase margin between the two stages is intrinsically above 60° , which ensures, by design, constructive interference.

6.2.4 Antagonistic objectives

Two antagonistic objectives are tracked.

- *Dynamic positioning of the output of the DDL.* This objective is mainly accessible by the active tracking of the fine stage. This

fine stage is enabling the fast and accurate realization of the main objective. Thus, the realization of objective one is enforcing the activity of the fine stage while the coarse stage is a source of perturbations.

- *Enlargement of the working area of the DDL and fine-stage saturation limits avoidance.* These objectives are realized by the coarse stage which maximize the distance to fine-stage-saturation and enlarge the complete stroke of the DDL. Thus, objective two is optimal when the fine stage remains in the center of its stroke.

The antagonism of the objectives for the DDL is directly visible through the activity of the two stages. Objective one is enforcing activity of the fine stage and minimizing activity of the coarse stage, while objective two is enforcing the contrary.

6.3 Simultaneous coordination of 2 DDLs

One particular configuration of the DDLs optical-system in Paranal foresees the use of a single active DDL to compensate the atmospheric turbulence, while the others are fixed (see Figure 6.12). This solution is easier to implement, but suboptimal in term of performance for stabilizing the light beams.

A higher level of coordination of each DDL on the controlled optical path enhances the overall performance in combining their effect two by two. This new degree of overactuation reduces the overall tracking error in combining their atmospheric rejection ratio.

Thanks to the proposed controller-structure (see Section 6.2.3), which relies on the fine stage as the main actuator, the DDL dual-stage system can be seen as a second-order system with the fine stage's characteristics, whenever it is not saturating. In fact, the coarse stage acts only to keep the fine stage within its stroke limits, while the accuracy is ensured by the latter. Calling respectively F_1 and F_2 the dynamic models of the two DDLs in closed-loop configuration (note that F_1 and F_2 should be identical by design), these

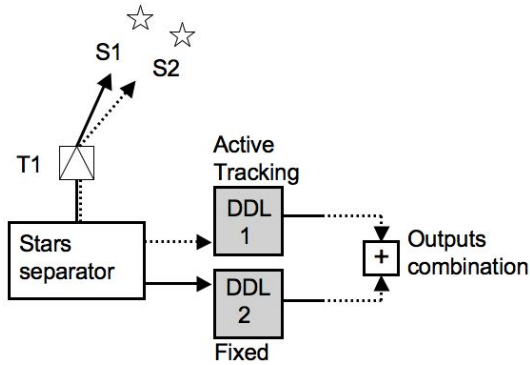


Fig. 6.12. The DDL global control structure (represented symbolically here) relies on a single DDL to track the reference, rejecting the atmospheric turbulence (here T_1 represents the first telescope). The controlled output is composed of the differential optical path between the two stars, with the same potential effect of each DDL on the optical path length.

are combined optimally without changing their respective controllers (see Figure 6.13). As can be seen in Figure 6.13, the two DDLs keep their own closed-loop controllers and structure. Note in the same Figure, that the two DDLs have their own decoupled feedback sensors, ensuring their respective stability.

The tracking error of the first DDL (F_1) is injected as a reference signal for the second DDL (F_2). In doing so, the second DDL will react and try to cancel the remaining error. In order to avoid an exaggerated response of the combined DDLs to the same tracking error, producing large overshoots, a prediction of the first DDL response to this reference ($P_1 y_1$) is added. This predictor has the dimension of a derivative. Thus a derivative of y_1 is subtracted from the tracking error fed to the second stage as a reference signal (see Figure 6.13). Under the initial hypothesis that both DDLs are similar ($F_1 = F_2 = F$) the following global transfer functions are obtained:

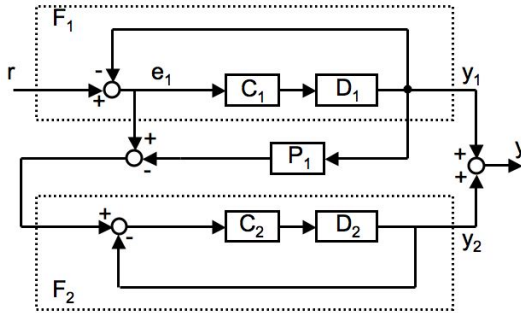


Fig. 6.13. The proposed multi-DDL control strategy relying on the two DDLs enables a more efficient reference tracking. F_1 and F_2 represent the two DDLs in closed-loop configurations. C_1 and C_2 are the controllers of the DDLs, each combining the effect of a fine and coarse stage. P_1 is the predictor of the first DDL response, it has a derivative structure.

$$Y = R(2F - F^2) - kF^2Rs$$

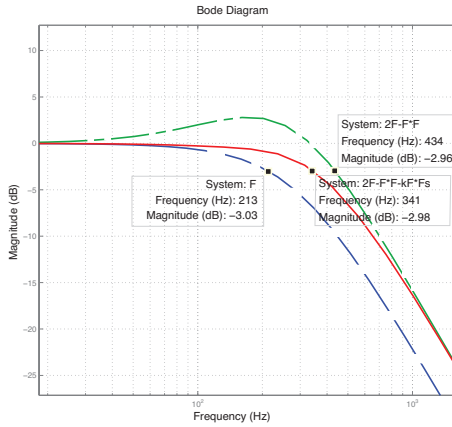
$$\frac{Y}{R} = 2F - F^2 - F^2P_1$$

Using the following decomposition $F = \frac{N(s)}{D(s)}$, we get:

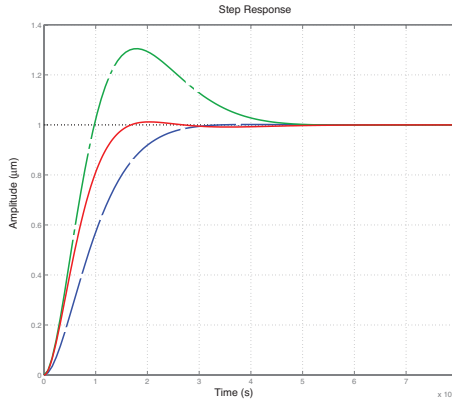
$$\frac{Y}{R} = \frac{2DN - N^2(1 + s)}{D^2}$$

The pole placement clearly does not change, when using this control scheme. However, its multiplicity is doubled and the zeros are modified. The predictive term, coming from P_1 , also introduces a new zero.

The results of this proposed control scheme using multi-DDL overactuation look very similar to the linear gain change of the controllers. The main difference is that a clear bandwidth enhancement by a factor of nearly 1.6 (visible in Figure 6.14(a)) is obtained through the overactuation characteristic of our complete system. The adequate coordination of the two DDLs results in this performance while



(a) Multi-DDL parallel control strategy: Comparison in the Bode plot. The bandwidth enhancement is clearly visible through the comparison of the frequencies at minus 3dB of the different schemes.



(b) Multi-DDL parallel control strategy: Comparison of the step responses.

Fig. 6.14. Comparison of the global control strategy. First, the case where a single DDL is active and the other one is fixed (dashed line). Second, the case where the two DDLs actively track the reference with (continuous line) and without (dash-dotted line) a prediction of the first DDL response.

no controller gain has changed. Thus, this result is obtained without encountering the risk of saturating the fine stage, which is clearly the case with high-gain controllers. Moreover, there are no stability issues since each DDL controller is designed individually, the two DDLs being combined uniquely through their references.

The simulations in Figure 6.14(b) illustrate clearly the faster response of this new scheme with respect to the classical one using only one DDL. In particular, the time constant comparison of the step responses is very conclusive.

6.4 DDL prototype performances

6.4.1 Experimental setup

DDL prototype and laser metrology

The DDL prototype available at the EPFL is built from a PM stepper motor NEMA 23 from "Ultramotion", combined with a lead-screw

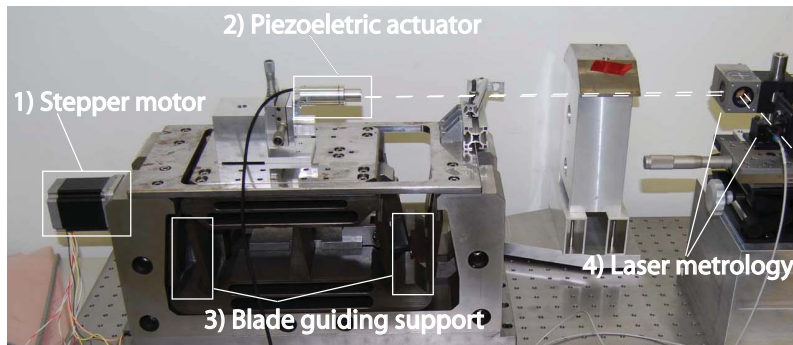


Fig. 6.15. Experimental setup: 1) Stepper motor, driving the coarse stage; 2) Piezoelectric actuator, driving the fine stage; 3) Double parallelogram flexure with notch-hinges; 4) Laser metrology with sub-nanometer resolution

which covers a full stroke of 70 mm. The motor is powered by a current amplifier developed by the PRIMA consortium. Also, the blade guiding system is a tailor-made product. The piezoelectric S-325 is from PI with a course of 30 μm and a bandwidth of approximately 300 Hz. A laser interferometer (Agilent 10897B) with 1.25 nm resolution is used to measure the displacement of the actuators which is provided to the VME rack. In Fig. 6.15 a schematic representation of the complete installation is given.

Data acquisition hardware

- **VME rack:** Two cards are installed into the VME rack to get access to the laser metrology: the Agilent 10897B laser board, which gives the position measured with sub-nanometer resolution, and the NI VME-MXI-2 board. The VME rack interfaces the memories of both boards, so that the measurements are available to a PC.
- **NI PCI-MXI-2:** This board is connected to the NI VME-MXI-2 board, so as to access the position measurement and to establish the real time control loop.
- **NI PCI-6025E and NI PCI-6251:** These cards provide the 3 analog outputs to control the piezoelectric actuator and the stepper motor. One of them is also used as timing source to synchronize the measurement and the excitation of the actuators.

Software

The EPFL prototype uses LabView 8.2 to implement the controllers. In a timed loop all the necessary operations are executed, where the loop is timed with the clock of one of the NI DAQ boards. To achieve good closed-loop performance, the sampling rate is selected to be 5kHz.

The final system installed at Paranal runs under VxWorks in an ESO-compatible environment which ensures the stability of the sampling (no jitter in the timing). The sampling rate will be 8kHz.

6.4.2 DDL overall performances

In pure tracking mode, a realization of a stochastic Kolmogorov process (with a frequency content up to 250 Hz) is used as a reference. This signal is representative of the atmospheric disturbances encountered. In reality, the reference is not a pure Kolmogorov signal. From time to time, there is a brusque change in position or even a switch in stroke from one end to the other. The behavior of the system in such cases can be tested through performing step responses with displacements of different amplitudes.

The controllers need to track the reference with less than 70 nm RMS error, in pure tracking, and cover the whole bandwidth of 250 Hz. In addition, they need to be robust all over the stroke range and for all the different kind of references.

As the controller of the piezoelectric stack actuator is fairly simple (hysteresis being compensated by internal electronics), the results presented hereafter are mainly discussing the PM (Permanent Magnet) stepper motor controller performances and their influence on the overall tracking performances.

Kolmogorov tracking

To analyze the quality of the tracking performance, several characteristics are evaluated.

- The root mean square error

$$\text{RMSE} = \sqrt{\frac{1}{n} \sum_{i=1}^n e_i^2}, \quad (6.3)$$

where n is the number of samples.

- The maximal absolute error

$$|e|_{max} = \max_e |e_i|. \quad (6.4)$$

- The mean absolute error

$$\bar{e} = \frac{1}{n} \sum_{i=1}^n |e_i|, \quad (6.5)$$

where n is the number of samples.

- The power dissipation

$$P_{RMS} = 2R (i_{a_{RMS}}^2 + i_{b_{RMS}}^2), \quad (6.6)$$

with $R = 0.5 \Omega$.

Final decoupled parallel SISO control scheme

The proposed global control structure based on a single metrology to close both loops combines optimally both stages. The global control structure (including the coarse stage feedback based on the coordinator) has been validated. No special unwanted oscillations between the two stages and no time-drift behavior due to the coordinator have been observed: this validates our closed-loop control structure. Moreover, thanks to the proposed double-stage coordination, the piezo-electric stack actuator never reaches its saturation limits while the complete system is working (see Figure 6.16).

The control approach, which relies on direct coil-current control of the PM stepper motor, results in very good tracking performances: the rms residual tracking error is as low as the measurement noise ($E < 8$ nm rms) and the movement of the coarse stage does not result in any visible tracking error of the overall system. The coordinator based control structure is the leading element that gives these outstanding results in stochastic trajectory tracking.

The interested reader will find more details in [70].

Comparison of obtained performances with respect to standard approaches

In order to validate the proposed coordination design (labeled direct coil control in this section), the performances of the prototype

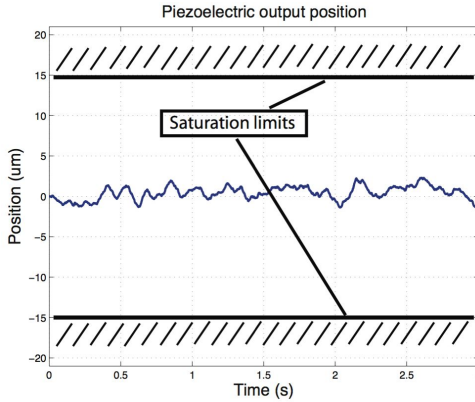


Fig. 6.16. The piezoelectric actuator controlled output never reaches its saturation limits during Kolmogorov-trajectory tracking.

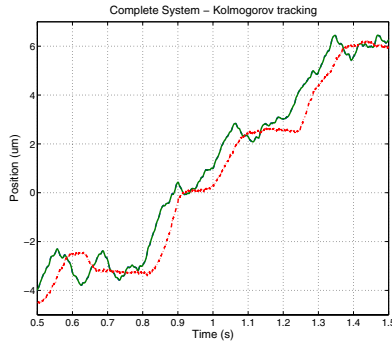
are compared to standard dual-stage/multi-variable control schemes (LQR, PQ, PI-linearized, Flatness-based).

Kolmogorov tracking: Kolmogorov-signal tracking was executed over 10 seconds. In Figure 6.18, only a detail is given in order to make differences visible. The tracking performance is evaluated with the same relationships as in section 6.4.2.

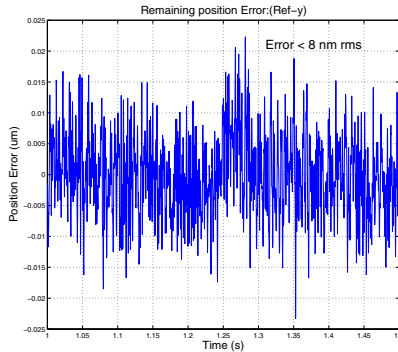
In Fig. 6.18(b) one can see that all the controllers guarantee that the coarse stage keeps the fine one within its saturation limits, which

Table 6.1. Tracking results in implementation: comparison of the control scheme I propose (*Direct Coil*) with respect to classical methods

	RMSE [nm]	$ e _{max}$ [nm]	\bar{e} [nm]	P [W]
<i>Direct Coil</i>	25	308	19.6	2.25
Flatness based	26.6	147.5	20.7	0.016
PI-linearized	22.8	133	17.7	0.017
PQ	40	270	31	0.012
LQR	44.8	640	30.7	0.015

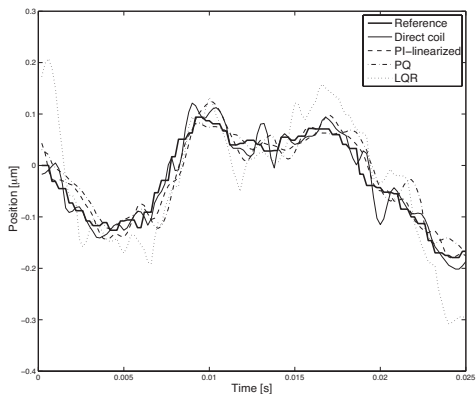


(a) Tracking of a Kolmogorov realization: direct voltage control. The continuous line is the position reference and perfectly superimposed is the measured final output; the dash-dotted line is the coarse stage estimated position.

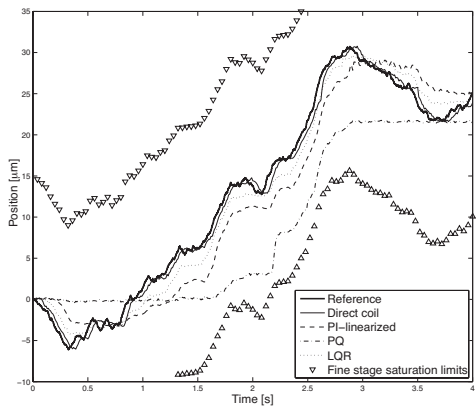


(b) Remaining tracking error.

Fig. 6.17. System response to the same realization of the stochastic Kolmogorov process with a frequency content of up to 200 Hz. Results obtained with the direct coil-voltage control of the PM stepper motor and the integral controller, giving a residual rms error less than 8 nm rms and a maximum instantaneous error of 30 nm.



(a) Detail of DDL output position; time scale 0 s to 0.025 s



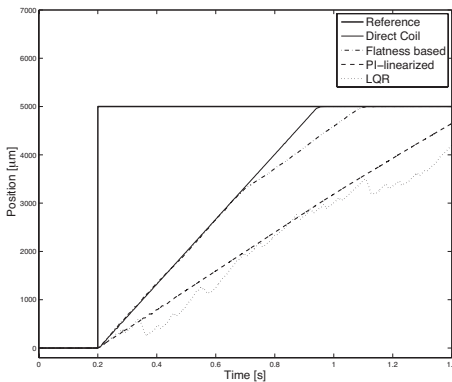
(b) Detail of the estimated coarse-stage position; time scale 0 s to 4 s; the fine-stage saturation limits are marked by the triangles

Fig. 6.18. Kolmogorov-signal tracking: comparison of different control-laws' performances.

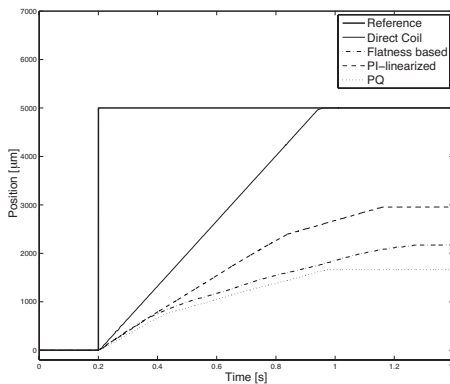
is necessary for the functionality of the system. In case of the PQ controller the coarse-stage action is quite at the limit of what is allowed (Fig. 6.18(b)); nevertheless the performance is similar to the one of the LQR controller in terms of RMS and mean error (Table 6.1 column 1 and 3). Furthermore, the three controllers based on the decoupled SISO design (direct coil, flatness based and PI-linearized) have similar RMS and mean errors (Table 6.1 column 1 and 3). Since they all use the same fine-stage controller, which gives the precision to the system, this is not surprising. In Fig. 6.18(a) the LQR shows a sort of oscillatory behavior and bigger deviation from the reference than the rest of the controllers. Checking the maximal error of the controllers (Table 6.1 column 2), one can see that just the LQR controller has the largest maximal error. Whereas for the direct coil and PQ controller the deviation peaks are less marked (Fig. 6.18(a)), also the maximal error of these controllers is smaller than for the LQR (Table 6.1 column 2). The PI-linearized controller does not show any oscillations around the reference (Fig. 6.18(a)), which is also confirmed by the smallest maximal error of all controllers (Table 6.1 column 2). In case of the PQ controller, one can also clearly see the effects of static friction on the coarse stage action (Fig. 6.18(b)), which leads to a sort of stepping behavior. The other controllers show a smoother coarse-stage movement especially the direct-coil controller (Fig. 6.18(b)). This controller also injects constantly a lot of energy into the system and thus the static friction does not affect the coarse-stage movement. Column 4 in Table 6.1 shows that all the controllers based on exact feedback linearization dissipate much less power in tracking than the direct-coil controller.

Based on the tracking performance in Table 6.1 the PI-linearized controller is rated best, since it has lowest values in RMS, absolute and maximal error and additionally the power dissipation is much less than for the direct-coil controller.

5000 μm step response: To test the system for sudden large displacements in the reference, step displacements of 5000 μm are applied to the DDL. One experience is done in the center of the stroke, where no force is applied to the blades (Fig. 6.19(a)), and another



(a) DDL output position for a $5000 \mu\text{m}$ step displacement at the center



(b) DDL output position for a $5000 \mu\text{m}$ step displacement towards the extremity of the stroke

Fig. 6.19. Tests of sudden large displacements in the tracking reference.

towards the end of the stroke, where a big reaction force acts on the coarse-stage actuator (Fig. 6.19(b)).

In order to obtain the results illustrated in Fig. 6.19, strict rate limitations for speed have been introduced, for the controllers based on the decoupled SISO structure, as mentioned in [70]. With these measurements, taken the system with direct-coil control performed best, since it allows the highest speed without destabilizing the system (Fig. 6.19(a)). In case of the LQR controller, no such speed limitation can be introduced, which leads to a random behavior caused by de-synchronization between rotor and the generated magnetic field (Fig. 6.19(a)). Similar behavior was also observed for the other methods based on exact feedback linearization depending on position and moving direction of the coarse stage. Towards the extremities of the stroke they also have problems to follow the reference. As one can see in Fig. 6.19(b), if the system is driven by a controller based on linearization, the DDL suddenly stops to move. The controllers do not allow the motor to generate enough torque to make the table move. With the direct coil controller, the system has no problems to follow the reference (Fig. 6.19(a)), because as soon as the difference between the reference and the real position increases a bigger torque is generated due to the particular structure of the controller. The input saturation is present by imposing a ramp instead of the true step reference. In case of a controller based on feedback linearization, this is different. The input I already saturates at the beginning of the ramp in order to follow it. When the tracking error starts to increase there is no more room to generate more torque, since the input is already saturated (Fig. 6.20).

The interested reader will find more details in [96].

Based on these comparisons (summarized in Table 6.2), the closed-loop coordination scheme using the direct-coil-control of the PM stepper motor I proposed is undoubtedly validated. The principles of this control scheme were implemented at the final installation of the DDLs, in Paran al, in August 2008.

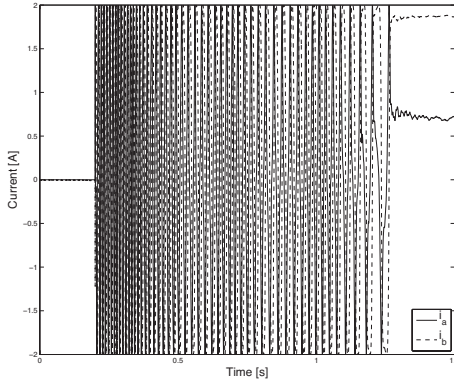


Fig. 6.20. Inputs i_a and i_b of the flatness-based controller during a 5000μ step displacement towards the extremity of the stroke

Table 6.2. Qualitative PM-stepper-motor controller comparison

	Decoupled SISO structure			Global structure	
	Amplitude = fixed Phase = controlled	Amplitude = controlled Phase = fixed		LQR	PQ
	<i>Direct coil</i>	PI-linearized	Flatness		
RMS error	++++	++++	++++	++	++
e_{max}	+++	++++	++++	+	++++
Power dissipation	-	++++	++++	++++	++++
Step response	++++	+	-	---	--
Robustness	++++	--	--	---	---

6.5 Conclusion

6.5.1 Link to preceding chapters

Close-loop coordination can be easily interpreted as a potential function scheme (see Chapter 5). Indeed, the closed-loop coordinator as main objective tends to minimize a potential function corresponding to the tracking error. Furthermore, the second objective (maximiz-

ing the distance to saturation for the fine stage) is also directly interpretable as a potential function to minimize. The links between these two chapters are thus obvious.

Moreover, the DDL underlying structure made from the combination of two collinear prismatic joints is very simple. Indeed, the DDL configuration space $\mathbb{R} \times \mathbb{R}$ is obviously simply connected and compact (from the saturation limits of the actuators). However, any more complex adaptative-optics (even so it doesn't exist now) including rotative joints could encounter some of the topological difficulties described in Chapter 4.

6.5.2 Contributions

The following four original contributions have been detailed in this chapter. First, in Section 6.2.3, the closed-loop scheme enabled a constructive coordination of the dual-stage mechatronic system (Figure 6.10). Saturation of the fine stage has been avoided and feedback signals have been distributed adequately. Second, all specifications were achieved successfully through the overactuation coordination scheme (Section 6.4.2). Third, a particular overactuation scheme using simultaneously several DDLs to track the same reference has been proposed (Section 6.3). This scheme would use the intrinsic characteristics of the piezoelectric more efficiently to even improve the overall performances. Fourth, the proposed closed-loop coordination scheme was successfully implemented on the DDLs, in Paranal, Chile, in August 2008 (see a selection of pictures in Appendix D).

Conclusions and perspectives

In this thesis, the coordination of overactuated systems has been investigated under the three following scopes: differential geometry, potential functions and closed-loop control. These three different insights were shown to be closely linked together through their coordination scheme introduced in Chapter 2. Each of these research axes brought a new insight on the general-coordination matter.

First, in Chapter 4, some *differential geometry* properties have been shown to be of great interest in order to enforce the repeatability and predictability of the responses to the inverse kinematic problem. Particularly, the involutivity of a vector-field-parameterization of the solution set was shown to enable closed responses of the joints whenever a periodic task was to be realized by the end-effector. In this context, a constructive method enforcing a foliation of the solution set using complementary 1-forms and involutive vector fields was proposed (Sections 4.3.3 and 4.3.4).

Second, in Chapter 5, a simultaneous multiple objectives coordination scheme using gradient of *potential functions* was proposed. In this context, secondary objectives were expressed by potential functions, the gradient of which were tracked in the null space of the main task. The proposed scheme, called soft extension of the jaco-

bian, enabled a full decoupling of the main task with any secondary one (Section 5.3.3). Furthermore, it was clearly demonstrated that the soft extension of the jacobian with potential functions, under certain conditions, drives the joints response toward a periodic cycle, when realizing a periodic task with the end-effector (Theorem 5.1). Moreover, a clear hierarchy of the different objectives was obtained through successive projections into reduced null spaces (Section 5.3.5). And finally, in Section 5.5, a compliant, flexible and periodic coordination scheme was obtained through the combination of the complementary 1-form (introduced in Section 4.3.4) with the task manifold (introduced in Section 5.1.1).

Third, in Chapter 6, the PRIMA-DDL project provided a very interesting application to our research. The success of the project (in term of tracking performances) entirely depended on the proposed *closed-loop coordination* scheme (Section 6.2). A particular high-level of overactuation using actively multiple DDLs to track the position reference was proposed (Section 6.3). The dual-stage optomechatronic system with its overactuated closed-loop coordination was successfully implemented in Paranal, Chile, at the ESO facility.

The concepts underlying the coordination of overactuated systems introduced in this thesis can be extended to any redundant system. As a matter of fact, a similar coordination scheme was applied to the model of a human-shoulder interpreted as an overactuated bio-mecanical system (see Appendix A).

This thesis intended to link together complex mathematical tools (differential geometry and topology) with robotics in its general expression. The mathematical tools such as topology and differential geometry request deep abstraction capabilities and, thus, they gain largely in clarity when they can be applied to a concrete field such as robotics. The latter in turns, gain in understanding of their underlying group structure. The author is convinced that, a global optimized joints trajectory is only possible when considering the topology of the concerned manipulator. The Hessian-like proposed algorithm is one attempt in this direction. The gap between the practical aspects of

robotics and the mathematical developments at our disposal is one of the main open research-area.

Concerning the PRIMA-DDL project, from the control point of view, a promising further development concerns the implementation of the high-level coordination scheme implying several DDLs simultaneously (Section 6.3). This scheme would clearly enlarge the bandwidth-response of the overall system. Moreover, another further development could take advantage of a combination of 1 PM stepper motor with several piezoelectric actuators. This potential new hardware scheme would take advantage of the optical nature of the output to improve the response of the DDL.



A

Shoulder coordination

A particular coordination scheme has been applied to the dynamical model of a human shoulder. The latter is indeed a highly overactuated system through its more than twenty muscles acting on the 6 degrees of freedom articulation. Constructive coordination, in this case, is achieved when the activation of the different muscles enables to follow a predefined motion with realistic forces.

A.1 The shoulder as an overactuated system

The shoulder is a very complex biomechanical system of four articulations, actuated by more than twenty muscles. Hence, the system is highly overactuated and there is an infinite number of possible muscle force combinations realizing the same task (see [1]). The muscle forces have a direct impact on the joint reaction force and the design of shoulder implants is highly influenced by the prevailing contact forces.

The shoulder is conceived as a dynamical system with input (neural excitation), states and output (humerus 3D position). Instead of using complex geometries, as it is done in FEM, simple, biomechanical concepts are considered. A physically comprehensible macroscopic model of the shoulder is obtained.

In order to solve the indetermination of the muscle-force distribution, as for redundant robots, the immersion map of the muscle forces (considered as actuators of the system) to the generalized forces (realizing the desired movement in space) has to be inverted. In this

context, the matrix of moment arms serves as immersion map. This matrix depends highly on the wrapping of the muscles around the glenohumeral joint.

The model is to be able to reproduce a predefined movement (parametrized in time), and to calculate the corresponding contact force in the glenohumeral joint. The humeral position is chosen as system output. The neural excitation of the muscles takes the role of the system input.

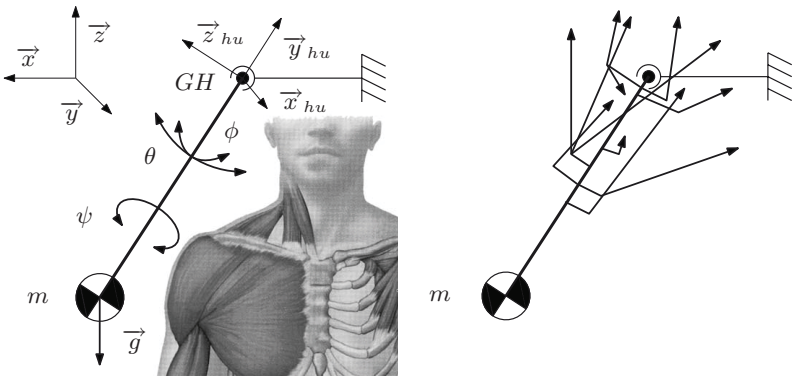


Fig. A.1. Simplified geometries: The glenohumeral joint is modeled by a spherical joint allowing three rotations: θ : abduction/adduction, ϕ : flexion/extension, ψ : rotation. A coordinate system is attached to the humerus which has its origin in the center of the glenohumeral joint. Eleven muscles actuate the humerus.

The glenohumeral joint (GHJ) is modeled by a spherical joint allowing three rotations but no translations (Figure A.1). The rotations are the Euler angles (XZY sequence): θ around the x-axis of the humerus (abduction/adduction), ϕ around the z-axis (flexion/extension) and ψ , rotation around the y-axis. The humerus embedded coordinate system is chosen according to the recommenda-

tions of [106] with its origin coincident with the rotation center of the GHJ. All the anthropometric data used in this model are provided by the ISG [13]. Furthermore, in this model, we consider the simple hypothesis that the position of the scapula is fixed on the thorax.

In the next section, a dynamical model of the shoulder is derived using the Lagrangian formalism.

A.2 Shoulder equation of motion

According to [10] the angular velocity $\vec{\omega}$ is defined as:

$$\vec{\omega} = \dot{\theta}\vec{a}_1 + \dot{\phi}\vec{a}_3 + \dot{\psi}\vec{a}_2'' \tag{A.1}$$

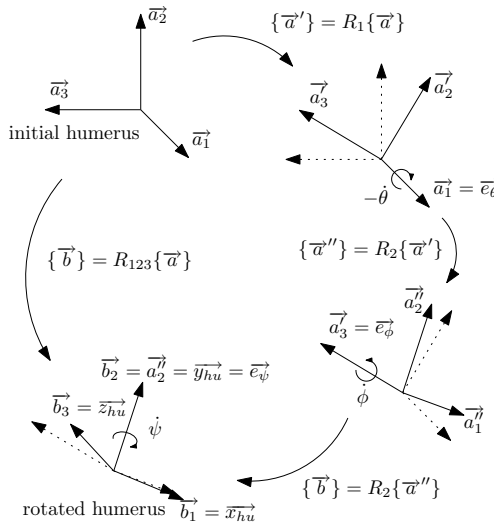


Fig. A.2. Rotation sequence XYZ: The initial coordinate system $\{\mathbf{a}\}$ is turned into $\{\mathbf{b}\}$ through 3 rotations around $\mathbf{e}_\theta = \mathbf{a}_1$, $\mathbf{e}_\phi = \mathbf{a}_3'$ and $\mathbf{e}_\psi = \mathbf{a}_2''$

As the three axis are not perpendicular, $\vec{\omega}$ is expressed in the humeral coordinate system:

$$\begin{aligned}\vec{\omega} = & (\dot{\theta} \cos(\psi) \cos(\phi) - \dot{\phi} \sin(\psi)) \cdot \vec{b}_1 \\ & + (-\dot{\theta} \sin(\phi) + \dot{\psi}) \cdot \vec{b}_2 \\ & + (\dot{\theta} \sin(\psi) \cos(\phi) + \cos(\psi) \dot{\phi}) \cdot \vec{b}_3\end{aligned}\quad (\text{A.2})$$

Considering the humerus as an infinite rigid body moving in 3D space, its kinetic energy is only due to rotation:

$$\begin{aligned}T = & \frac{1}{2} \cdot I_{arm}^t \cdot (\omega_1^2 + \omega_3^2) + \frac{1}{2} \cdot I_{arm}^l \cdot \omega_2^2 \\ = & \frac{1}{2} \left(I_{arm}^t \cdot \left[(\dot{\theta} \cos(\psi) \cos(\phi) - \dot{\phi} \sin(\psi))^2 \right. \right. \\ & \left. \left. + (\dot{\theta} \sin(\psi) \cos(\phi) + \cos(\psi) \dot{\phi})^2 \right] \right. \\ & \left. + I_{arm}^l \cdot (-\dot{\theta} \sin(\phi) + \dot{\psi})^2 \right)\end{aligned}\quad (\text{A.3})$$

where I_{arm}^t and I_{arm}^l are the transversal and longitudinal moment of inertia of the arm. Its potential energy V is due to gravity:

$$V = m_{arm} \cdot g \cdot L_{arm} \cdot [1 - \cos(\phi) \cos(\theta)] \quad (\text{A.4})$$

Using the Lagrangian approach we have:

$$L = T - V \quad (\text{A.5})$$

Considering $q_1 = \phi$, $q_2 = \theta$ and $q_3 = \psi$ as the generalized coordinates, we have:

$$\frac{d}{dt} \left(\frac{\partial L}{\partial \dot{q}_i} \right) - \frac{\partial L}{\partial q_i} = Q_i \quad i = 1, 2, 3. \quad (\text{A.6})$$

where Q_i are the generalized forces corresponding to the generalized coordinates. Virtual work has the form:

$$\delta W = \overline{M^{tot}} \cdot \vec{\delta\theta} \quad (\text{A.7})$$

with $\vec{\delta\theta}$ the virtual rotation which can be expressed in function of the generalized coordinates:

$$\vec{\delta\theta} = \sum_{i=1}^3 \frac{\partial \vec{\omega}}{\partial \dot{q}_i} \delta q_i. \quad (\text{A.8})$$

Substituting (A.8) into (A.7) gives:

$$\delta W = \sum_{i=1}^3 Q_i \delta q_i = \overrightarrow{M^{tot}} \cdot \frac{\partial \vec{\omega}}{\partial \dot{q}_i} \delta q_i. \quad (\text{A.9})$$

Therefore, the generalized forces correspond to the projections of the resulting angular momentum $\overrightarrow{M^{tot}}$ on the axes about which the Euler-angle rotations have been performed. Defining (see Figure A.2)

$$\vec{e}_\theta = \frac{\partial \vec{\omega}}{\partial \dot{\theta}} = \vec{a}_1, \quad \vec{e}_\phi = \frac{\partial \vec{\omega}}{\partial \dot{\phi}} = \vec{a}_3', \quad \vec{e}_\psi = \frac{\partial \vec{\omega}}{\partial \dot{\psi}} = \vec{a}_2'' \quad (\text{A.10})$$

it follows

$$\begin{aligned} Q_\theta &= \vec{e}_\theta \cdot \overrightarrow{M^{tot}}(\phi, \theta, \psi) \\ Q_\phi &= \vec{e}_\phi \cdot \overrightarrow{M^{tot}}(\phi, \theta, \psi) \\ Q_\psi &= \vec{e}_\psi \cdot \overrightarrow{M^{tot}}(\phi, \theta, \psi) \end{aligned} \quad (\text{A.11})$$

which reformulated in matrix form gives:

$$\begin{aligned} \begin{pmatrix} Q_\theta \\ Q_\phi \\ Q_\psi \end{pmatrix} &= [B] \overrightarrow{M^{tot}} = \begin{bmatrix} \vec{e}_\theta^T \\ \vec{e}_\phi^T \\ \vec{e}_\psi^T \end{bmatrix} \cdot \begin{pmatrix} M_x^{tot} \\ M_y^{tot} \\ M_z^{tot} \end{pmatrix} \\ &= \begin{bmatrix} -\sin(\psi) & 0 & \cos(\psi) \\ \cos(\phi) \cos(\psi) & -\sin(\phi) \cos(\phi) \sin(\psi) \\ 0 & 1 & 0 \end{bmatrix} \\ &\quad \cdot \begin{pmatrix} M_x^{tot} \\ M_y^{tot} \\ M_z^{tot} \end{pmatrix} \end{aligned} \quad (\text{A.12})$$

The following eleven muscles are included in the model: Deltoidus (divided into a posterior, medial and anterior part), coracobrachialis,

infraspinatus, teres minor, teres major, supraspinatus, subscapularis, latissimus dorsi and pectoralis major. In the work of Breteler [13], every muscle is divided into 2-11 fibers. In order to simplify the dynamical model, one resulting fiber per muscle is considered. Therefore, the fibers are summed up and weighted by their Physiological Cross-Sectional Area (PCSA). Moreover, the muscle force is modeled using a linear law (see Equation A.13) with respect to the muscle activity a . This allows to easily find the mapping between the muscle force and the muscle activity.

$$F_M = a \cdot F^{max} \quad (\text{A.13})$$

The maximal muscle force F^{max} is obtained from the PCSA and is supposed to be:

$$F_{max} = PCSA \cdot 40 \left[\frac{N}{cm^2} \right] \quad (\text{A.14})$$

The factor of 40 $\left[\frac{N}{cm^2} \right]$ is very controversial in the literature. It has been chosen according to [71]. a is called the activity of the muscle. It corresponds to the internal state of the muscle and its very fast dynamics is neglected with respect to the neural excitation s .

$$a \approx s \quad (\text{A.15})$$

where s is the neural excitation ($0 < s < 1$) and τ ($40[\mu s]$) its small time constant (see [97] for a similar simplification). s is the input variable of the dynamical system.

To sum up, there are eleven inputs (the neural excitations), 17 states (11 corresponding to the activities of the muscles and 6 corresponding to the generalized coordinates with their time derivatives) and 3 outputs (the 3D position of the humerus extremity).

Now that the dynamical model of the shoulder has been established with its corresponding states, inputs and outputs, a muscle-coordination scheme based on the pseudo-inverse map (introduced in Section 4.3.1) is developed in the next section. The aim is to coordinate the muscle acting on the shoulder in order to realize a predefined positioning task of the humerus.

A.3 Muscles coordination

A.3.1 The matrix of moment-arms

The total muscle moment of force:

$$\overrightarrow{M}_{tot} = \sum_j \overrightarrow{M}_j = \sum_j \overrightarrow{r}_j \times \overrightarrow{d}_j \cdot F_{M_j} \quad (\text{A.16})$$

can be written as a matrix multiplication [48], [59]:

$$\overrightarrow{M}_{[3 \times 1]} = [B]_{[3 \times 11]} \overrightarrow{F}_{[11 \times 1]} \quad (\text{A.17})$$

Where

$$[B] = \left[\overrightarrow{r}_1 \times \overrightarrow{d}_1 \cdots \overrightarrow{r}_{11} \times \overrightarrow{d}_{11} \right] \text{ et } \overrightarrow{F} = \begin{pmatrix} F_{M_1} \\ \vdots \\ F_{M_{11}} \end{pmatrix} \quad (\text{A.18})$$

Applying the projection matrix P we find the mapping between the muscle forces \overrightarrow{F} and the generalized forces \overrightarrow{Q} that we call the matrix of moment-arms $[W]_{[3 \times 11]}$:

$$\overrightarrow{Q}_{[3 \times 1]} = [P]_{[3 \times 3]} [B]_{[3 \times 11]} \overrightarrow{F}_{[11 \times 1]} = [W]_{[3 \times 11]} \overrightarrow{F}_{[11 \times 1]} \quad (\text{A.19})$$

$[W]$ can be thought of an immersion map from a 11 dimensional space to a 3 dimensional one. This map allows to find directly the generalized forces corresponding to the muscle forces. Thus, determining the individual forces of each muscles in order to realize a predefined movement (parametrized by the generalized forces) corresponds to the problem of inverting this map. However, as we consider a positioning task in the 3D space of the extremity of the humerus together with 11 muscles, the system is overactuated by a degree of 8 and therefore not uniquely invertible.

A.3.2 Pseudo-inverse map: 1st coordination

In order to find a reasonable distribution of the muscle forces for a given set of generalized forces, an optimization problem is formulated with the following cost function:

$$\min_{(\vec{F}, \vec{\lambda})} G_1(\vec{F}, \vec{\lambda}) \quad (\text{A.20})$$

with

$$G_1(\vec{F}, \vec{\lambda}) = \vec{F}^T [E] \vec{F} - \vec{\lambda}^T ([W] \vec{F} - \vec{Q}). \quad (\text{A.21})$$

$[E]_{[11 \times 11]}$ is a diagonal weighting matrix. This cost function allows us to find

$$\vec{F}_{\text{eff}} = [E]^{-1} [W]^T ([W] [E]^{-1} [W]^T)^{-1} \vec{Q} = [W^+] \vec{Q} \quad (\text{A.22})$$

where $[W^+]$ is the pseudo-inverse of $[W]$. $[E]_{[11 \times 11]}$ allows both to balance the muscle forces and to modify the cost function. Whenever the sum of the square muscles forces is minimized, $[E]$ is equal to the identity matrix and the pseudo-inverse has the classic Moore-Penrose form $[W^+] = [W]^T ([W] [W]^T)^{-1}$ (see [59]). Van der Helm [100] has shown that the the results correspond best to the EMG (electromyogram) measures if the distribution is obtained by minimizing the sum of the square muscle stresses $\min(\sum \sigma_i^2)$. In this case, the diagonal elements e_i of $[E]$ are:

$$e_i = \frac{1}{PCSA_i^2} \quad (\text{A.23})$$

Where PCSA is the physiological cross sectional area of the muscle. In this paper, the latter form of $[E]$ has been chosen in order to compare the results to those found in literature. Equation (A.22) allows to find a set of F_{M_i} called effective forces \vec{F}^{eff} . They can be positive or negative. A negative muscle force makes physically no sense, as it would correspond to a muscle which pushes. Therefore F_{M_i} must verify

$$f_{\min}^i < F_{M_i} < f_{\max}^i \quad (\text{A.24})$$

A.3.3 Nullspace constraints: 2nd coordination

A possibility to modify the muscle force vector \vec{F} without any impact on the generalized forces \vec{Q} is to consider the *null space* of $[W]$. Here, $\text{null}(W)$ is a matrix $[N]_{[11 \times 8]}$ with 8 column vectors n_j which are linearly independent. A linear combination of n_j has to be found which verifies (A.24).

$$\begin{aligned} f_1^{\min} &\leq f_1^{\text{eff}} + n_{[1,1]}\mu_1 + \dots + n_{[1,8]}\mu_8 \leq f_1^{\max} \\ &\vdots \\ f_{11}^{\min} &\leq f_{11}^{\text{eff}} + n_{[11,1]}\mu_1 + \dots + n_{[11,8]}\mu_8 \leq f_{11}^{\max} \end{aligned} \quad (\text{A.25})$$

where μ_i are the unknown multipliers. Reformulated in matrix form:

$$\vec{F}^{\min} \leq \vec{F}^{\text{eff}} + [N]\vec{\mu} \leq \vec{F}^{\max} \quad (\text{A.26})$$

\vec{F}^{\min} and \vec{F}^{\max} are obtained by evaluating the symbolic vector \vec{F} with the muscle activities $a_i = 0$ et $a_i = 1$ considering the linear muscle model (see Equation A.13). Formally, the complete muscle forces, verifying all the constraints while realizing the positioning task, are:

$$\vec{F} = \vec{F}^{\text{eff}} + [N]\vec{\mu} = \vec{F}^{\text{eff}} + \vec{F}^{\text{null}} \quad (\text{A.27})$$

In order to find the unknown multipliers μ_i , a new optimization problem can be defined taking into consideration the constraints on the muscle forces. This second optimization problem has been solved using quadratic programming. To this end, a new cost function is formulated:

$$\begin{aligned} \text{minimize: } & G_2(\vec{\mu}) = \frac{1}{2}\vec{\mu}^T[H]\vec{\mu} \\ \text{subject to: } & [A] \cdot \vec{\mu} \leq \vec{b} \\ & [A_{eq}] \cdot \vec{\mu} = \vec{b}_{eq} \end{aligned} \quad (\text{A.28})$$

The following manipulations allow to formulate our optimization problem in the form demanded in (A.28)

- Calculation of $G_{inter}(\vec{\mu}) = \frac{1}{2}\vec{F}^T[E]\vec{F}$

- Calculation of the matrix $[H]$: $h_{i,j} = \frac{\partial^2 G_{inter}}{\partial \mu_i \partial \mu_j}$

The matrix $[A]$ and the vector \mathbf{b} of the inequalities (A.28) are obtained as follows:

$$\left[\begin{array}{c|c} [N] & [0]_{11 \times 8} \\ \hline [0]_{11 \times 8} & -[N] \end{array} \right] \begin{pmatrix} \mu_1 \\ \vdots \\ \mu_{16} \end{pmatrix} \leq \begin{pmatrix} f_1^{max} - f_1^{eff} \\ \vdots \\ f_{11}^{max} - f_{11}^{eff} \\ -f_1^{min} + f_1^{eff} \\ \vdots \\ -f_{11}^{min} + f_{11}^{eff} \end{pmatrix} \quad (\text{A.29})$$

the matrix $[A_{eq}]$ and the vector \vec{b}_{eq} of the equalities:

$$\left[[I]_{8 \times 8} \mid -[I]_{8 \times 8} \right] \begin{pmatrix} \mu_1 \\ \vdots \\ \mu_{16} \end{pmatrix} = \begin{pmatrix} 0 \\ \vdots \\ 0 \end{pmatrix} \quad (\text{A.30})$$

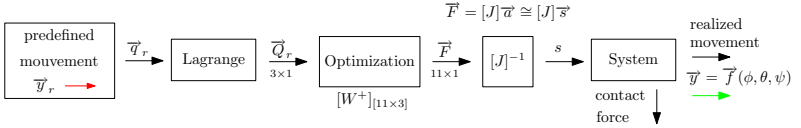


Fig. A.3. Overview of the proposed algorithm. y_r : predefined movement, q_r : generalized coordinates, Q_r : generalized forces, $[W^+]$: pseudo-inverse of the moment arm matrix, F : muscle forces, s : neural excitations (system input), y : realized movement.

Once the muscle force vector \vec{F} is known, the corresponding neural excitations are calculated using the mapping between the muscle force and the muscle activity a . Thanks to the linear force law, the

mapping is simply the Jacobian matrix $[J]$ obtained from equation (A.13). As $[J]$ is square and positive definite, it is invertible:

$$\vec{F}_{[11 \times 1]} = [J]_{[11 \times 11]} \vec{a}_{[11 \times 1]} \Rightarrow \vec{a} = [J^{-1}] \vec{F} \quad (\text{A.31})$$

As the dynamics of the muscle activity are very fast compared to the realized movements, the muscle activity a is supposed to be approximately equal to the neural excitation s for the mapping. Hence $\vec{s} \approx [J^{-1}] \vec{F}$.

A.4 Conclusion

A particular open-loop coordination scheme was applied to the dynamical model of a human shoulder, which was considered as a highly overactuated system. Constructive coordination was achieved with the correct activation of the different muscles in order to realize a predefined motion with realistic forces. The successful muscle-coordination results are illustrated in movies (see Appendix E).

B

Blade guiding analysis

A detailed description of the model of the double parallelogram flexure with notch hinges used to constrain the rectilinear movement of the DDL is made (see [82]). A particular focus on its first resonant mode and its dependency with respect to position is made.

Conceptually, the blade guiding support of the DDL can be schematized by two rigid bodies, with respective masses M and m , interconnected by two sets of blades, the main ones with rigidity k_1 , and the auxiliary ones with rigidity k_{1p} . The auxiliary blades guarantee the horizontal displacement of the main mass M . The parasitic vertical deflexion of the main set of blades is exactly compensated by the auxiliary one, since the blade length is equivalent. The mass M remains indeed perfectly horizontal (see Figure B.1). Only m , the intermediate platform, adapts its height accordingly. x_1 is the horizontal displacement of M and x_2 is the horizontal movement of the small mass m . x_3 is the corresponding deflection of the small mass m .

The coordinates x_1 , x_2 and x_3 are not free, but linked by geometrical constraints:

$$C_1 = 2x_2 - x_1 = 0 \tag{B.1}$$

$$C_2 = x_3 + 3x_2^2/5/l = 0 \tag{B.2}$$

C_1 results from a mechanical lever (not represented in Figure B.1), constraining the horizontal displacement of the two masses, while C_2 indeed results from the blade mechanical coupling (see [40]).

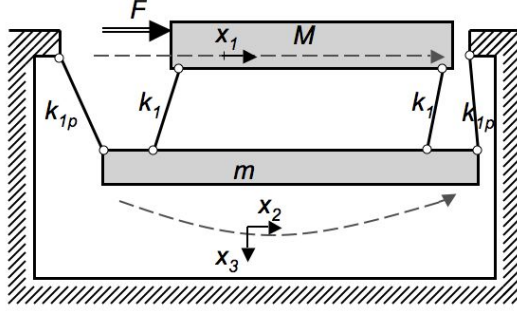


Fig. B.1. Schematic representation of the blade guiding support with its coordinates and parameters. The dashed lines correspond to the vertical deflection of the intermediate mass m and the horizontal motion of the main mass M .

Using the Lagrangian formalism, the system can be described as follow:

$$\mathcal{L} = \frac{1}{2} (M\dot{x}_1^2 + m(\dot{x}_2^2 + \dot{x}_3^2) - k_{1p}x_2^2 - k_1(x_2 - x_1)^2)$$

$$\frac{d}{dt} \left(\frac{\partial \mathcal{L}}{\partial \dot{x}_i} \right) - \frac{\partial \mathcal{L}}{\partial x_i} = F_i - \sum_{j=1}^2 \frac{\partial C_j}{\partial x_i} \lambda_j, \quad \text{for } i = 1, 2, 3$$

$$M\ddot{x}_1 = u + k_1(x_2 - x_1) - \frac{\partial C_1}{\partial x_1} \lambda_1 - \frac{\partial C_2}{\partial x_1} \lambda_2$$

$$m\ddot{x}_2 = -k_{1p}x_2 - k_1(x_2 - x_1) - \frac{\partial C_1}{\partial x_2} \lambda_1 - \frac{\partial C_2}{\partial x_2} \lambda_2$$

$$m\ddot{x}_3 = -\frac{\partial C_1}{\partial x_3} \lambda_1 - \frac{\partial C_2}{\partial x_3} \lambda_2$$

The control variable u (which delivers the force F) acts directly on the first dynamical equation related to x_1 , which reflects the impact

of the PM stepper motor directly on the coarse stage output (see Figure B.1).

The small-signal linearization of the above equations gives for the operating point \bar{x}_1 :

$$\dot{\delta}x = A\delta x + B\delta u$$

$$A = \begin{bmatrix} 0 & 1 & 0 & 0 & 0 & 0 \\ -10\alpha & 0 & 10\beta & 0 & 0 & 0 \\ 0 & 0 & 0 & 1 & 0 & 0 \\ -5\alpha & 0 & -5\beta & 0 & 0 & 0 \\ 0 & 0 & 0 & 0 & 0 & 1 \\ -3\frac{\bar{x}_1}{l}\alpha & 0 & 3\frac{\bar{x}_1}{l}\beta & 0 & 0 & 0 \end{bmatrix}$$

$$B = \delta \begin{bmatrix} 0 \\ 100l \\ 0 \\ 50l \\ 0 \\ 30\bar{x}_1 \end{bmatrix}$$

$$\alpha = 5k_1l\delta$$

$$\beta = 5(k_1 - k_{1p})l\delta$$

$$\delta = \frac{l}{25l^2(m + 4M) + 9m\bar{x}_1^2}$$

The 6 states are not independent since the conditions $C_1 = 0$, $C_2 = 0$, $\dot{C}_1 = 0$ and $\dot{C}_2 = 0$ should be satisfied at any time.

This full six-order state-space model becomes controllable once the constraints (B.1) and (B.2) (together with their time derivatives) are taken into account. This leads to the following equivalent second-order state-space realization:

$$\dot{x}_r = A_r x_r + B_r u$$

where $x_r = (x_1 \dot{x}_1)^T$ and

$$A_r = \begin{bmatrix} 0 & 1 \\ \omega_0^2 & 0 \end{bmatrix}, \quad B_r = \begin{bmatrix} 0 \\ 100l\delta \end{bmatrix}, \quad \omega_0^2 = 10\alpha - 5\beta.$$

As foreseen, this simplified model corresponds to an ideal spring behavior. However, the main resonant frequency of the equivalent spring model (Figure B.2) changes with respect to position (ω_0 is a function of \bar{x}_1). Thus, this resonant mode cannot be directly canceled

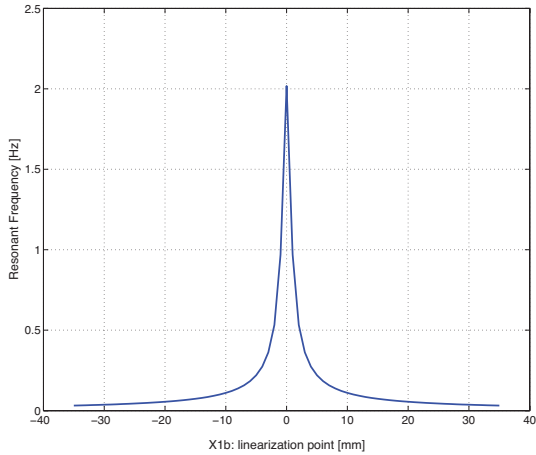


Fig. B.2. Evolution of the main resonant frequency of the blade guiding support with respect to its position within the full stroke.

by pole-zero placement in the controller, since its frequency evolves.

Moreover, the second conclusion from this analysis is that the load of the coarse stage actuator changes drastically with position (the force varies from minus 150 N to 150 N). These two characteristics drive the design of the coarse stage controller, which should be robust enough to handle this load and resonant-frequency change throughout the full stroke.

C

Piezoelectric hysteresis compensation

In the context of compensating the hysteresis of the stack piezoelectric actuator, an hysteresis compensation-method based on a Preisach model is described in this appendix.

The Preisach-based model of the piezoelectric hysteresis has been adapted using electromagnetism theory by Ge and Jouaneh [28]. Some improvements of this method have also been proposed, such as the generalized Preisach model, which relaxes the congruency property [30]. Ge and Jouaneh developed a compensation method based on the Preisach model [29]

C.1 Preisach model of hysteresis

The basic idea of the Preisach model lies in the description of the hysteresis through an infinite number of operators $\gamma_{\alpha\beta}[u(t)]$ (Fig. C.1a). For piezoelectric actuators, $\gamma_{\alpha\beta}[u(t)]$ is set to +1 if the input $u(t)$ exceeds the switching value α or to 0 if the input $u(t)$ is below the switching value β . The operators are multiplied by a weighting function $\mu(\alpha, \beta)$ and connected in parallel (Fig. C.1b). Such a representation takes into account the fact that the hysteresis is a nonlinearity with nonlocal memory effect, which means that the current displacement of the actuator, namely $x(t)$, depends upon the history of the input voltage $u(t)$. The classical Preisach model can then be mathematically written as:

$$x(t) = \iint_{\alpha > \beta} \mu(\alpha, \beta) \gamma_{\alpha\beta}[u(t)] d\alpha d\beta \quad (\text{C.1})$$

This equation can be interpreted thanks to a limiting triangle T_0 , also called $\alpha - \beta$ diagram. It is defined in such a way that $u_{max} \geq \alpha \geq \beta \geq u_{min}$, where u_{max} and u_{min} are the limiting values of the input voltage $u(t)$. The surface S^+ , which corresponds to the operators $\gamma_{\alpha\beta}[u(t)]$ set to +1, grows from bottom to top when the hysteresis is in an ascending loop and decreases from right to left in a descending loop (Fig. C.2). Since the operator $\gamma_{\alpha\beta}[u(t)]$ is equal to 0 out of the surface S^+ , Equation (C.1) can be written as:

$$x(t) = \iint_{S^+} \mu(\alpha, \beta) d\alpha d\beta \quad (\text{C.2})$$

So as to both simplify the calculation and suppress the double integration, the Preisach function is defined as follows:

$$X(\alpha', \beta') = x_{\alpha'} - x_{\alpha'\beta'} \quad (\text{C.3})$$

where $x_{\alpha'}$ is the piezoelectric expansion on the major ascending branch for an input voltage α' , and $x_{\alpha'\beta'}$ is the piezoelectric expansion on the first order reversal curve for an input voltage β' (Fig.

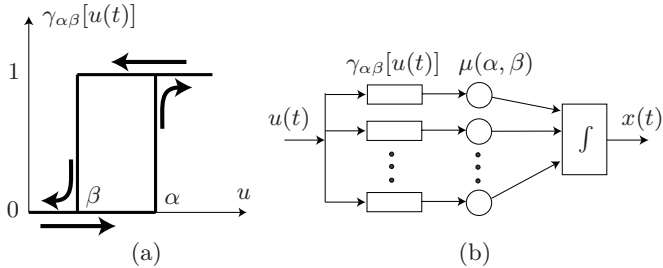


Fig. C.1. (a) Hysteresis operator $\gamma_{\alpha\beta}[u(t)]$. (b) Block diagram of the Preisach model.

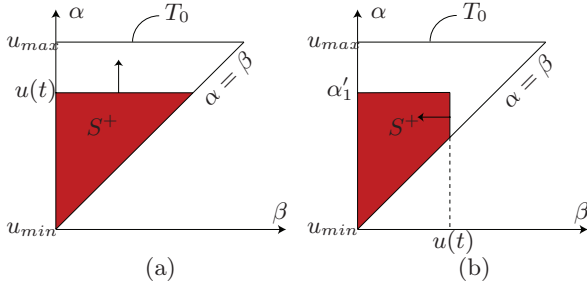


Fig. C.2. Limiting triangle T_0 for (a) an ascending loop and (b) a descending loop.

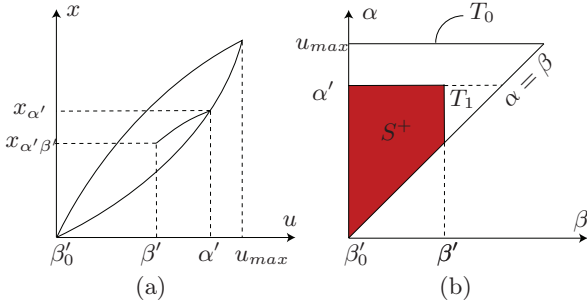


Fig. C.3. (a) Expansion of the actuator for a input voltage increasing until α' and then decreasing until β' . (b) Limiting triangle T_0 related to (a).

C.3). α' and β' represent the maxima, resp. the minima, of the input voltage $u(t)$. Figure C.3b shows that Equation (C.3) can also be written as:

$$X(\alpha', \beta') = \iint_{T_1} \mu(\alpha, \beta) d\alpha d\beta \quad (\text{C.4})$$

If the hysteresis loop contains several extrema, the surface S^+ is composed of several trapezoidal regions S_k (Fig. C.4). All the extrema α'_k and β'_k that depend on the past values of the input voltage $u(t)$ are stored in the history. For the region S_1 , the following equation is deduced:

$$\iint_{S_1} \mu(\alpha, \beta) d\alpha d\beta = X(\alpha'_1, \beta'_0) - X(\alpha'_1, \beta'_1) \quad (\text{C.5})$$

The other regions are calculated in the same way. Because the integration on the surface S^+ is the sum of the integrations on all the surfaces S_k , the total piezoelectric expansion $x(t)$ for an input voltage $u(t)$ is determined thanks to (C.2), depending on the current slope of $u(t)$:

$$\dot{u}(t) > 0$$

$$x(t) = \sum_{k=1}^N [X(\alpha'_k, \beta'_{k-1}) - X(\alpha'_k, \beta'_k)] + X(u(t), \beta'_N) \quad (\text{C.6})$$

$$\dot{u}(t) < 0$$

$$x(t) = \sum_{k=1}^{N-1} [X(\alpha'_k, \beta'_{k-1}) - X(\alpha'_k, \beta'_k)] + X(\alpha'_N, \beta'_{N-1}) - X(\alpha'_N, u(t)) \quad (\text{C.7})$$

where N is the number of maxima α'_k and minima β'_k that are stored.

So as to compute the values $X(\alpha', \beta')$, a mesh of α and β is created within T_0 . The reference values $X(\alpha, \beta)$ are measured on the piezoelectric actuator for all α and β of the mesh and stored at each corresponding node (Fig. C.5). Once the cell in which a given pair (α', β') lies is determined, the corresponding value $X(\alpha'_i, \beta'_j)$ is computed using a bilinear-spline interpolation:

$$X(\alpha', \beta') = a_{00} + a_{10}\alpha' + a_{01}\beta' + a_{11}\alpha'\beta' \quad (\text{C.8})$$

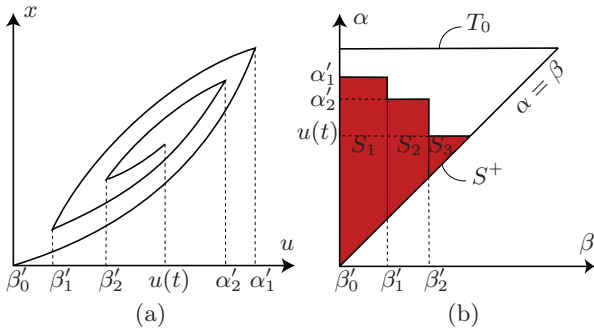


Fig. C.4. (a) Hysteresis loop with several extrema α' and β' . (b) Limiting triangle T_0 related to (a).

For every $X(\alpha', \beta')$, the interpolation coefficients a_{00}, a_{10}, a_{01} and a_{11} , are obtained through the same spline interpolation based on

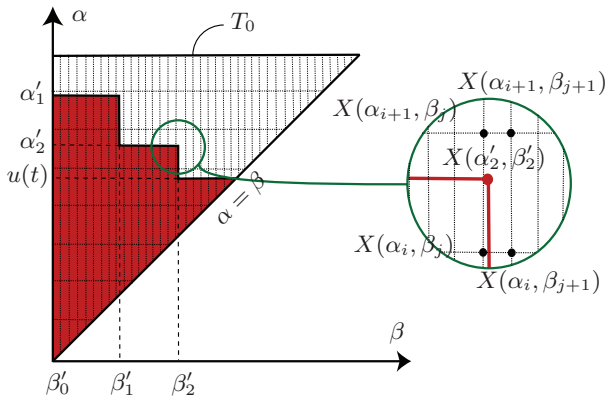


Fig. C.5. Division of the limiting triangle T_0 into a finite number of rectangles and triangles.

the values of the nodes surrounding the cell $X(\alpha_i, \beta_j)$, $X(\alpha_i, \beta_{j+1})$, $X(\alpha_{i+1}, \beta_j)$ and $X(\alpha_{i+1}, \beta_{j+1})$ (Fig. C.5). The expansion is determined using either (C.6) or (C.7).

To work properly, the Preisach model still needs an additional property, namely the wipe-out property. It allows to erase the pair $(\alpha'_N, \beta'_{N-1})$ from the history once $u(t)$ exceeds α'_N . Similarly, the pair (α'_N, β'_N) can be erased from the history once $u(t)$ becomes smaller than β'_N . This avoids the excessive growing of the stored values.

C.2 Hysteresis compensation

So as to compensate the hysteresis of the actuator, the Preisach model (Appendix C) has to be inverted. In other words, the voltage $u(t)$ that produces the desired expansion $x(t)$ must be determined, based on the model. This inversion is complicated by the fact that the hysteresis is a nonlinearity with a nonlocal memory. The inversion of the hysteresis model is achieved by modifying Equations (C.6) and (C.7) so as to express the voltage $u(t)$ as a function of the desired expansion $x(t)$. The history of the hysteresis must however be carefully taken into account. The cases of either ascending or descending branches are treated separately.

- $\dot{u}(t) > 0$

If t_0 is defined as the time at which the input voltage reaches a local minimum, the expansion is:

$$x(t_0) = \sum_{k=1}^N [X(\alpha'_k, \beta'_{k-1}) - X(\alpha'_k, \beta'_k)] \quad (\text{C.9})$$

where all values $X(\alpha'_k, \beta'_{k-1})$ and $X(\alpha'_k, \beta'_k)$ are already stored in the history. As the voltage grows, the expansion is obtained with (C.6). Combining this result together with (C.9), the following relation holds:

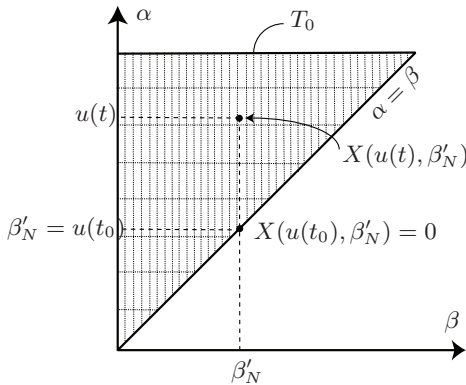


Fig. C.6. Inverse Preisach model principle when $\dot{u}(t) > 0$.

$$X(u(t), \beta'_N) = x(t) - x(t_0) \quad (\text{C.10})$$

Equations (C.8) and (C.10) lead to the voltage

$$u(t) = \frac{x(t) - x(t_0) - a_{01}\beta'_N - a_{00}}{a_{10} + a_{11}\beta'_N} \quad (\text{C.11})$$

The only remaining problem is that the interpolation coefficients, a_{00} , a_{10} , a_{01} and a_{11} , depend on the cell which contains the value $X(u(t), \beta'_N)$. Nevertheless, it can be solved by reasoning in the $\alpha - \beta$ diagram, as illustrated in Fig. C.6. When the voltage is at his local minimum, the value $X(u(t), \beta'_N)$ is located on the straight line $\alpha = \beta$ and is equal to zero. As the voltage grows, the point that contains $X(u(t), \beta'_N)$ moves up on the vertical line $\beta = \beta'_N$. By calculating the values $X(\alpha, \beta'_N)$ that lies at the intersection of the line $\beta = \beta'_N$ with the horizontal lines of the mesh, the cell which should contain the value $X(u(t), \beta'_N)$ can be determined. As the interpolation coefficients are known for each cell, the voltage $u(t)$ is the only remaining unknown value and is obtained thanks to (C.11). As for the classical Preisach model, the wipe-out property can be used to simplify the

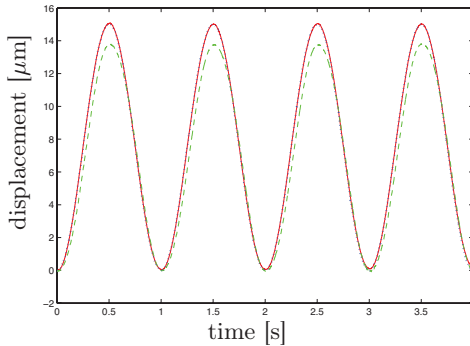


Fig. C.7. Open-looped tracking of a 1 Hz sinusoidal reference (dotted line) with and without the compensation algorithm (continuous and dashed line).

storage of the extrema.

The case $\dot{u}(t) < 0$ is quite similar to the above one. The interested reader will find the details of this approach in [102].

C.3 Implementation results

The hysteresis compensation algorithm is validated on the real system (piezoelectric only) with different input signals. All the experimentations are realized in open loop. Comparisons are done between the system controlled with and without the compensation of the hysteresis.

For a low frequency input signal, Figures C.7 and C.8 show a large improvement by using the compensation algorithm. The error decreases from 902 nm rms to approximately 79 nm rms. The maximum error is about 150 nm, which is only 1.1% of the total stroke. The major part of the error comes from the modeling and not from the inversion. With input signals of higher frequency, the sampling

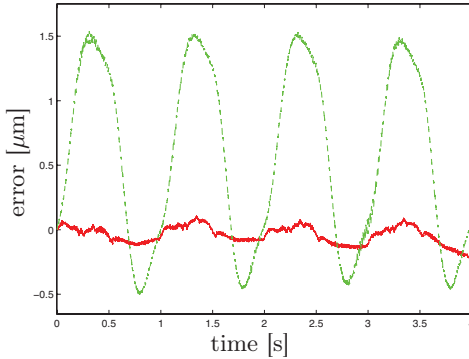


Fig. C.8. Tracking error for a 1 Hz sinusoidal reference with and without the compensation algorithm (continuous and dashed line).

period necessary for the inversion involves a higher error, which is also increased by the dynamics of the piezoelectric actuator. Nevertheless, the compensation algorithm still provides far better results than a simple open-loop control.

The response to a stochastic signal plotted in Figure C.9 also shows a great improvement obtained by the addition of the compensation algorithm. An error of 44 nm rms can be seen in Figure C.10 instead of 134 nm rms for a simple open-loop control, that means a diminution of approximately 67%. The maximum error is about 120 nm, which is 6% of the maximal stroke of 2 μm . In fact the results are promising even if the stochastic signal contains high frequencies that cannot be represented optimally with the model built at low frequency. However, as the amplitude of the input signal diminishes, the dynamics of the piezoelectric are less visible than with a high-amplitude sinusoidal signal. As the effect of the hysteresis slowly decreases with an increasing frequency [20], a dynamic model could be implemented to improve the performances [93]. Since both the signal is stochastic and the future values are unknown, the determination of the frequency or of the current slope can however be

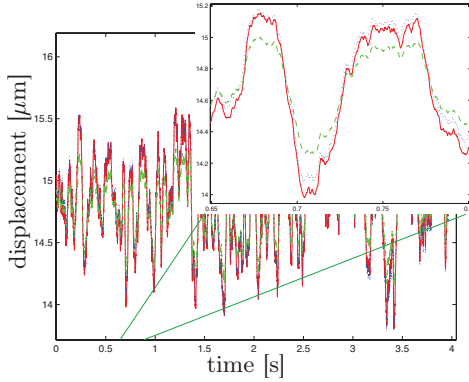


Fig. C.9. Open-loop tracking of a stochastic signal (dotted line) with and without the compensation algorithm (continuous and dashed line).

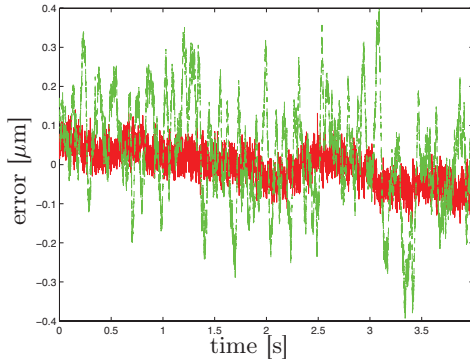


Fig. C.10. Tracking error for a stochastic reference with and without the compensation algorithm (continuous and dashed line).

particularly tricky.

The interested reader will find the details in [102].

D

Illustrations of the Differential Delay Line

In this appendix, a selection of pictures and drawing of the DDL system is presented. These pictures are not commented and are integrate to the present work as illustrations of the final system implemented in Paranal, August 2008.



(a) VLTI at Paranal: main telescopes

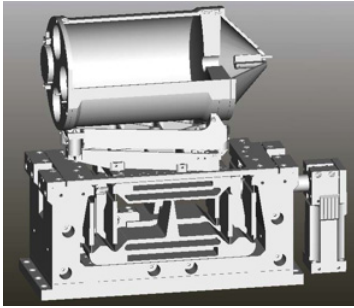


(b) VLTI at Paranal: main telescopes

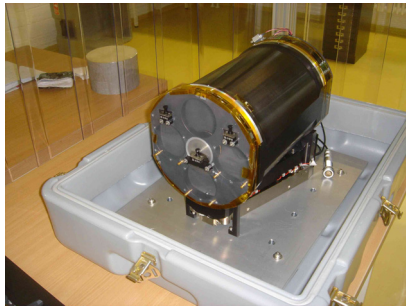


(c) VLTI at Paranal: auxiliary telescopes

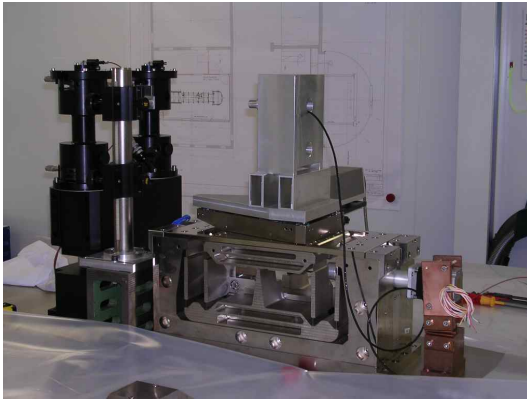
Fig. D.1. ESO Very Large Telescope Interferometer (VLTI) infrastructure in Paranal, Chile.



(a) DDL: 3D draw



(b) DDL: cat's eye alone

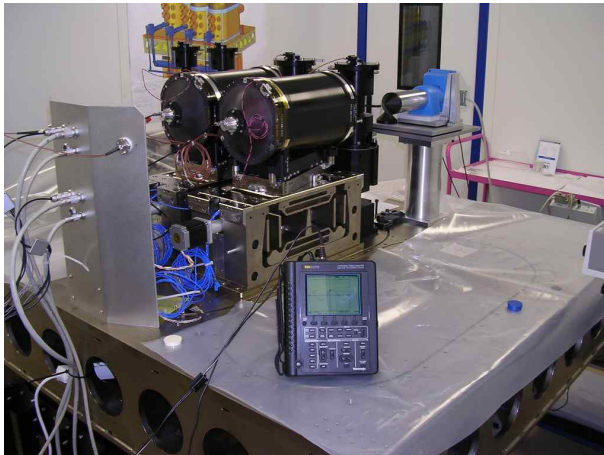


(c) DDL prototype with the dummy cat's eye mounted on the top of the blade guiding structure.

Fig. D.2. Differential Delay Line (DDL) prototype with its dedicated optics (cat's eye).

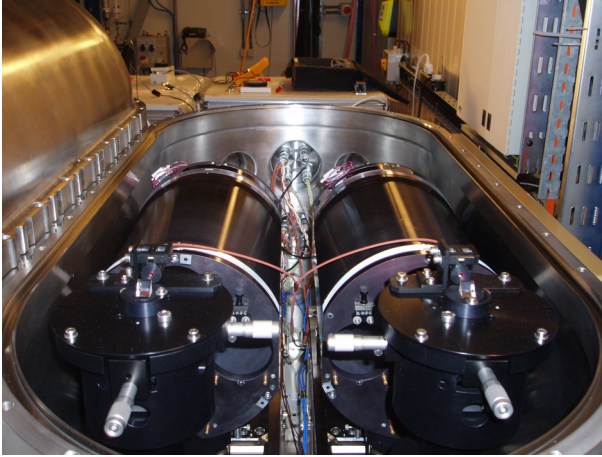


(a) DDL: complete system rear side view



(b) DDL: complete system front side view

Fig. D.3. Differential Delay Line (DDL) final testing before packing to Chile.



(a) DDL: final implementation in Chile



(b) VLTi

Fig. D.4. VLTi & DDL: in Paranal on Monte Cerro, Chile

E

Links to illustrative movies

In the context of overactuation, where the number of degrees of freedom is usually large, movies are very useful to illustrate the concepts successfully.

- 5R3D manipulator:
-<http://lawww.epfl.ch/page24555.html>
- Shoulder coordination:
-<http://lawww.epfl.ch/Jahia/site/la/op/edit/pid/29277>
- Differential Delay Line coordination:
-<http://lawww.epfl.ch/Jahia/site/la/op/edit/pid/25947>

References

- [1] M. Aeberhard. Modélisation dynamique de l'épaule. Master's thesis, Ecole Polytechnique Fédérale de Lausanne, 2008.
- [2] M. Aiello, R. Rekowski, M. Bodson, J. Chiasson, and D. Schuerer. Experimental results of using an exact linearization controller on a pm stepper motor. *Proceedings of the Conference on Decision and Control*, 1990.
- [3] A. Al Mamun, I. Mareels, T. H. Lee, and A. Tay. Dual stage actuator control in hard disk drive - a review. *IECON '03. The 29th Annual Conference of the IEEE Industrial Electronics Society, 2003.*, 3:2132–2137, 2003.
- [4] J. Aldrich and R. E. Skelton. Time-energy optimal control of hyper-actuated mechanical systems with geometric path constraints. *IEEE Conference on Decision and Control and the European Control Conference in Seville*, December 2005.
- [5] H. Asada and J.-J. E. Slotine. *Robot Analysis and Control*. Wiley-Interscience Publication, 1rst edition, 1985.
- [6] B. A. Awabdy, W.-Ch. Shih, and D. M. Auslander. Nanometer positioning of a linear motion stage under static load. *IEEE Transactions on mechatronics*, 3(2), 1998.

- [7] B. A. Awabdy, W.-Ch. Shih, and D. M. Auslander. Nanometer positioning of a linear motion stage under static load. *IEEE Transactions on mechatronics*, 3(2), 1998.
- [8] J. Baillieul. Kinematic programming alternatives for redundant manipulators. *Proc. IEEE Conf. Robotics Automation*, pages 722–728, 1985.
- [9] J. Baillieul, J. Hollerbach, and R. W. Brockett. Programming and control of kinematically redundant manipulators. *Proceedings of the 23rd IEEE Conference on Decision and Control*, pages 768–774, December 1984.
- [10] H. Baruh. *Analytical Dynamics, 1st Edition*. McGraw-Hill, 1999.
- [11] M. Bodson and J. Chiasson. Application of nonlinear control method to the positioning of a permanent magnet stepper motor. *Proceedings of the Conference on Decision and Control*, 1989.
- [12] M. Bodson, J. N. Chiasson, R. T. Novotnak, and R. B. Rekowski. High-performance nonlinear feedback control of a permanent magnet stepper motor. *IEEE Trans. on Control Systems Technology*, 1(1), March 1993.
- [13] M. D. K. Breteler, C. W. Spoor, and F. C. Van der Helm. Measuring muscle and joint geometry parameters of a shoulder for modeling purposes. Technical Report 11, Vrije Universiteit, Faculty of human movement sciences, 1996.
- [14] R. W. Brockett. Robotic manipulators and the product of exponentials formula. *Proc. MTNS Conf., Beer-Sheva, Israel*, pages 120–129, June 1983.
- [15] J. W. Burdick. *Kinematic Analysis and Design of Redundant Manipulators*. PhD thesis, Stanford University, 1988.
- [16] J. W. Burdick. On the inverse kinematics of redundant manipulators: characterization of the self-motion manifolds. *Proceedings of 1989 International Conference on Robotics and Automation*, 1989.

- [17] T. Chettibi, H. E. Lehtihet, M. Haddad, and S. Hanchi. Minimum cost trajectory planning for industrial robots. *European Journal of Mechanics And Solids*, pages 703–715, 2004.
- [18] L. Chrifi-Alaoui and A. Lebrun. h_∞ feedback control of a permanent magnet stepper motor. *Oxford Science Publications*, 1994.
- [19] D. Croft, G. Shed, and S. Devasia. Nonlinear inversion-based output tracking. *Journal of Dynamic Systems, Measurement and Control*, 123:35–43, 2001.
- [20] D. Damjanovic. Stress and frequency dependence of the direct piezoelectric effect in ferroelectric ceramics. *Journal of Applied Physics*, 82:1788–1797, 1997.
- [21] F. Delplancke et al. Phase-referenced imaging and micro-arcsecond astrometry with the vlti. In *Proc. SPIE, Interferometry in Optical Astronomy*, volume 4006, pages 365–376, July 2000.
- [22] F. Derie et al. Phase referenced imaging and micro-arcsec astrometry (prima) technical description and implementation. In *ESA Special Publication*, volume 522, March 2003.
- [23] S. Devasia. Nonlinear inversion-based output tracking. *IEEE Transactions on Automatic Control*, 41(7), 1996.
- [24] M. Dimmler, U. Holmberg, and R. Longchamp. Hysteresis compensation of piezo actuators. *Proceedings of 1999 European Control Conference*, 1998.
- [25] M. Farkas. *Periodic Motions, Applied Mathematical Sciences, Vol. 104*. Springer-Verlag, 1994.
- [26] B.A. Francis and W.M. Wonham. The internal model principle of control theory. *Automatica*, 12:457–465, 1976.
- [27] W. Fulton. *Algebraic topology. A first course*. Graduate Texts in Mathematics, New York: Springer, 1995.
- [28] P. Ge and M. Jouaneh. Modeling hysteresis in piezoceramic actuators. *Precision Engineering*, 17:211–221, 1995.
- [29] P. Ge and M. Jouaneh. Tracking control of a piezoceramic actuator. *IEEE Transactions on Control Systems Technology*, 4:209–216, 1996.

- [30] P. Ge and M. Jouaneh. Generalized preisach model for hysteresis nonlinearity of piezoceramic actuators. *Precision Engineering*, 20:99–111, 1997.
- [31] C. V. Giessen, Q. Zou, and S. Devasia. Inversion-based precision-positioning of switching inertial reaction devices. *Proceedings of 2004 American Control Conference*, 2004.
- [32] A. Glindemann et al. The vlt interferometer: a unique instrument for high-resolution astronomy. *Proc. SPIE, Interferometry in Optical Astronomy*, 4006:2–12, 2000.
- [33] H. Goldstein. *Classical Mechanics*. Reading, MA: Addison-Wesley, 2nd edition, 1980.
- [34] D. H. Gottlieb. Robots and topology. *Proceedings of 1986 International Conference on Robotics and Automation*, 1986.
- [35] E. Y. L. Gu. A configuration manifold embedding model for dynamic control of redundant robots. *The International Journal of Robotics Research*, 19(3):289–304, 2000.
- [36] E. Y. L. Gu. Configuration manifolds and their applications to robot dynamic modeling and control. *IEEE Transactions on Robotics and Automation*, 16(5):517–527, 2000.
- [37] Y.-L. Gu. Dynamics and control for redundant robots. *Proceedings of Int. Conf. On Robotics and Automation*, pages 194–199, 1988.
- [38] J. Guckenheimer and P. Holmes. *Nonlinear Oscillations, Dynamical Systems, and Bifurcations of Vector Fields*. Springer-Verlag, new york edition, 1983.
- [39] O. Harkegard and S. T. Glad. Resolving actuator redundancy: Optimal control vs. control allocation. *Automatica*, 41:137–144, 2005.
- [40] S. Henein. *Conception des structures articulées à guidages flexibles de haute précision*. PhD thesis, Ecole Polytechnique Fédérale de Lausanne, 2000.
- [41] D. Hernandez, S.-S. Park, R. Horowitz, and A. K. Packard. Dual-stage track-following servo design for hard disk drives. *Proceedings of ACC*, 1999.

- [42] J. M. Hollerbach and K. C. Suh. Redundancy resolution of manipulators through torque optimization. *Proc. IEEE Conf. Robotics Automation*, pages 1016–1021, 1985.
- [43] R. Hooper and D. Tesar. Motion coordination based on multiple performance criteria with a hyper-redundant serial robot example. *Proceedings of the 1995 IEEE International Symposium on Intelligent Control*, pages 133–138, August 1995.
- [44] X. Hu, W. Guo, T. Huang, and B. M. Chen. Discrete-time lqg/ltr dual-stage controller design and implementation for high track density hdds. *Proceedings of the American Control Conference*, 1999.
- [45] D. Huston, B. Esser, G. Spencer, D. Burns, and E. Kahn. Hierarchical actuator systems. *Smart structures and materials 2005: Industrial and Commercial Application of Smart Structures Technologies*, 5762:311–319, 2005.
- [46] C.-L. Hwang. High bandwidth nano-positioner : A robust control approach. *Review of Scientific Instruments*, 73(9), 2002.
- [47] C.-L. Hwang. Trajectory tracking of large-displacement piezoelectric actuators using a nonlinear observer-based variable structure control. *IEEE Transaction on control Systems technology*, 13(1), 2005.
- [48] S. Kawamura, H. Kino, and Ch. Won. High-speed manipulation by using parallel wire-driven robots. *Robotica*, 18:13–21, 2000.
- [49] T. Kenjo and A. Sugawara. *Stepping Motors and their Microprocessor Controls*. Oxford Science Publications, 2nd edition, 1994.
- [50] O. Khatib. Real-time obstacle avoidance for manipulators and mobile robots. *International Journal of Robotics Research*, 5(1):500–505, 1986.
- [51] O. Khatib. A unified approach for motion and force control of robot manipulators: the operational space formulation. *IEEE Journal of Robotics and Automation*, RA-3(1):43–53, february 1987.

- [52] O. Khatib, L. Sentis, J. Park, and J. Warren. Whole-body dynamic behaviour and control of human-like robots. *International Journal of Humanoid Robotics*, 1(1):29–43, 2004.
- [53] Y.-H. Kim and S.-H. Lee. An approach to dual-stage servo design in computer disk drives. *Transactions on Control Systems Technology*, 12(1), 2004.
- [54] W. C. A. Kishore, S. Sen, and G. Ray. Disturbance rejection and control allocation of over-actuated systems. *IEEE International Conference on Industrial Technology*, December 2006.
- [55] Ch. A. Klein and Sh. Ahmed. Repeatable pseudoinverse control for planar kinematically redundant manipulators. *IEEE Transactions on Systems, Man, and Cybernetics*, 25, December 1995.
- [56] Ch. A. Klein and Ch.-H. Huang. Review of pseudoinverse control for the use with kinematically redundant manipulators. *IEEE Transactions on Systems, Man, and Cybernetics*, 13, 1983.
- [57] B. H. Koh, Z. Li, P. Dharap, S. Nagarajaiah, and M. Q. Phan. Actuator failure detection through interaction matrix formulation. *Journal of Guidance Control and Dynamics*, 28(5):895–901, 2005.
- [58] S. Kwon, W. K. Chung, and Y. Youm. On the coarse/fine dual-stage manipulators with robust perturbation compensator. *Proceedings of the IEEE International Conference on Robotics and Automation*, 2001.
- [59] P. Lafourcade, M. Llibre, and C. Reboulet. Design of a parallel wire-driven manipulator for wind tunnels. In *Proceedings of the WORKSHOP on Fundamental Issues and Future Research Direction for Parallel Mechanisms and Manipulators, Quebec, Canada, 1-7, 2002*.
- [60] R. Launhardt, S. Frink, D. Segransan, and J. Setiawan. Astrometric survey for extra-solar planets with prima - scientific proposal. Technical Report Planets-PRI-SCI-0001, DDL consortium - ESO, Geneva Observatory, Leiden Observatory, MPIA Heidelberg, September 2003.

- [61] K.K. Leang and S. Devasia. Design of hysteresis-compensating iterative learning control for piezo-positioners: Application to atomic force microscopes. *Mechatronics*, 16:141–158, 2006.
- [62] S.-H. Lee, Y.-H. Kim, and S.-E. Baek. Modeling and control of a dual-stage actuator for hard disk drive servo systems. *Proceedings of the American Control Conference.*, 6:4254–4258, June 2000.
- [63] S.-H. Lee, Y.-H. Kim, and Ch. Ch. Chung. Dual-stage actuator disk drives for improved servo performance : Track follow, track seek, and settle. *IEEE Trans. on Magnetics*, 37(4), 2001.
- [64] A. Liegeois. Automatic supervisory control of the configuration and behavior of multibody mechanisms. *IEEE Transactions on Systems, Man, and Cybernetics*, SMC-7(12):868–871, 1977.
- [65] H. Liu, B. Lu, Y. Ding, Y. Tang, and D. Li. A motor-piezo actuator for nano-scale positioning based on dual servo loop and nonlinearity compensation. *Journal of Micromechanics and Microengineering*, (13):295–299, 2003.
- [66] H. Liu, B. Lu, Y. Ding, Y. Tang, and D. Li. A motor-piezo actuator for nano-scale positioning based on dual servo loop and nonlinearity compensation. *Journal of Micromechanics and Microengineering*, (13):295–299, 2003.
- [67] A. Liégeois. Automatic supervisory control of the configuration and behavior of multibody mechanisms. *IEEE Transactions on Systems, Man, and Cybernetics*, 7, December 1977.
- [68] J. Lugon. Trajectory planification and control of a redundant serial manipulator. Master’s thesis, Ecole Polytechnique Fédérale de Lausanne, 2008.
- [69] A. Al Mamun, I. Mareels, T. H. Lee, and A. Tay. Dual stage actuator control in hard disk drive – A review. *29th Annual Conference of the IEEE*, 3, 2003.
- [70] Y. Michellod, Ph. Mullhaupt, and D. Gillet. Strategy for the control of a dual-stage nano-positioning system with a single metrology. *Proceedings of IEEE International Conference on Robotics, Automation and Mechatronics*, June 2006.

- [71] Hellmuth Michels and Claas Lennart Neumann. *Kurzlehrbuch Anatomie Hellmuth Michels, Claas*. Elsevier, Urban & Fischer, 2007.
- [72] A. Muller and P. Maisser. A lie-group formulation of kinematics and dynamics of constrained mbs and its application to analytical mechanics. *Multibody System Dynamics*, 9(4):311–352, 2003.
- [73] Ph. Mullhaupt. *Introduction à l'Analyse et à la Commande des Systèmes Non Linéaires*. Presses Polytechniques et Universitaires Romandes, 2008.
- [74] P. Murdin, editor. *Encyclopedia of Astronomy and Astrophysics*. Nature Publishing Group and Institute of Physics Publishing, 2001.
- [75] D. N. Nenchev. Redundancy resolution through local optimization: A review. *Journal of Robotic Systems*, (6):769–798, 1989.
- [76] F. Nicolato and M. K. Madrid. Recursive algorithm for the inverse kinematics of redundant robotic manipulators. *Proceedings of 16th IFAC World Congress*, 2005.
- [77] P. J. Olver. *Equivalence, invariants, and symmetry*. Cambridge University Press, 1995.
- [78] Ch. Khiang Pang, G. Guo, B. M. Chen, and T. H. Lee. Self-sensing actuation for nanopositioning and active-mode damping in dual-stage hdds. *IEEE/ASME Trans. Mechatron.*, 11(3), 2006.
- [79] K. Peng, B. M. Chen, and T. H. Lee. Design and implementation of a dual-stage actuated hdd servo system via composite nonlinear control approach. *Mechatronics*, 14(9):965–988, 2004.
- [80] H. R. Rapley and W. C. Messner. Designing controllers for two stage disk drive actuator systems using the PQ method and the s-Bode plot. *IEEE Trans. on Magnetics*, 37(2), March 2001.
- [81] M. Rotunno and R. A. de Callafon. Fixed order H_∞ control design for dual-stage hard disk drives. *Proceedings of the 39th IEEE Conference on Decision and Control*, 2000.

- [82] L. Sache. VLT-TRE-DDL-15723-0009, DDL Translation Assembly, Final Analysis and Performance Report. Technical report, Ecole Polytechnique Fédérale de Lausanne, 2006.
- [83] G. Schitter, R. W. Stark, and A. Stemmer. Sensors for closed-loop piezo control : strain gauges versus optical sensors. *Measurement Science and Technology*, 13, 2002.
- [84] M. G. E. Schneiders, M. J. G. van de Molengraft, and M. Steinbuch. Benefits of over-actuation in motion systems. *Proceedings of ACC*, 2004.
- [85] F. Schossau. Atmospheric disturbance compensation in the vlti telescope. Master's thesis, Ecole Polytechnique Fédérale de Lausanne, 2007.
- [86] S. J. Schroeck, W. C. Messner, and R. J. McNab. On compensator design for linear time-invariant dual-input single-output systems. *IEEE/ASME Trans. Mechatron.*, 6, 2001.
- [87] J. M. Selig. Lie groups and lie algebras in robotics. *Computational Noncommutative Algebra and Applications: Proceedings of the NATO Advanced Study Institute*, 2004.
- [88] J.M. Sellig. *Lie Groups and Lie Algebra in Robotics*. chapter in: Computational Noncommunicative Algebra and Applications, 2004.
- [89] L. Sentis and O. Khatib. Task-oriented control of humanoid robots through prioritization. *IEEE International Conference on Humanoid Robots*, 2004.
- [90] L. Sentis and O. Khatib. A whole-body control framework for humanoid operating in human environments. *Proceedings of 2006 International Conference on Robotics and Automation*, 2006.
- [91] T. Shamir and Y. Yomdin. Repeatability of redundant manipulators: Mathematical solution of the problem. *IEEE Transactions on Automatic Control*, 33, November 1988.
- [92] H. Sira-Ramirez. Trajectory planning in the regulation of a pm stepper motor: A combined passivity and flatness approach. *Proceedings of the American Control Conference*, 2000.

- [93] D. Song and J. Li. Modeling of piezo actuator's nonlinear and frequency dependent dynamics. *Mechatronics*, 9:391–410, 1999.
- [94] G. Song, J. Zhao, X. Zhou, and J.A. De Abreu-Garcia. Tracking control of piezoceramic actuator with hysteresis compensation using inverse preisach model. *IEEE/ASME Transactions on Mechatronics*, 10:198–209, 2005.
- [95] M. Stalder. Dedicated controller design for a dual-stage mechatronic system. Master's thesis, Ecole Polytechnique Fédérale de Lausanne, 2008.
- [96] M. Stalder, Y. Michellod, Ph. Mulhaupt, and D. Gillet. Dedicated controller design for a dual-stage opto-mechatronic system. *IEEE/ASME International Conference on Advanced Intelligent Mechatronics*, in Xi'an, July 2008.
- [97] S. Stroeve. Impedance characteristics of a neuromusculoskeletal model of the human arm i. posture control. *Biological Cybernetics*, 81(5):475–494, November 1999.
- [98] S.-M. Suh, Ch. Ch. Chung, and S.-H. Lee. Discrete-time lqg/ltr dual-stage controller design in magnetic disk drives. *IEEE Transactions on Magnetics*, 37:1891–1895, 2001.
- [99] K. Takahashi. Reliability and availability of redundant satellite orbit systems. *IEEE Transactions on Aerospace and Electronic Systems*, 18(3):258–267, 1982.
- [100] F. C. van der Helm. A finite element musculoskeletal model of the shoulder mechanism. *J Biomech*, 27(5):551–569, May 1994.
- [101] S. Weerasooriya and D. T. Phan. Discrete-time lqg/ltr design and modeling of a disk drive actuator tracking servo system. *IEEE Transactions on Industrial Electronics*, 42:240–247, 1995.
- [102] F. Weibel, Y. Michellod, Ph. Mullhaupt, and D. Gillet. Real-time compensation of hysteresis in piezoelectric-stack actuator tracking a stochastic reference. *In Proc. of American Control Conference, Seattle*, 2008.
- [103] D. E. Whitney. Resolved motion rate control of manipulators and human prostheses. *IEEE Transactions on Man-Machine Systems*, MMS-10(2):47–53, 1969.

- [104] R. L. Williams and J. B. Mayhew. Obstacle-free control of the hyper-redundant nasa inspection manipulator. *Proceedings of Fifth National Conference on Applied Mechanisms and Robotics*, October 1997.
- [105] D. Wu, G. Guo, and T. C. Chong. Comparative analysis on resonance compensation in hdd dual stage actuation systems. *Transactions On Industrial Electronics*, 50(9), 2003.
- [106] G. Wu, F. C T van der Helm, H. E. J. D. Veeger, M. Makhsous, P. Van Roy, C. Anglin, J. Nagels, A. R. Karduna, K. McQuade, X. Wang, F. W. Werner, B. Buchholz, and International Society of Biomechanics. Isb recommendation on definitions of joint coordinate systems of various joints for the reporting of human joint motion—part ii: shoulder, elbow, wrist and hand. *J Biomech*, 38(5):981–992, May 2005.
- [107] Y. K. Yong, S. Aphale, and R. Moheimani. Design, analysis and control of a fast nanopositioning stage. *Proceedings of IEEE/ASME International Conference on Advanced Intelligent Mechatronic, Xian, China*, 2008.
- [108] Y. Zhang, V. S. Suresh, B. Jiang, and D. Theilliol. Reconfigurable control allocation against aircraft control effector failures. *Proceedings of the 2007 IEEE Conference on Control Applications*, 1-3:1304–1309, 2007.
- [109] M. Zribi and J. Chiasson. Position control of a pm stepper motor by exact linearization. *IEEE Trans. on Automatic Control*, 36(5), 1991.

Index

- 1-form, 25, 69, 73
 - complementary, 43, 44, 74, 76
 - exact, 25
 - integrable, 25

- accessibility area, 14
- antagonism, 11, 32, 56, 100

- baseline, 80
- blade-guiding structure, 84

- cat's eye, 84
- closed trajectory, 18, 32, 62
- compact, 38
- compliance, 72, 75, 77
- condition
 - connexity, 28, 45
 - integrability, 28
- configuration
 - manifold, 6
- coordination, 2, 5, 28, 76, 92, 99, 101
 - constructive, 2, 11, 30, 32, 44, 51, 55, 77, 95
- coordinator, 96
- cotangent bundle, 25, 42

- DDL, 80, 82, 85, 87, 94, 96
- de-synchronization, 92
- delay line, 80
- destructive interference, 99
- diffeomorphism, 17, 24, 39
- differential delay line, 4, 79
- differential geometry, 27
 - integrability condition, 5
 - Lie bracket, 5, 28
 - simply connected, 5
- differentiation, 10, 31, 94
- DISO, 85
- double parallelogram flexure with notch hinges, 85, 91
- dual feed, 81
- dual space, 25

- eigenvalue, 70

- eigenvector, 70, 77
- end-effector, 13
- ESO, 80

- feed-forward, 88, 99
- feedback, 86, 98
- flatness, 90
- flexibility, 1, 10, 12, 31, 43, 51, 54, 72, 75, 77
- foliation, 31, 44
- fringes, 80

- HDD, 84, 96, 99
- hessian, 51, 68, 70, 71
 - matrix, 69, 77
- hierarchy, 52, 55, 67, 68
- homeomorphism, 24, 62, 73
- humanoid, 6
- hyper-surface, 25, 43
- hysteresis, 88, 89
 - Preisach model, 90

- integrability, 25
- integrable distribution, 36
- interferometry, 80
- internal model principle, 88
- intrinsic characterization, 10, 94
- invariant set, 65, 66
- involutive, 25, 28, 31, 36, 39, 42
 - basis, 44

- jacobian, 22, 33, 44, 56
 - matrix, 5, 29
 - rigid extension, 5, 57, 58, 68
 - soft extension, 59, 60, 62, 68, 77
- joint
 - configuration, 15, 29
 - coordinate, 21
 - motion, 29
 - prismatic, 93
 - space, 5

- kernel, 41
- kinematic, 5
 - direct problem, 20, 70
 - inverse problem, 21, 27, 51, 57, 60, 62, 69, 75
 - open chain, 13, 15
- kolmogorov, 83, 87

- Lagrange multipliers, 23
- Lie bracket, 25, 36, 39
- Lie group, 43
- limit cycle, 62, 76, 77
 - convergence, 71
- Lissajou, 17, 34, 37, 44, 66
- loop transfer recovery, 86
- LQG, 86
- Lyapunov, 61, 63

- manifold, 17
 - configuration, 29
 - integral, 38, 74
 - output, 17, 29, 31, 34, 52, 66
 - redundant, 54, 67
 - task, 52, 53, 62, 68, 70, 72, 77
 - working, 31, 69
- manipulator, 13
- map, 15
 - surjective, 21
- moving attractive point, 62
- multi-tasking, 6, 10, 51, 60, 68, 76, 77

- null space, 56, 61
 - jacobian, 56, 59, 66

- reduced, 67, 68
- obstacle avoidance, 3
- OPD, 80
- operational space, 6
- optical path difference, 80
- output manifold, 29
- overactuation, 2, 9, 12, 29, 30, 51, 93
- Park transformation, 90
- piezoelectric, 84, 88
- PM stepper motor, 84, 88, 90
- Poincaré
 - Bendixon, 38
 - map, 18, 19, 46
 - section, 18
- potential function, 51, 62, 65
 - gradient, 55, 59, 61, 65, 76
- PQ, 99
- predictability, 62, 72, 77
- PRIMA, 80, 81
- prioritization, 6, 68
- pseudo-inverse, 5, 22, 28, 33, 37, 56, 59, 63
 - map, 66
 - Moore-Penrose, 5, 23
- redundancy, 4, 15
 - fiber, 53, 63, 65, 73
- repeatability, 18, 51, 55, 57, 75
- self-motion, 15, 53, 57, 60, 62, 77
- simply connected, 38
- singularities
 - accessibility, 12, 56
 - algorithmic, 56, 58, 59, 68, 71
 - integration, 12
- SISO, 85, 96
- submanifold, 38
- submersion, 5, 29, 32, 34, 39
- tangent bundle, 17, 25, 29, 39, 44, 73
- topology, 6, 69, 71
- UTs, 80
- vector fields, 28
 - distribution, 25
- versatility, 11, 12, 31
- VLT, 80
- voice-coil, 84
- working space, 14, 95

Glossary

AT : Auxiliary Telescopes
DDL : Differential Delay Line
DISO : Dual Input Single Output
DOF : Degree Of Freedom
dOPD : Differential Optical Path Difference
ESO : European Souther Observatory
FEM : Finite Element Model
GHJ : Glenohumeral Joint
HDD : Hard Disk Drive
ISG : International Shoulder Group
LQR : Linear-Quadratic Regulator
LQG : Linear-Quadratic Gaussian Regulator
MIMO : Multi-Input Multi-Output
NI DAQ : National Instrument Digital Acquisition board
OG : Observatoire de Genève
OPD : Optical Path Difference
PCSA : Physiological Cross-Sectional Area
PID : Proportional Integral Derivative
Pinv : Pseudo-Inverse
PM : Permanent Magnet

PRIMA : Phased-Referenced Imaging and Microarcsecond Astrometry

PZT : Piezoelectric stack actuator

RMS : Root Mean Squared

SISO : Single Input Single Output

UT : Unit Telescope

VLTI : Very Large Telescope Interferometer

Yvan Michellod

Chemin de Plampro 31
1936 Médières (Suisse)
+ 41 27 565 23 43

Born in Martigny the 27th November 1978
Nationality: Valaisan

Education

- 2004-2008: École Polytechnique Fédérale de Lausanne, **Doctoral studies and research** in Automatic Control.
- 1999-2004: École Polytechnique Fédérale de Lausanne, **Master of Science** in Electrical Engineering.

Publications

- Launhardt, R. et al. Towards High-Precision Ground-Based Astrometry: Differential Delay Lines for PRIMA@VLTI. In *Astrometry in the Age of the Next Generation of Large Telescopes (Astrometry 04)*, Lowell Observatory, Flagstaff, 2004.
- Gillet, D, Salzmann Ch., Michellod, Y. and Perritaz D. Hands-on Introduction to Automatic Control with focus on Teleoperation and Real-Time Interaction. In *Advances in Control Education (ACE) 2006, Madrid*, 2006.
- Michellod, Y., Mullhaupt, Ph. and Gillet, D. Strategy for the Control of a Dual-stage Nano-positioning System with a Single Metrology. In *2006 IEEE International Conference on Robotics, Automation and Mechatronics (RAM), Bangkok, Thailand*, 2006.
- Michellod, Y., Mullhaupt, Ph. and Gillet, D. Trajectory Tracking through Overactuation for an Optical Delay Line. Submitted to *IEEE/ASME Transactions on Mechatronics*, 2008.

- Stalder, M., Michellod, Y., Mullhaupt, Ph. and Gillet, D. Dedicated controller design for a dual-stage opto-mechatronic system. In *IEEE/ASME International Conference on Advanced Intelligent Mechatronics, Xian, China*, 2008.
- Michellod, Y., Mullhaupt, Ph. and Gillet, D. On Achieving Periodic Joint-Motion for Redundant Robots. In *IFAC World Congress, Seoul*, 2008.
- Weibel, F., Michellod, Y., Mullhaupt, Ph. and Gillet, D. Real-time compensation of hysteresis in piezoelectric-stack actuator tracking a stochastic reference. In *American Control Conference, Seattle*, 2008.
- Launhardt, R. et al. The PRIMA Astrometric Planet Search Project. In *The Power of Optical/IR Interferometry: Recent Scientific Results and 2nd Generation Instrumentation, Eso Astrophysics Symposia.*, Springer, 2008, p. 55.
- Aeberhard, M., Michellod, Y., Mullhaupt, Ph., Terrier, A., Pioletti, D. P. and Gillet, D. Dynamical biomechanical model of the shoulder: null space based optimization of the overactuated system. In *2008 IEEE International Conference on Robotics and Biomimetics, Bangkok*, 2008.